

# **Age-dependent upregulation of mechanosensitive channel Piezo1 impairs hippocampal synaptic plasticity**

Thesis

for the degree of  
doctor rerum naturalum (Dr. rer. nat.)

approved by the Faculty of Natural Sciences of Otto von Guericke University Magdeburg

by M.Sc. Hadi Mirzapourdelavar

born on February 7, 1985 in Babol (Iran)

Examiner: Prof. Dr. Alexander Dityatev

Prof. Dr. Vishnu Suppiramanian

submitted on: November 29, 2022

defended on: September 11, 2023

## Summary

Aging gives rise to widespread cellular and molecular changes in the central nervous system. Age-dependent or inflammation-induced accumulation of the extracellular matrix molecules coincides with increased tissue stiffness, which may result in dysregulated  $\text{Ca}^{2+}$  homeostasis via the activation of mechanosensitive channels. Therefore, this study aimed to investigate the expression and function of mechanosensitive channels in the aging mouse brain.

First, I compared the expression of the main mechanosensitive channels in the hippocampus of young 2- to 4-months-old (2-4 m) and over 30-months-old (>30 m) C57BL6/J male mice. Using qPCR, I found an aging-associated increase in the expression of the Piezo mechanosensitive channels, *Piezo1* and *Piezo2*, and some members of the TRP channel family including *TRPV1*, *TRPV4*, and *TRPA1*. Further analysis of 6-month-old (6 m) 5xFAD mice as a model of familial Alzheimer's disease revealed the same pattern of overexpression of hippocampal *Piezo1* and *Piezo2* when compared to control mice. Next, I focused on *Piezo1* because it is expressed at a much higher level than *Piezo2* in the hippocampus and is a pure mechanosensitive channel, unlike the mentioned TRP channels which have additional important functions. The immunocytochemical analysis confirmed overexpression of *Piezo1* in neurons of aged mice.

To study the effects of *Piezo1* hyperactivity separately from other abnormalities accompanying aging, we treated hippocampal acute slices from young mice with Yoda1, a chemical activator of *Piezo1*. We observed that *Piezo1* activation increased the resting intracellular calcium level. Using extracellular recordings of field postsynaptic potentials in the CA1 region, I demonstrated that theta-burst stimulation of CA3 axons resulted in impaired long-term potentiation (LTP) in slices treated with Yoda1 compared to a vehicle. Subsequent immunohistochemistry, qPCR, and western blot analyses suggested that mechanisms underlying this impairment may involve the activation of p38 MAPK, calpain protease, and transcriptional regulators YAP/TAZ. Inhibitors of p38 MAPK and calpain abrogated the effects of Yoda1 on CA1 LTP.

Inspired by these findings, I attempted to rescue the impaired CA1 LTP and hippocampus-dependent cognitive function in aged mice by knock-down of *Piezo1* expression via delivery of *Piezo1* shRNA encoding adeno-associated virus. Our behavioral and LTP analyses showed a partial rescue of synaptic and cognitive functions in aged mice following the *Piezo1* knockdown. Similar effects were observed after the degradation of the neural extracellular matrix by an overexpression of ADAMTS5 proteinase.

Taken together, the results of this thesis provide the first evidence that mechanosignaling through mechanosensitive ion channels is upregulated in aged mice and suggest that inhibiting mechanosignaling in neurons could be a potential target to rescue the impaired cognitive phenotype during aging.

## ZUSAMMENFASSUNG

Das Altern führt zu weit verbreiteten zellulären und molekularen Veränderungen im zentralen Nervensystem. Die altersabhängige oder entzündungsbedingte Akkumulation der extrazellulären Matrixmoleküle geht mit einer erhöhten Gewebesteifigkeit einher, die über die Aktivierung mechanosensitiver Kanäle zu einer fehlregulierten  $Ca^{2+}$ -Homöostase führen kann. Daher zielte diese Studie darauf ab, die Expression und Funktion von mechanosensitiven Kanälen im alternden Mausgehirn zu untersuchen.

Zuerst habe ich die Expression der wichtigsten mechanosensitiven Kanäle im Hippocampus von jungen 2-4 Monate alten (2-4 M) und über 30 Monate alten (>30 M) männlichen C57BL6/J-Mäusen verglichen. Mittels qPCR fand ich eine altersbedingte Zunahme der Expression der mechanosensitiven Piezo-Kanäle Piezo1 und Piezo2 und einiger Mitglieder der TRP-Kanalfamilie, einschließlich TRPV1, TRPV4 und TRPA1. Eine weitere Analyse von 6 Monate alten (6 M) 5xFAD-Mäusen als Modell der familiären Alzheimer-Krankheit ergab das gleiche Muster der Überexpression für hippocampales Piezo1 und Piezo2 im Vergleich zu den Kontrollmäusen. Als nächstes habe ich mich auf Piezo1 konzentriert, weil es im Hippocampus sehr viel stärker exprimiert wird als Piezo2 und ein rein mechanosensitiver Kanal ist, im Gegensatz zu den erwähnten TRP-Kanälen, die zusätzliche wichtige Funktionen haben. Die immunzytochemische Analyse bestätigte die Überexpression von Piezo1 sowohl in Neuronen als alter Mäuse.

Um die Auswirkungen der Piezo1-Hyperaktivität getrennt von anderen mit dem Altern einhergehenden Anomalien zu untersuchen, behandelten wir akute Hippocampus-Schnitte von jungen Mäusen mit Yoda1, einem chemischen Aktivator von Piezo1. Wir haben beobachtet, dass die Piezo1-Aktivierung den intrazellulären Kalziumspiegel im Ruhezustand erhöht. Anhand extrazellulärer Aufzeichnungen von postsynaptischen Feldpotenzialen in der CA1-Region habe ich gezeigt, dass die Theta-Burst-Stimulation von CA3-Axonon zu einer beeinträchtigten Langzeitpotenzierung (LTP) in mit Yoda1 behandelten Schnitten im Vergleich zu einem Träger führte. Nachfolgende immunhistochemische, qPCR- und Western-Blot-Analysen deuteten darauf hin, dass die Mechanismen, die dieser Beeinträchtigung zugrunde liegen, mit der Aktivierung von p38 MAPK, Calpain-Protease und der Transkriptionsregulatoren YAP/TAZ zusammenhängen könnten. Tatsächlich hoben Inhibitoren für p38 MAPK und Calpain die Wirkung von Yoda1 auf CA1-LTP auf.

Inspiziert von diesen Erkenntnissen versuchte ich, die beeinträchtigte CA1-LTP und Hippocampus-abhängige kognitive Funktion in gealterten Mäusen zu retten, indem ich die Piezo1-Expression durch die Abgabe von Piezo1-shRNA, die ein Adeno-assoziiertes Virus kodiert, ausschaltete. Unsere Verhaltens- und LTP-Analysen zeigten eine teilweise Wiederherstellung synaptischer und kognitiver Funktionen bei

gealterten Mäusen nach dem Piezo1-Knockdown. Ähnliche Effekte wurden nach dem Abbau der neuralen extrazellulären Matrix durch Überexpression der ADAMTS5-Proteinase beobachtet.

Zusammengenommen liefern die Ergebnisse dieser Dissertation den ersten Beweis dafür, dass die Mechansignalübertragung durch mechanosensitive Ionenkanäle in gealterten Mäusen hochreguliert ist und legen nahe, dass die Hemmung der Mechansignalübertragung in Neuronen ein potenzielles Ziel sein könnte, um den beeinträchtigten kognitiven Phänotyp während des Alterns zu retten.

## Table of Contents

<b>1 INTRODUCTION</b> .....	12
1.1 Central nervous system aging .....	12
1.2 Mechanisms of synaptic plasticity and cognitive loss in aging.....	13
1.3 Age-related changes in the brain extracellular matrix .....	18
1.4 Age-related changes in the brain's tissue stiffness.....	22
1.5 Mechanical properties of plasma neuronal membrane, axonal growth, and dendrites.....	24
1.6 Mechanically-relevant components of the cell.....	26
1.6.1 Actin and spectrin.....	26
1.6.2 Microtubules and neurofilaments.....	28
1.6.3 Extracellular matrix.....	28
1.6.4 Mechanosensitive ion channels .....	30
1.6.4.1 Transient receptor potential channels .....	31
1.6.4.2 Piezo channel family .....	33
1.7 Piezo1 structure.....	33
1.8 The kinetics of Piezo channels.....	36
1.9 Cellular pathways activated by Piezo channels.....	39
1.9.1 HIPPO (YAP/TAZ) pathway.....	39
1.9.2 Mitogen-activated protein (MAP) kinases.....	40
1.9.3 Calpain protease.....	41
1.10 Role of Piezo1 in the CNS immunomodulation.....	42
<b>2 AIMS AND OBJECTIVES</b> .....	<b>45</b>
<b>3 MATERIALS AND METHODS</b> .....	<b>46</b>
3.1 Animals.....	46
3.2 Hippocampal tissue isolation, RNA, and protein purification.....	46
3.3 cDNA synthesis and quantitative real-time PCR.....	46
3.4 SDS-PAGE and western-blot.....	48
3.5 Immunohistochemistry.....	50
3.6 Generation, and characterization of Adeno-associated viruses containing Piezo1 shRNA.....	51
3.7 Primary neural culture preparation.....	52

3.8	Injection of AAV encoding control and Piezo1 shRNA into the dorsal hippocampus.....	52
3.9	Behavioral experiments.....	53
3.9.1	Open field.....	53
3.9.2	Novel object location and recognition tests.....	53
3.10	Preparation of acute hippocampal slices.....	54
3.11	Analysis of synaptic transmission and plasticity.....	54
3.12	Chemical LTP induction.....	56
3.13	Statistical analysis.....	56
3.14	List of chemicals and equipment.....	57
<b>4</b>	<b>RESULTS.....</b>	<b>58</b>
4.1	Increased expression of some mechanosensitive ion channels in the hippocampus of aged mice.....	58
4.2	Expression of Piezo1 channel is increased at the protein level in neurons but not in astrocytes of aged mice.....	62
4.3	YAP/TAZ expression is decreased following Piezo1 knockdown <i>in vitro</i> .....	64
4.4	Piezo1 knockdown changes the expression pattern of ECM molecules and ECM-related enzymes <i>in vitro</i> .....	65
4.5	Aging-mimicking activation of Piezo1 impairs synaptic plasticity in the young hippocampus.....	66
4.6	Piezo1 activation mimics the aged brain and increases the p38 MAPK pathway.....	69
4.7	Piezo1 activation impairs chemical LTP induction in the young hippocampus.....	72
4.8	Piezo1 activation mimics aging in brain and reduces the CaMKII phosphorylation.....	73
4.9	Synaptic plasticity is impaired in the aged mice compared to the young mice.....	74
4.10	Piezo1 knockdown tends to improve the impaired cognitive function in aged mice.....	76
4.11	ECM cleavage downregulates Piezo1 expression <i>in vitro</i> and rescues synaptic plasticity deficits in aged mice <i>ex vivo</i> .....	79
<b>5</b>	<b>Discussion.....</b>	<b>81</b>
5.1	mRNA levels of mechanosensitive ion channels and YAP/TAZ are upregulated in the aged and 5xFAD mice.....	82
5.2	Piezo1 activation mimics the aged brain by increasing p38 MAPK phosphorylation.....	83
5.3	Piezo1 activation dephosphorylates YAP.....	85
5.4	Piezo1 activation mediated calpain-dependent spectrin cleavage.....	85

5.5	Piezo1 activation mimics an aged brain and reduces the CaMKII phosphorylation.....	86
5.6	Piezo1 knockdown tends to improve impaired cognitive function and enhances synaptic plasticity in the aged mice.....	86
5.7	ECM cleavage downregulates Piezo1, 2, and YAP/TAZ expression <i>in vitro</i> and rescues synaptic plasticity deficits in aged mice <i>ex vivo</i> .....	87
5.8	Limitations and outlook.....	87
<b>6</b>	<b>Conclusions.....</b>	<b>89</b>
<b>7</b>	<b>References.....</b>	<b>90</b>

## LIST OF ABBREVIATIONS

AAV	Adeno-associated virus
ACAN	Aggrecan
ACSF	Artificial cerebrospinal fluid
AD	Alzheimer's disease
ADAMTS	A disintegrin and metalloproteinase with thrombospondin motifs
AMPA	$\alpha$ -amino-3-hydroxy-5-methyl-4-isoxazolepropionic acid
APP	Amyloid precursor protein
BCAN	Brevican
BSA	Bovine serum albumin
C4S	Carbon 4 sulfation
C6S	Carbon 6 sulfation
CA1	Cornus ammonis 1
CA2	Cornus ammonis 2
CA3	Cornus ammonis 3
CaMKII	Ca <sup>2+</sup> /Calmodulin-dependent protein kinase
cAMP	Cyclic AMP
chABC	Chondroitinase ABC
CNS	Central nervous system
CREB	cAMP response element-binding protein
CSPGs	Chondroitin sulfate proteoglycans
CTD	C-terminal domains
CTGF	Connective tissue growth factor
CYR61	Cysteine-rich angiogenic inducer 61

DG	Dentate gyrus
DIV	Days <i>in vitro</i>
DMEM	Dulbecco's Modified Eagle's Medium
DZNE	Deutsches Zentrum für Neurodegenerative Erkrankungen e.V.
ECM	Extracellular matrix
EPSPs	Excitatory postsynaptic potentials
ER	Endoplasmic reticulum
fEPSPs	Field excitatory postsynaptic potentials
GABA	Gamma-aminobutyric acid
GAGs	Glycosaminoglycan
GFAP	Glial fibrillary acidic protein
HA	Hyaluronan acid
HAPLN	Hyaluronan and proteoglycan link proteins
IBA1	Allograft Inflammatory Factor 1
IHC	Immunohistochemistry
IL	Interleukin
IL-1 $\beta$	Interleukin 1 beta
LATS1/2	Large tumor suppressor kinase 1 and 2
LPS	Lipopolysaccharides
LTCC	L-type voltage-gated Ca <sup>2+</sup> channels
LTD	Long-term depression
LTP	Long-term potentiation
MST1/2	Mammalian sterile20-like 1 and 2
MAPK	Mitogen-activated protein kinase

MMP	Matrix metalloproteinase
N	Novel objects
NB	Neurobasal medium
NCAM	Neuronal cell adhesion molecule
NCAN	Neurocan
NGS	Normal goat serum
NMDA	N-Methyl-D-aspartate
NO	Nitric oxide
NOLT	Novel object location test
NORT	Novel object recognition test
NSCs	Neural stem cells
PB	Phosphate-buffered
PBS	Phosphate-buffered saline
pCREB	Phosphorylated CREB
PD	Parkinson's disease
PFA	Paraformaldehyde
PGs	Proteoglycans
PNN	Perineuronal nets
PSD	Postsynaptic density protein
PV	Parvalbumin
qPCR	Quantitate polymerase chain reactions
ROS	Reactive oxygen species
RT-PCR	Reverse transcription-polymerase chain reaction
shRNA	Short hairpin RNA

SBDPs	Spectrin breakdown products
TBS	Theta-burst stimulation
TIMP	Tissue inhibitor of metalloproteinase
TNF- $\alpha$	Tumor necrosis factor- $\alpha$
TNR	Tenascin-R
TRP	Transient receptor potential
WFA	<i>Wisteria floribunda</i> agglutinin
YAP	Yes-associated protein

# 1. INTRODUCTION

## 1.1 Central nervous system aging

Aging is defined as a progressive loss of physiological integrity, which causes the function to be compromised and increases mortality risk. In the central nervous system (CNS), aging gives rise to widespread cellular and molecular changes in the brain (Azam et al 2021, Burke & Barnes 2010). At the cellular level, aging is associated with changes in the vascular endothelial structure, neuronal shrinkage and loss, glial senescence, and loss of function of adult stem cell and progenitor cell populations (Sikora et al 2021, Smith et al 1999, White et al 2020, Xu et al 2017). At the molecular level, aging results in genomic instability, transcriptomic changes, telomere shortening, epigenetic alterations, loss of proteostasis, mitochondrial dysfunction, cellular senescence, stem cell exhaustion, and altered intercellular communication (Figure 1.1) (Baidoe-Ansah et al 2022, Gonzalo 2010, Iourov et al 2021, Rizvi et al 2014, Tyrrell et al 2020), all of which correlate with cognitive disability susceptibility.

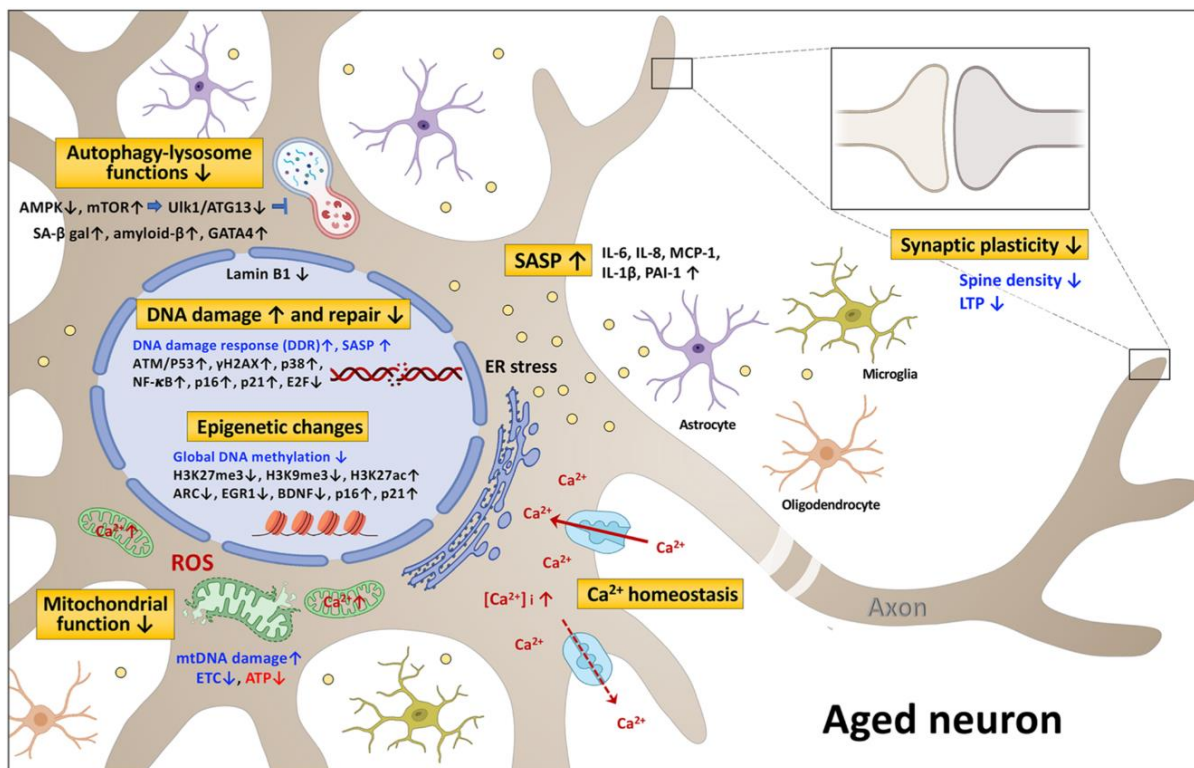


**Figure 1.1 Multiple changes happen at the cellular and molecular level in the aged brain.** The image is adopted from (Chao et al 2021).

Aging is also associated with declines in performance in cognitive tasks in both humans and animals (Baidoe-Ansah et al 2022, Glisky 2007, Kujawski et al 2021). Though there are many listed risk factors for neurodegeneration, aging alone is the primary risk factor for most neurodegenerative diseases, including Alzheimer's disease (AD) and Parkinson's disease (PD)(Guerreiro & Bras 2015, Hindle 2010). AD affects

10% of people over the age of 65, and its prevalence rises with age (Hogan et al 2016, von Strauss et al 1999). Figure 1.1 illustrates the main cellular and sub-cellular signaling pathways impaired in the aged neurons.

## **1.2 Mechanisms of synaptic plasticity and cognitive loss in aging**

The hippocampal formation is an important and well-studied structure of the neurobiological foundations of higher cognitive tasks in both animals and humans. The importance of the hippocampus in cognitive functioning was discovered decades ago when an epileptic patient exhibited signs of memory impairment following a bilateral media temporal lobe removal. His memory loss has been widely interpreted as an inability to transfer transitory, immediate information into stable long-term memory (Squire 2009). The hippocampus's significance in learning and memory is its most well-known function. It is thought that the hippocampus collects and consolidates information, allowing for the creation of long-term memories through synaptic modifications, the most studied form of which is long-term potentiation (LTP). The hippocampus has a simple and well-organized structure which makes it an ideal place to dissect synaptic transmission in the mammalian brain. In the transversal view, the hippocampus is split into four distinct zones labeled CA1, CA2, CA3, and dentate gyrus. The CA1 area is the biggest and is bordered laterally by the presubiculum and medially by the CA2 with 90% glutamatergic projection neurons and 10% inhibitory interneurons. The CA2 layer is limited laterally by the CA1 layer and medially by the CA3 layer and receives inputs from the hypothalamic supramammillary area. The CA3 layer is oriented towards the dentate gyrus hilus and is medially constrained by the CA2 layer. Some refer to the CA3's most superficial cells as CA4. Mossy fibers from the dentate gyrus are sent to the apical dendrites of the CA3 layer. CA3 pyramidal cell axons contribute to the alveus, fimbria, and fornix. The collaterals of the axonal processes originating from the CA3 pyramidal cells are known as Schaffer collaterals which form synapses with dendrites in the *striatum radiatum* of the CA1 region. This pathway is the well-studied pathway for understanding LTP in the hippocampus (Chauhan et al 2021).

The groundbreaking study of Bliss and Lomo in 1973 (Bliss & Lomo 1973) inspired numerous neuroscientists to conduct studies on the characteristics of LTP. Long-term synaptic plasticity has been found in several forms in the mammalian CNS. LTP and long-term depression (LTD) are two primary types of neuronal plasticity. LTP is a long-term and stable activity-dependent facilitation of synaptic transmission that can be induced by different paradigms such as classic high-frequency stimulation (HFS), theta-burst stimulation (TBS), pairing, and spike-timing protocol. Conversely, LTD is a long-term reduction in synaptic potentiation and can be induced by low-frequency stimulation (LFS), pairing, and spike-timing protocols. LTP, along with other kinds of synaptic plasticity, is widely regarded as the most accurate neural model for studying the cellular mechanisms underlying learning and memory storage.

Molecular mechanisms of LTP are now well known and may be simply divided into a few steps including induction, expression, and maintenance. In the basal condition,  $\text{Na}^+$  and  $\text{K}^+$  pass via the  $\alpha$ -amino-3-hydroxy-5-methyl-4-isoxazolepropionic acid (AMPA) receptor channel but not the N-Methyl-D-aspartate (NMDA) receptor channel, because  $\text{Mg}^{2+}$  blocks the NMDA receptor. Postsynaptic membrane depolarization following a strong stimulus removes the  $\text{Mg}^{2+}$  barrier of the NMDA receptor, enabling  $\text{Na}^+$ ,  $\text{K}^+$ , and, most crucially,  $\text{Ca}^{2+}$  to pass through. Postsynaptic  $\text{Ca}^{2+}$  is required and sufficient for the induction of LTP, which initiates the process that leads to postsynaptic signaling molecules activation such as CaMKII and an increase in AMPA receptor transmission. GluA1 and GluA2 knockout mice studies showed a distinct need for these two subunits for LTP. GluA1 is required (Jiang et al 2021a), while GluA2 is not (Meng et al 2003). C-terminal domains (CTD) of GluAs show the largest subunit divergence and they are anchored in the protein matrix of the postsynaptic density. Therefore, these domains act as the substrate for subunit-specific modulation of AMPA receptor trafficking and LTP. CaMKII phosphorylates the GluA1 intracellular CTD, which increases during LTP (Diaz-Alonso & Nicoll 2021). Other phosphorylation sites in the GluA1 CTD mediated by various kinases have been found. Raising intracellular calcium level promotes the phosphorylation of the cAMP-responsive element binding protein (CREB) transcription factor that regulates the transcription of genes with a CRE site in their promoter resulting in the expression of the immediately early genes (IEG) such as *c-Fos* and *Ark* (Hayashi 2022). Studies reported that *c-Fos* deletion impairs learning and memory (Fleischmann et al 2003) and *ARC* knockout impairs spatial and fear memory consolidation (Peebles et al 2010).

In multiple brain areas, including the hippocampus, retrosplenial cortex, prefrontal cortex, and anterior cingulate cortex, aging is associated with impairments or declines in the efficiency of certain components of learning and memory (Ash et al 2016, Liu et al 2018b, Zhou et al 2014).

The hippocampus is especially sensitive to age-related changes. Lots of studies have shown that aging diminishes hippocampus synaptic strength and plasticity, which is associated with memory problems in both elderly animals and aged humans (Burke & Barnes 2010, Li et al 2018, Ojo et al 2015, Wong et al 2021). Previous research with electron microscopy showed that certain synapses may be weaker in older rats with reduced hippocampus-dependent memory (Nicholson et al 2004), while synapse quantity does not indicate cognitive state (Calhoun et al 2008).

At the synaptic level, impaired synaptic strength can be caused by one of three mechanisms: (1) loss of synaptic connections, (2) decreased presynaptic neurotransmitter release, or (3) decreased postsynaptic response to the transmitter. All of these can be determined by electrophysiology approaches like extracellular recordings of field excitatory postsynaptic potentials (fEPSPs) in the hippocampal slices of aged animals. At the cellular level, age-related neuronal loss and impaired neurogenesis have been reported

in several studies (Daynac et al 2016, Mortera & Herculano-Houzel 2012, Takei 2019) that couple to increased intracellular calcium level and impaired calcium hemostasis that is frequently underpinning the pathologies associated with aging and age-related neurodegeneration. Changes in calcium signaling impair the functioning of the ionotropic glutamate receptors, AMPA and NMDA, which are pivotal in LTP induction and expression. AMPA receptors are subject to strict regulatory processes by a range of direct and indirect interacting proteins that control their biosynthesis, membrane trafficking, degradation, and various post-translational modifications due to their critical role in regulating brain function. AMPA receptors may be less functional (silent) rather than reduced in number in aged brains because treatment of positive allosteric modulators of AMPA receptors improved memory and synaptic potentiation deficiencies in aged rats (Bloss et al 2008).

In many animals, the NMDA receptor's binding densities and functions are compromised with age (Magnusson et al 2010). Functional NMDA receptors are heterotetramers consisting of two essential GluN1 subunits and two optional GluN2 or GluN3 subunits. In the CNS, four distinct GluN2 subunits (GluN2A-D) are produced differently, both developmentally and temporally. Each GluN2 subunit provides unique ion channel characteristics and intracellular trafficking mechanisms on NMDA receptors. GluN2B and GluN2D are significantly expressed throughout development and decline after birth, but GluN2A and GluN2C rise and remain even in maturity (Paoletti et al 2013). Meanwhile, there is a change in the distribution of certain NMDA receptor subunits throughout aging, with GluN2B-containing NMDA receptors diffusing laterally to extra-synaptic dendritic spine locations (Avila et al 2017). Synaptic NMDA receptors activate positive regulators of synaptic plasticity pathways like the ERK-Jacob-CREB pathway (Mulholland et al 2008). Synaptic NMDA receptors activity causes ERK1/2 activation and subsequent binding and phosphorylation of Jacobs (a synapto-nuclear protein encoded by the NSMF gene) at Ser180, which is required for Jacob to depart from the synapse (Grochowska et al 2021). Calpain I protease is also activated by the synaptic activity of NMDA receptors that cleaves internexin and Jacob protein. This may lead to the production of a soluble  $\alpha$ -internexin fragment and its interaction with pJacob and pERK to protect them from dephosphorylation. The presence of pJacob in the nucleus is associated with increased CREB phosphorylation and increased synthesis of genes involved in plasticity. Upon the activation of extrasynaptic NMDA receptors, ERK is not activated, and therefore Jacob is not phosphorylated before nuclear translocation. This leads to CREB shut-off which invokes proapoptotic proteins and suppression of synaptic plasticity and survival pathways (Karpova et al 2013).

In the presynaptic perspective, aged hippocampus and cortex have shown a considerable increase in bouton size and synaptophysin-positive terminals (Grillo et al 2013, Shimada et al 2003), indicating that aging may

inhibit glutamate release and cause presynaptic compartments and synaptic structure to enlarge as a compensatory mechanism.

Calcium ions enter neurons via ionotropic glutamate receptors and voltage-dependent  $\text{Ca}^{2+}$  channels, where they regulate a variety of cellular processes such as synaptic strength regulation and  $\text{Ca}^{2+}$ -mediated cell death. Calcium causes synaptic vesicle exocytosis at the presynapse which can regulate short-term synaptic plasticity, whereas, in the postsynaptic dendrites,  $\text{Ca}^{2+}$  modulates multiple signaling cascades involved in long-term synaptic plasticity and gene transcription.

Dysregulated  $\text{Ca}^{2+}$  homeostasis has become a prevalent underlying mechanism of neuronal death and has been linked to several age-dependent conditions like neurodegenerative disease (Delekate et al 2014, Kuchibhotla et al 2009). A few mechanisms have been proposed following elevated intracellular calcium leading to impaired neuronal function and phenotype such as poor mitochondrial and ER  $\text{Ca}^{2+}$  handling, increased expression of voltage-gated  $\text{Ca}^{2+}$  channels, decreased activation of  $\text{Ca}^{2+}$  binding proteins such as CAMKII, and  $\text{Ca}^{2+}$ -dependent gene expression, e.g. of brain-derived neurotrophic factor (BDNF) (Jung et al 2020).

A well-know mechanism is mediated by the declined mitochondria calcium buffering capacity which is vital to proper cellular function. Studies in different models have revealed that neuronal potential is decreased due to mitochondrial  $\text{Ca}^{2+}$  uptake impairment and elevation of intracellular  $\text{Ca}^{2+}$  in an age-dependent manner (Pandya et al 2015). The triggering of cell death by  $\text{Ca}^{2+}$  overload requires the opening of the mitochondrial permeability transition pore (mPTP), followed by cytochrome c release and subsequent apoptosis activation. Cytochrome c released into the cytoplasm induces apoptotic cascades by binding to the IP3-R on the ER, desensitizing its autoinhibition by calcium and inducing additional calcium release from ER reserves.

The principal mediators of depolarization-induced calcium entry into neurons are voltage-gated calcium channels. Early findings suggested that in some types of neurons, such as the principal cells in the hippocampal CA1 region, there is an increased  $\text{Ca}^{2+}$  influx mediated by increased VOCC activity in aged neurons especially L-type calcium channel (LTCC) which leads to enhanced calcium current and afterhyperpolarization (AHP) mainly mediated by calcium-dependent potassium currents. The AHP that occurs after an action potential (AP) is commonly regarded as an inhibitory mechanism that regulates neuronal activity by boosting firing frequency adaptation and AP burst termination (Faber & Sah 2007). Interestingly, chemical inhibition of LTCC is effective in reversing age-related learning impairments, increasing the basal firing rate of CA1 neurons, and increasing the intrinsic excitability of CA1 neurons by lowering post-burst AHP (Oh et al 2010).

As mentioned above, in normal conditions, postsynaptic calcium entry leads to the activation of CaMKII, one of the most abundant proteins in neurons and a key regulator of LTP induction with a high localization in the postsynaptic density. CaMKII activity was considerably diminished in the aged hippocampal neurons (Bodhinathan et al 2010). In addition to its main role in the phosphorylation of elements in LTP induction, CaMKII responds to  $Ca^{2+}$  influx to promote activity-dependent transcription of several important genes such as BDNF by phosphorylating CREB and inducing expression of BDNF. A decline in BDNF expression coincides with hippocampal volume shrinkage and impaired cognitive performance which has been reported previously in the aged brain (Erickson et al 2010).

In addition to neurons, glial cell functions are modified and undergo significant changes during aging. In fact, glial cells are the first cells in the CNS to respond to stress conditions in aging (Palmer & Ousman 2018). In physiological conditions, they support neurons physically and metabolically, including neuronal insulation and communication, as well as nutrition and waste removal. Glial cells, which are mostly composed of microglia, astrocytes, and oligodendrocyte lineage cells, make up a significant portion of the mammalian brain. Astrocytes interact with neurons actively and dynamically, reacting to neurotransmitters and regulating neuronal and synaptic activity by releasing gliotransmitters. Astrocyte function is mainly dependent on calcium signaling, and therefore, understanding the intricacies of calcium dynamics within astrocytes is crucial for unraveling their roles in processes such as synaptic transmission and neuroprotection.

RNA sequencing was used to determine the transcriptional patterns of astrocytes in several brain areas of adult and elderly mice. It was found that aged astrocytes exhibit a partly reactive state, with increased expression of the complement system and neuroinflammatory genes in all brain areas (Boisvert et al 2018). In humans, a meta-analysis of transcriptome data found that aged astrocytes in the human prefrontal cortex showed a reactive behavior (Payan-Gomez et al 2018). However, brain astroglial networks are critical for neuronal homeostasis, hippocampal development, and spatial cognition (Hosli et al 2022). Structural and functional changes in astrocytes including, the decreased volume fraction of process, compromised  $K^+$  and glutamate uptake and impaired calcium oscillation result in affected synaptic plasticity in aged animals (Popov et al 2021, Verkhratsky 2019).

Microglia are resident immune cells in the brain that not only perform immunological responsibilities but also play crucial roles in maintaining homeostatic activities in a healthy brain. They are involved in regulating neuronal activity throughout development, controlling synapse formation, maturation, and elimination (Andoh & Koyama 2021, Cangalaya et al 2020, Stevens et al 2007). In the hippocampus, they influence neurogenesis and synaptic plasticity (Cornell et al 2022, Diaz-Aparicio et al 2020, Sierra et al 2010). These glial cells are increasingly being linked to age-related pathological conditions like Parkinson's

and Alzheimer's disease (Ferreira & Romero-Ramos 2018, Hemonnot et al 2019). Like astrocytes, microglia in the aged brain go through transcriptional changes (Godbout et al 2005) with less migratory properties and continuously produce pro-inflammatory signaling molecules, indicating compromised homeostatic function. In the physiological conditions, IL-1 $\beta$  secreted by microglia supports LTP induction and maintenance (Avital et al 2003, Schneider et al 1998), while in proinflammatory conditions like aging, it plays a role as a negative regulator of LTP in the synapse (Prieto et al 2019). Interestingly, IL-1 $\beta$  serves in a synapse-specific manner on the hippocampal synaptic plasticity (Hoshino et al 2017).

### **1.3 Age-related changes in the brain extracellular matrix**

The extracellular matrix (ECM), which is found in tissues and organs, is a dynamic three-dimensional structure of macromolecules that includes proteoglycans, collagens, fibronectin, laminins, fibrillins, and several other glycoproteins (Dityatev & Rusakov 2011, Lockhart et al 2011). ECM is uniquely structured in a tissue-specific type. The ECM of the neural tissue is distinct in its composition and can be divided into three different categories: The basement membrane, neural interstitial matrix, and perineuronal net (PNN). The basement membrane covers the cerebral vasculature. Generally, in the brain, the ECM contains less collagen than other connective tissues, and the collagens are primarily restricted to the cerebral vasculature and meninges in the basal lamina. PNN mostly surrounds inhibitory neuronal cell bodies and has a significant influence on synaptic input and the physiology of fast-spiking inhibitory neurons for producing synchronized activity in local networks. Finally, there is the neural interstitial matrix that is dispersed throughout the parenchyma and occupies the space between neurons and glial cells (Lau et al 2013) (Figure 1.2).

In addition to the structural support, the neural ECM has a variety of physiological functions during development (e.g., controlling the closure of critical periods in brain regions) and in the mature brain (e.g., determining synaptic plasticity and stability, cognitive flexibility, and context discrimination)(Dityatev & Rusakov 2011, Dityatev et al 2021). Recent research indicates that the content and integrity of the ECM are dynamic and change significantly, which influences the function of the tissue in aging, epilepsy, neurodegeneration, dementia, depression, bipolar disorder, and schizophrenia (Berretta 2012, Blanco & Conant 2021, Dityatev 2010, Morawski et al 2014, Vegh et al 2014b).

Brain ECM occupies the space between neurons and glial cells and this extracellular space volume accounts for approximately 20% of the total volume of the adult brain (Bonneh-Barkay & Wiley 2009). Secreted ECM molecules produced by both neurons and glial cells aggregate in the extracellular space. ECM composition and density may vary within the tissue in a region-specific manner to produce unique conditions for diverse physiological functions (Hobohm et al 1998). Cell attachment to the ECM during development is influenced by ECM receptors like discoidin domain receptors, integrins, and syndecans,

which are present in varying amounts across the tissue and affect cell proliferation, migration, and differentiation.

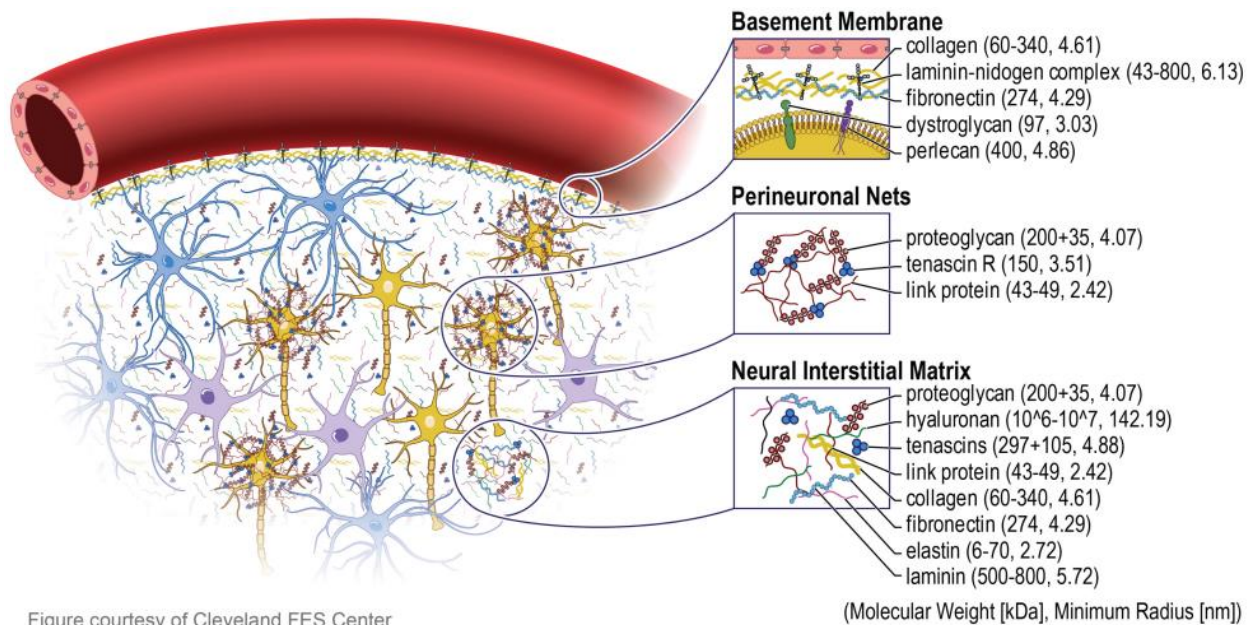
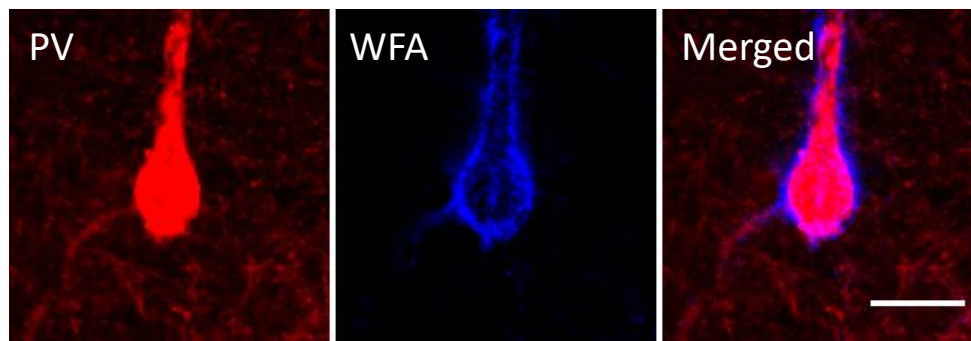


Figure courtesy of Cleveland FES Center

**Figure 1.2** Various components of the brain extracellular matrix form three distinct structures, basement membrane, perineuronal net, and interstitial matrix. The scheme is adopted from (Kim et al 2018).

PNN is a specialized form of the ECM in the CNS that is condensed with heterogeneous glycosaminoglycan-rich ECM and mainly surrounds parvalbumin (PV)-expressing, fast-spiking GABAergic interneurons in several brain regions (Figure 1.3). The time of maturation of PNNs coincides with the closure of critical periods in many brain regions (El-Tabbal et al 2021, Pizzorusso et al 2002).



**Figure 1.3** WFA-labeled of a PV+ inhibitory neuron in the mouse hippocampus.

The primary components of the neuronal ECM in the adult brain are a family of chondroitin sulfate proteoglycans (CSPGs) known as lecticans and their binding partners, the glycoprotein tenascin-R (TNR) and the glycosaminoglycan hyaluronic acid as the backbone of the ECM (Dityatev et al 2014). Together,

they cross-linked by extensive interactions with TNFR. Transmembrane hyaluronan synthase enzyme which synthesizes hyaluronan links these chains to the cell membrane surface (Siiskonen et al 2015).

According to the proposed tetrapartite model of the synapse, the ECM in addition to the other three classical components of synapses - including the presynaptic button, postsynaptic spine, and the astroglial processes - is involved in the stabilization and maintenance of synapses (Dityatev et al 2006, Dityatev & Rusakov 2011).

Synapses are connected with a range of membrane-bound molecules that interact with the adjacent ECM. The integrin family as the main ECM receptors make a link between the ECM from outside the cell and the neuronal cytoskeleton inside the cell and ultimately modulate synaptic structure (Shi & Ethell 2006). The ECM can regulate synaptic function both pre- and postsynaptically. For instance, at the presynaptic level, the role of laminins, heterotrimeric proteins of the ECM, has been reported in the regulation of vesicle release machinery at synapses in the adult brain (Hunter et al 2019). A well-studied example of the postsynaptic modulation by ECM is through the ECM receptor integrin. Activation of postsynaptic beta1 integrins by extracellular matrix ligands such as fibronectin results in the activation of subsets of kinase involved in synaptic plasticity and ultimately phosphorylation of GluN2A and GluN2B subunits of NMDA receptors, while integrin inhibition by antibody reverses the effect (Bernard-Trifilo et al 2005). Furthermore, the ratio of excitatory to inhibitory synapses is altered in quadruple knockout mice lacking the ECM components tenascin-C, tenascin-R, neurocan, and brevican, demonstrating the role of the ECM in regulating the neural network activity (Gottschling et al 2019).

Using proteomic analysis in the hippocampus of young and aged mice, Vegh and colleagues demonstrated that a small group of proteins showed the most substantial age-dependent shift in synaptic protein levels, all of which were gradually up-regulated with age. Three of these four proteins are ECM proteins (neurocan, brevican, and HAPLN1) and their upregulation was correlated with hippocampus-dependent spatial learning in a Barnes maze test (Vegh et al 2014b) (Figure 1.4).

Sulfation patterns of the chondroitin sulfate-glycosaminoglycans (GAGs) determine their charge structure, binding affinities, and biological roles. Changes in the pattern have been seen during development and persist through maturity and aging when carbon 6 sulfation (C6S) decreases gradually (Foscarin et al 2017). While C6S has been found to promote axonal development and regeneration and is required for neuroplasticity (Lin et al 2011, Yang et al 2021), carbon 4 sulfation (C4S), on the other hand, is regarded to be the most inhibitory type of CS for axonal development and guidance (Wang et al 2008). When C6S is overexpressed, PNN development in the visual cortex is significantly impeded, and mice become more plastic (Miyata et al 2012).

Interestingly, ECM removal either by ECM-degrading enzyme hyaluronidase or Chondroitinase ABC (ChABC), which is a bacterial enzyme that digests the chondroitin sulfate glycosaminoglycans of ECM can improve neuronal connectivity *in vitro*, and cognitive impairments *in vivo*, demonstrating that ECM build-up does indeed generate a restrictive environment for both structural and functional plasticity. The effects of ECM removal on cognitive function and synaptic plasticity in different parts of the brain have been well-documented (Senkov et al 2014). ChABC-mediated ECM removal in the amygdala promoted the extinction of fear conditioning and drug-seeking behavior in mice (Gogolla et al 2009, Xue et al 2014). In the hippocampus, ECM digestion resulted in impaired CA1 LTP and contextual fear conditioning memory in APP/PS1 mice (Vegh et al 2014a). However, in normal adult mice, ECM is required for LTP induction as it has been shown that ECM removal via ChABC leads to increased SK channel activity, decreased neuronal excitability, and impaired LTP in CA1, which can be rescued by the application of apamin, an SK channel inhibitor in hippocampal slices (Dembitskaya et al 2021). Hyaluronidase-mediated ECM removal also showed similar results with a decrease in contextual fear conditioning and impaired LTCC-dependent LTP in the CA1 (Kochlamazashvili et al 2010a).

In a study with a quadruple knockout mouse deficient in the ECM molecules tenascin-C, tenascin-R, neurocan, and brevican, Gottschling and colleagues showed an increase in the excitatory synapses, a decrease of inhibitory synapses, higher neuronal network activity *in vitro*, and a reduction of PNNs *in vivo* followed by alterations in the gene expression profile in the hippocampus of this quadruple knockout mouse (Gottschling et al 2019). In a previous study, brevican knockout mice showed an increased LTP in the CA1 region but no change in shuttle box cognitive function was seen (Brakebusch et al 2002). Moreover, in the auditory cortex, learning causes transitory overexpression of brevican which is required during long-term memory consolidation (Niekisch et al 2019). Enzymatic digestion of the ECM in mature neural cultures increased neuronal activity but prevented the disinhibition-induced hyperexcitability seen in age-matched control cultures with intact ECM. Furthermore, ECM degradation followed by disinhibition had a considerable effect on network interaction, resembling the pattern found in naive growing cultures (Bikbaev et al 2015). In an *in vivo* study, ECM removal by ChABC reduced striatal PNNs and diffusive ECM in a 22-month treated mouse with increased motor learning in the accelerating rotarod test (Richard et al 2018). ECM also plays a fundamental role in cognitive flexibility as ECM removal *in vivo* results in enhanced reversal learning of frequency-modulate discrimination in the auditory cortex of Mongolian gerbils (Happel et al 2014).

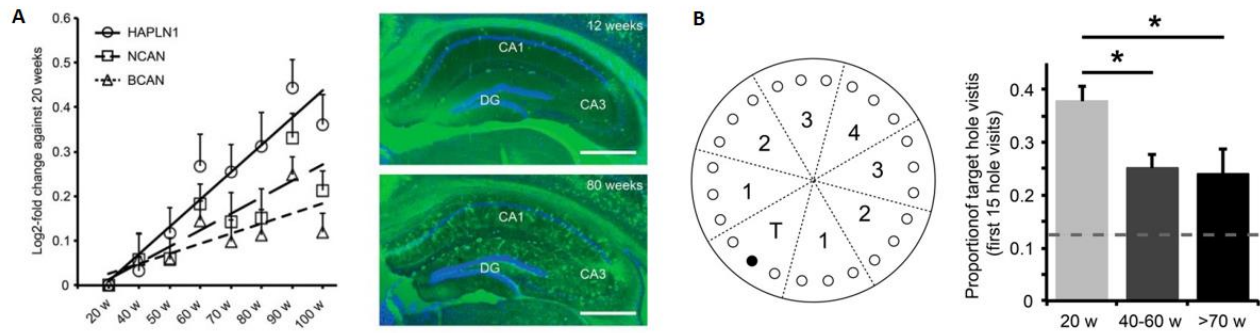


**Figure 1.4 Age-dependent accumulation of ECM and impaired spatial memory.** (A) Age-dependent changes of some ECM components and PNN upregulation in the mouse hippocampus. (B) Performance in the Barnes maze spatial task is impaired in the elderly animal. The panels are adopted from (Vegh et al 2014b).

Numerous pathophysiological features of schizophrenia, including impaired connectivity and neuronal migration, synaptic anomalies, and altered GABAergic, glutamatergic, and dopaminergic neurotransmission, may be attributed to ECM abnormalities (Berretta 2012, Matuszko et al 2017). Following social defeat and stress (depression), a similar association was also identified in rats. In this case, an overlap between hippocampus time-dependent cognitive impairment and ECM imbalance was seen (Koskinen et al 2020).

### 1.4 Age-related changes in the brain's tissue stiffness

Normal brain tissue cells reside in a polysaccharide-rich environment. Its composition affects the characteristics of the brain's biomechanical properties like stiffness. The GAG/collagen ratio is around 10:1, resulting in very low stiffness of the brain (Akhmanova et al 2015). Changes in the microstructure of the extracellular matrix and tissue stiffness following pathological conditions influence cell responses, especially astrocytes as multifunctional cells responding to mechanical and inflammatory stimuli (Johnson et al 2015). In such situations, astrocytes are converted from a dormant to a reactive state in which glial fibrillary acidic protein (GFAP) and vimentin are frequently upregulated (Liddelow & Barres 2017, O'Leary et al 2020). Therefore, modifications in the brain's ECM stiffness may have an impact on the growth and neurophysiology of brain cells (Murphy et al 2016, Ryu et al 2021).

Cells can modify their force generation in response to the local stiffness when grown on 2D substrates or in 3D microenvironments (Doss et al 2020, Langhans 2018). Various heterogeneous components like cells, vessels, ECM, and interstitial fluid can determine the biomechanical characteristics of the brain such as stiffness (Franze et al 2013). According to the definition, stiffness is the degree of a material's resistance to deformation under the application of force (Baumgart 2000). *In vitro* studies have shown that some properties of the cells, like proliferation, differentiation, and migration of neural stem cells, progenitor cells, and mature neurons can be regulated depending on the stiffness of the surrounding environment (Arulmoli

et al 2015, Kapr et al 2021). In physiological conditions, the adult brain seems to be 3–4 times stiffer than the child brain in humans (Chatelin et al 2012). In line with this observation, the prefrontal cortex progressively stiffens with age in the rat brain (Segel et al 2019) (Figure 1.5). Ryu and colleagues also observed that the stiffness of hippocampus tissue increased from the neonatal to the early adult stage in all subregions of the hippocampus (Ryu et al 2021). They also discovered that CS-56 immunoreactivity, which detects the unique oligosaccharide structure of CSPGs, including both C6-sulfation and C4-sulfation, decreased with maturation. ECM digestion with ChABC enzyme enhanced tissue stiffness in neonatal hippocampus slices, demonstrating that the ECM plays a role in tissue stiffness (Ryu et al 2021).

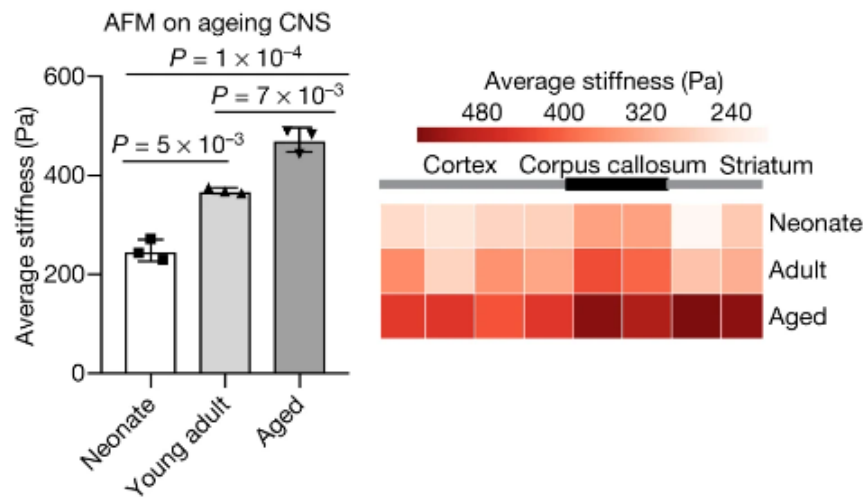


**Figure 1.5 Age-dependent changes in tissue stiffness in different parts of the rodent’s brain.** The image is adopted from (Segel et al 2019).

In Alzheimer’s disease,  $A\beta$  plaque deposits are associated with increased brain stiffness (Velasco-Estevez et al 2018). Since the structure of amyloid plaques is extremely hard and brittle, it affects the surface morphology of the brain tissue and makes it rougher.

Brain stiffness at different ages can be determined precisely by atomic force microscopy (AFM) indentation measurements. AFM is a high-resolution, non-optical imaging type of microscopy first illustrated by Binnig, Quate, and Gerber in 1985 (Binnig et al 1986), which uses piezoelectric elements that allow precise control of the movement with nanometer precision (Figure 1.6). Local material qualities such as adhesion and stiffness may be studied in addition to topographic high-resolution information by measuring tip-sample interaction forces. Though it is an invasive approach for determining stiffness due to the necessity for the tissue slices, it is routinely being used to characterize the biomechanical properties of the cells and tissue *in vitro* and *ex vivo*.

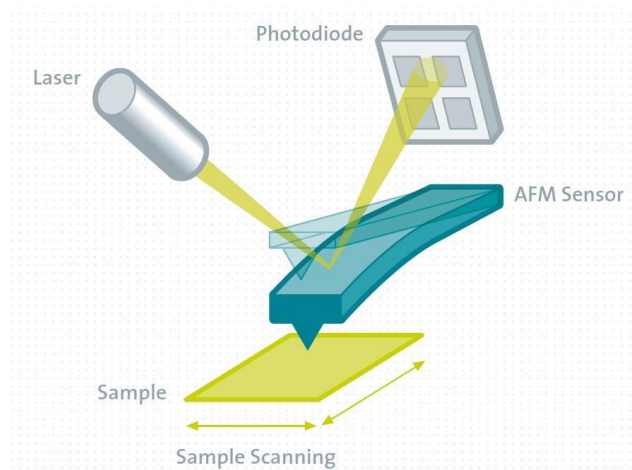


**Figure 1.6 Simple schematic view of the main components of an AFM.** The image is adopted from <https://raman.oxinst.de/>

### 1.5 Mechanical properties of plasma neuronal membrane, axonal growth, and dendrites

A multitude of physical, mechanical, and chemical factors, including stored curvature elastic stress (lateral pressure), the bulk lipid phase, lipid rafts, and membrane viscoelasticity, may be used to characterize lipid bilayer properties. Plasma membranes are dynamic, undergoing structural changes across a wide range of time and length scales, from nanoscopic (nanosecond and nanometer) to microscopic and mesoscopic (microsecond and millimeter). Plasma membranes react to force as nonlinear functions of strain, indicating that they are viscoelastic or non-Newtonian fluids (Crawford & Earnshaw 1987, Tyler 2012). In response to a variety of intracellular and intercellular stresses, the membrane is constantly deformed inward and outward, and the deformation is described by their compression ( $K_C$ ), area expansion ( $K_A$ ), and bending ( $K_B$ ) moduli (Figure 1.7).

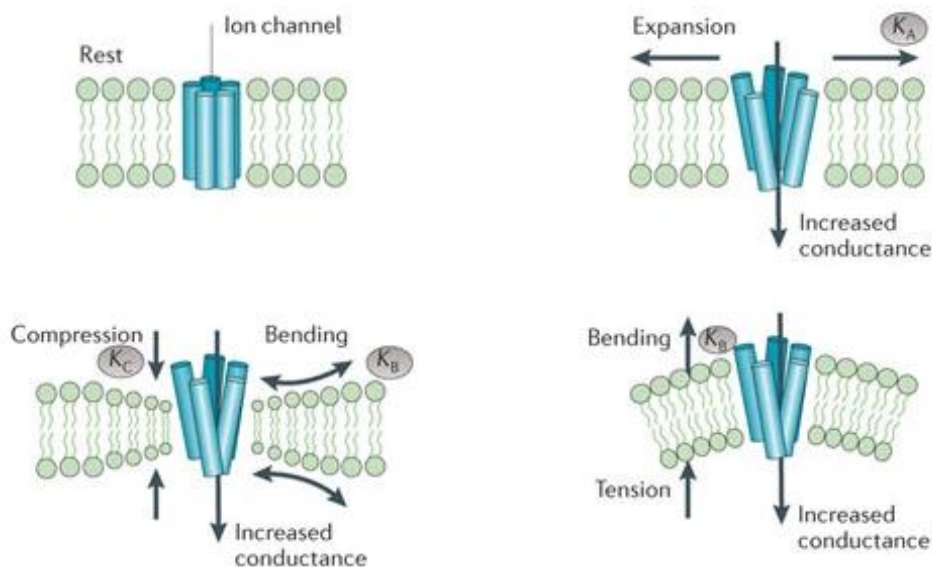


**Figure 1.7 A schematic view of how the conformational shape of the ion channel can alter as a result of membrane expansion, compression, bending, and tension, modulating the ion channel's opening and membrane conductance.** The image is adopted from (Tyler 2012).

The force-from-lipids theory of cellular mechanosensation was first inspired by a patch-clamp study of an E-coli membrane under mechanical forces (Martinac et al 1987) and proposed that ion channel gating reacts directly to changes in the physical state of the membrane, such as lateral tension. In the neuronal membrane case, changes in membrane formation lead to millisecond-scale neuronal activity.

The remarkable sensitivity of the neuronal plasma membrane to bending deformation supports its flexibility to exocytose and recapture vesicles, as well as respond to protrusive and repulsive pressures experienced during growth and motility (Hui et al 2009, Steinkuhler et al 2019). Neuronal membranes' innate viscoelastic characteristics are further regulated by cytoskeletal components, which create structural tension within a cell (Tyler 2012).

In recent years, there has been a focus on the mechanical components related to neuronal development and maturation, with particular emphasis on their role in processes such as axon growth and guidance. During neural development, neurons send out axons to reach their postsynaptic partner. Axons often follow very precise paths and use various guidance cues to navigate in the nervous system, and how they manage to find their way so accurately remains an area of intense research.

Growth cone motility and axonal pathfinding involve a precise spatial and temporal remodeling of growth cone architecture resulting in mechanotransduction and motility. The role of mechanics in facilitating outgrowth cones was first proposed three decades ago by Tim Mitchison and Marc Kirschner as the “clutch hypothesis” (Jay 2000, Mitchison & Kirschner 1988). Based on this model, ECM-adhesion molecules interaction would drive to the acto-myosin cytoskeleton via a clutch protein, which ultimately generates a mechanical force to promote motility.

While spine formation and structural plasticity have been extensively studied for decades, many areas still require further clarification. Components in synapse formation and plasticity including cytoskeleton, molecular motors, cell-adhesion molecules, and the extracellular matrix can be either force-generating or force-bearing, therefore dendritic spine formation can be viewed as a mechanical phenomenon. The BAR-domain superfamily proteins, which deform membranes into tubular structures, mediate a membrane-bended remodeling to form proto-protrusions that eventually create the dendritic filopodia. Figure 1.8 illustrates the mechanically relevant component of spine formation.

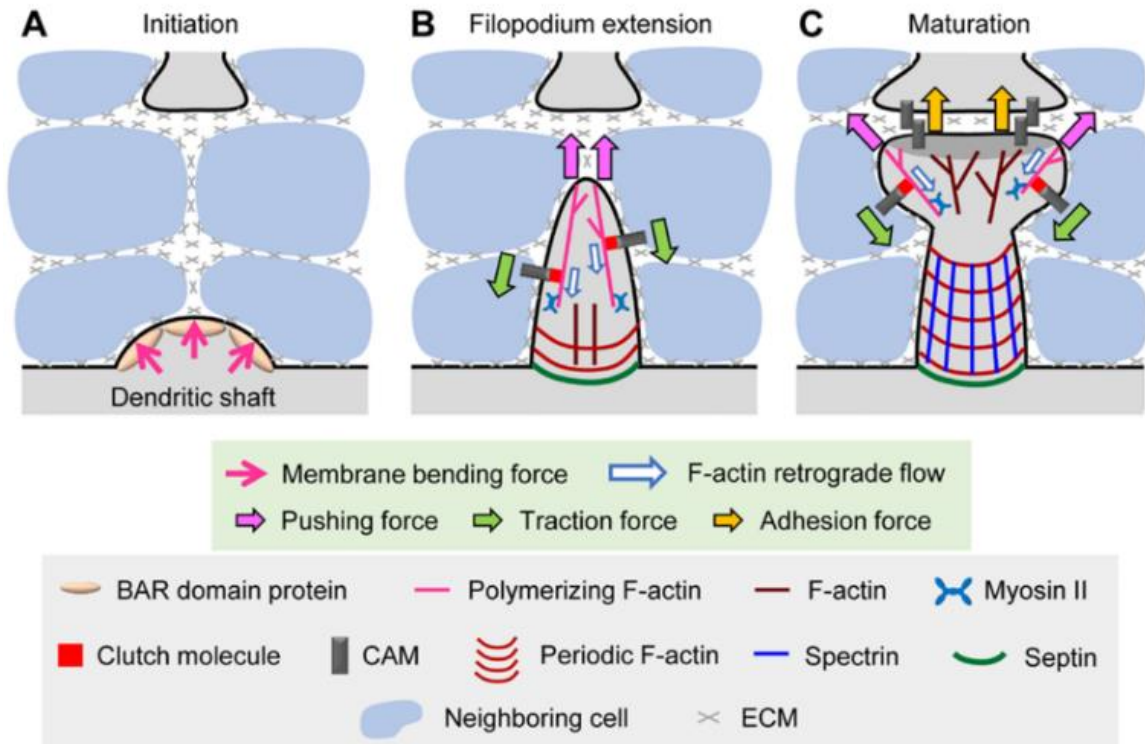


**Figure 1.8 Mechanically-relevant components of spine formation and maturation.** The scheme is adopted from (Minegishi et al 2022).

## 1.6 Mechanically relevant components of the cell

### 1.6.1 Actin and Spectrin

Cells' mechanical and functional qualities are heavily reliant on their cytoskeleton, which is made up of networks of biopolymers such as microtubules, actin, and intermediate filaments. Dendritic spines are tiny protrusions that accept input from mostly a single excitatory presynaptic terminal, enabling synapse-by-synapse control of synaptic strength. There are 1–10 spines per micrometer of dendrite length (Sorra & Harris 2000), and some neurons, such as hippocampal neurons, have thousands of spines in their dendritic arbors. There is strong evidence that structural changes in dendritic spines, driven by the remodeling of the actin cytoskeleton—a versatile and ubiquitous cytoskeletal protein—play a major role in shaping the structure and function of neurons. These changes are responsible for consolidating memories following learning. That is why medications that inhibit actin polymerization inhibit LTP (Fukazawa et al 2003). Kenneth Holmes, Wolfgang Kabsch, and colleagues discovered the three-dimensional structures of individual actin molecules and actin filaments in 1990. Actin globular monomer (G-actin) is a globular protein of 375 amino acids (43 kD). Monomers have tight binding sites that facilitate head-to-tail contacts with two other actin monomers, allowing actin monomers to polymerize to create filamentous actin (F-actin). Various actin structures are connected with distinct mechanical loads that are tailored to the

structure's unique cellular activities. Mechanical forces result in changes in the shape of filaments as well as how they interact with Actin-Binding Proteins (ABP) (Figure 1.9).

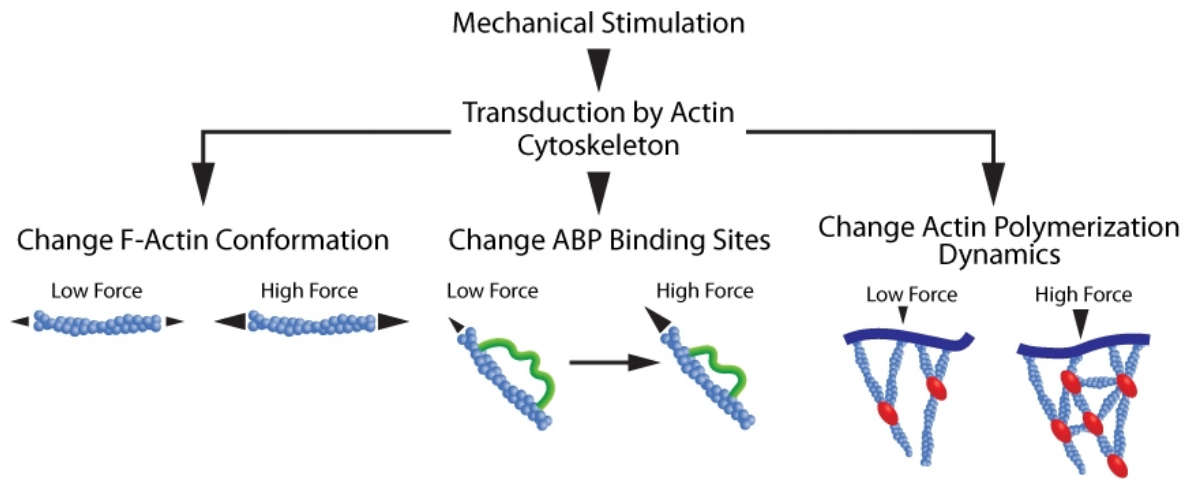


**Figure 1.9 Mechanical forces are translated by the actin cytoskeleton conformational changes and polymerization and actin binding-protein site changes.** The image is adopted from <https://www.cytoskeleton.com/>

Mechanically-induced changes in F-actin length and its binding partners result in the formation of stabilized F-actin, facilitating the more efficient development of stress fibers. This represents a crucial aspect of a cell's mechanotransduction processes (Tojkander et al 2012). Actin can also interact with adhesion family members, such as E-cadherin, N-cadherin, and P-cadherin, to make a mechanotransduction complex (Leckband & de Rooij 2014).

Spectrin is a big, cytoskeletal, heterodimeric protein made up of modular and subunits. Spectrin repeats are 106 consecutive amino acid sequence motifs that are frequently found in the spectrin proteins. This structural protein is well recognized as a membrane skeletal protein that is essential for cell shape maintenance and mechanical support of the plasma membrane (Deng et al 2020). The spectrin family contains  $\alpha$  and  $\beta$  spectrin II, also known as brain spectrin. The subunits normally form heterotetramers within the membrane skeleton by generating antiparallel heterodimers that interact head-to-head to create a tetramer. Spectrin binds the actin cytoskeleton to cell membranes via interacting with transmembrane proteins such as ankyrin (Czogalla & Sikorski 2005). Evidence revealed by stochastic optical reconstruction microscopy (STORM) showed that actin has a periodicity of between 180 and 190 nanometers, formed ring-like structures that wrapped around the circumference of axons, and was equally spaced along axonal shafts. Actin rings and the actin-capping protein adducin colocalized with spectrin, and the space between their neighboring rings was about the same as the length of a spectrin tetramer (Xu et al 2013).

### **1.6.2 Microtubules and neurofilaments**

Microtubules are critical structural elements in biological systems, and their mechanical qualities are required for a wide range of cellular operations such as cell shape, division, motility, intracellular transport, and the formation of various cellular morphologies. Their structure, which makes them the stiffest intracellular cytoskeletal filaments, provides the foundation for their mechanical robustness. Microtubules are made up of a cylindrical shell of tubulin protein. This tubulin is found in two forms: alpha and beta tubulin, which form a tight dimeric complex. The cylindrical tubule is then formed by stacking them side by side.

Mechanical stimuli influence microtubule formation and proliferation as well. For instance, passive stretching of the heart muscle has been found to have a direct impact on microtubule formation. Tubulin mRNA and protein levels were shown to be elevated in this case in response to passive stretching of newborn cardiac myocytes (Watson et al 1996). In somatosensory neurons, microtubule acetylation by  $\alpha$ -tubulin acetylase (dTAT) modulates mechanosensation in a wide and specific manner (Yan et al 2018).

Though many studies have concentrated on reconstituted networks of filamentous actin, which dominate the mechanics of many cells' cytoskeleton, intermediate filaments also play an essential role in the mechanics of the cytoskeleton. In fact, they form the most important network in several cell types. In contrast to other tissue-specific classes of intermediate filaments (IFs), neurofilaments (NFs) are heteropolymers made up of four subunits, each of which has a different domain structure and function. These subunits are NF-L (neurofilament light), NF-M (neurofilament middle), NF-H (neurofilament heavy), and -internexin or peripherin (Yuan et al 2017). In adult axons, type IV intermediate filaments known as neurofilaments are the most prevalent cytoskeletal component, outnumbering both microtubules and actin (Wong et al 1995).

### **1.6.3 Extracellular matrix**

Living cells are exposed to mechanical stimuli all the time, whether originating from the surrounding ECM or neighboring cells. Mechanical properties of the ECM, including composition, stiffness, and topography have been shown to impact the function (Dowell-Mesfin et al 2004) and mechanical properties of the surrounding cells (Young et al 2016).

Integrin clusters as the adhesion receptor and principle receptor for the ECM, detecting extracellular changes in stiffness, tension, or other mechanical cues. Upon interaction with the ECM via the extracellular domain, they are activated and these morphological alterations or redistribution recruit focal adhesion kinase (FAK) via cytoplasmic tail linked to the actin cytoskeleton, and a variety of docking proteins such as talin rod, vinculin, and paxillin to create the focal adhesion inner site (Figure 1.10).

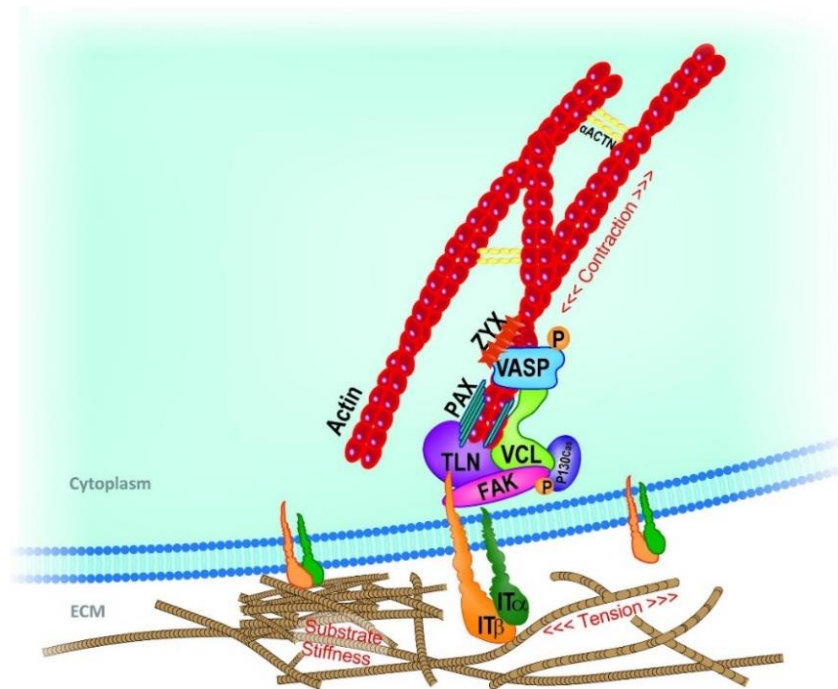


**Figure 1.10 Key mechanosensing players engaged in cell-ECM interaction at the focal adhesion site.** The scheme is adopted from (Martino et al 2018).

On 2D substrates from *in vitro* studies, it has been known that many cell types may respond to the elastic characteristics of the underlying surface, which can regulate several biological processes, including cell motility, cell proliferation, and differentiation (Blaschke et al 2020, Nichol et al 2019). In line with this, studies on 3D structures revealed that the ECM is a biopolymer network, made up of a variety of biomolecules and has a highly nonlinear mechanical response (Storm et al 2005) which is extremely relevant to cell-ECM interactions (Hall et al 2016, van Helvert & Friedl 2016). Biopolymers that form networks within the cytoskeleton such as F-actin, vimentin, fibrin, or extracellular matrix, exhibit distinctive physicochemical behavior that is not found in synthetic soft materials utilized as cell substrates or scaffolds for tissue engineering (Wen & Janmey 2013). Purified biogels made by native molecules show similar behavior and are force stiffening, with an elastic modulus that can raise the stress equivalent to cell and tissue deformation *in vivo*. Theoretically, depending on filament stiffness, different models have been proposed to explain this behavior (Wen & Janmey 2013). The force-dependent properties of several cytoskeletal components and synthetic ECM polymers are shown in Figure 1.11.

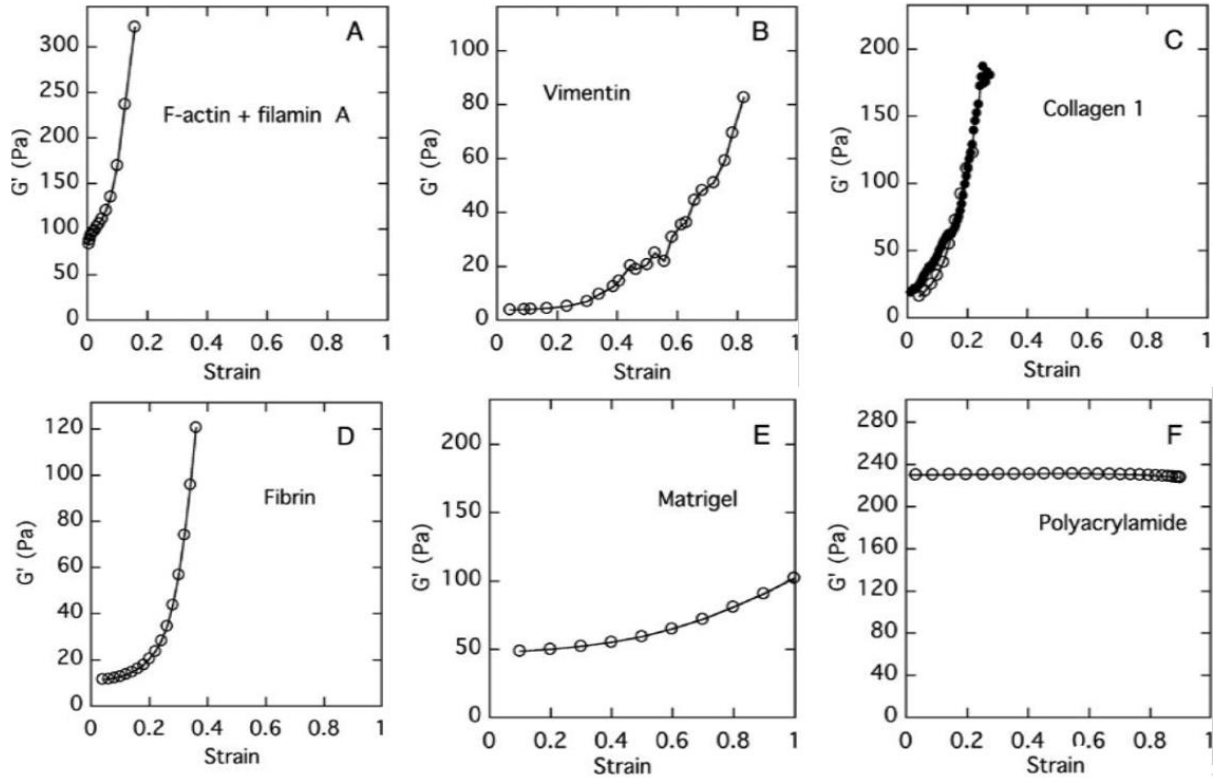


**Figure 1.11** Non-linear response to different strain magnitudes for cytoskeletal component F-actin, vimentin, collagen 1, and fibrin and linear response in synthetic polymers matrigel and polyacrylamide. The panel is modified from (Wen & Janmey 2013).

### 1.6.4 Mechanosensitive ion channels

Mechanotransduction, the process by which mechanical inputs are translated into electrochemical signals, is required for several biological processes such as neuronal cell formation, pain sensation, and red blood cell volume regulation (Cahalan et al 2015, Chighizola et al 2019, Lewin & Moshourab 2004).

Mechanosensitive channels, mechanosensitive ion channels, and stretch-gated ion channels are a subset of proteins that translate mechanical signals into biochemical responses. A broad range of mechanosensitive channels (MSCs) in the CNS and PNS can be activated by mechanical cues such as pressure, tension, stretch, and shear stress. In the CNS, the extending bulk of evidence shows that neurons and glial cells can respond to the direct mechanical forces in the microenvironment by regulating the expression of mechanosensitive ion channels (Johnson et al 2021, Ma et al 2022a). In the mammalian CNS, among ion channels with mechanosensation activity, two families have been categorized well: Transient receptor potential (TRP) and the Piezo family.

### 1.6.4.1 Transient receptor potential channels

TRPs are versatile signaling molecules found in a variety of tissues and cell types. The majority of TRPs are polymodal channels, or coincidence detectors, that respond to both physical (temperature, voltage, pressure, and tension) and chemical stimuli (Startek et al 2019, Zheng 2013). Some TRPs act as non-selective cation channels in the plasma membrane, whereas others control  $\text{Ca}^{2+}$  release in intracellular organelles (Zhang et al 2018).

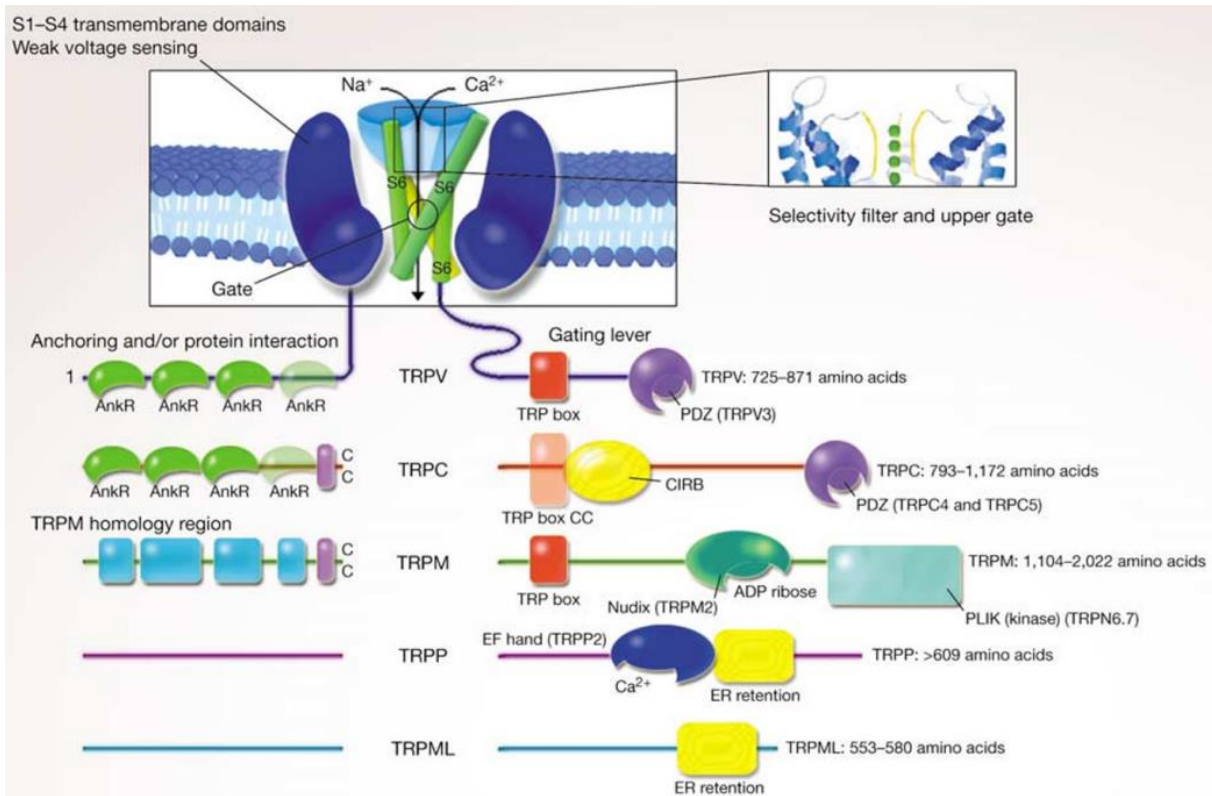


**Figure 1.12 Schematic view of the structure and distinct domains of each TRP member in the cell membrane.** The scheme is adopted from (Clapham 2003).

The proteins of the TRP family form tetrameric non-selective cation channels. TRP channels depolarize the membrane potential when activated and allow cations to enter the intracellular compartment, depolarizing the plasma membrane and potentially modulating voltage-gated ion channels (Gees et al 2010, Wu et al 2010). According to the published data, it is well known that some subfamilies of TRP channel members including TRP canonical (TRPC), TRP melastatin (TRPM), and TRP vanilloid (TRPV), are highly expressed in the brain with distinct physiological functions (Figure 1.12) (Held & Toth 2021, Kougioumoutzakakis et al 2020, Menigoz & Boudes 2011). They modulate widespread physiological function, including developmental and homeostatic functions in both neuronal and glial cells (Echeverry et al 2016, Guo et al 2022, Verkhatsky et al 2014). Table 1.1 describes some of the TRP ion channels that are potentially involved in mechanotransduction in the PNS and CNS.

**Table 1.1** TRP mechanosensitive ion channels expressed in the brain

Channel	Cell type	Ref
TRPV1	Retinal ganglion cell neurons	(Sappington et al 2015)
	Microglia	(Marrone et al 2017)
	Astrocyte	(Yang et al 2019)
TRPV2	Sensory neurons	(Katanosaka et al 2018)
	Astrocyte	(Shibasaka et al 2013)
TRPV4	Astrocytes	(Kim et al 2015)
	Microglia	(Redmon et al 2021)
	DRG neurons	(White et al 2016)
TRPC1	Sensory neurons	(Alessandri-Haber et al 2009)
	Pyramidal neuron	(Martinez-Galan et al 2018)
TRPC3	Sensory neurons	(Quick et al 2012)
	Astrocyte	(Hoffmann et al 2010)
TRPC4	Pyramidal neuron	(Arboit et al 2020)
	DRG neurons	(Wu et al 2008)
TRPC5	Pyramidal neuron	(Arboit et al 2020)
TRPA1	Sensory neurons	(Zappia et al 2017)
	Astrocyte	(Shigetomi et al 2011)
TRPM3	Oligodendrocyte	(Hoffmann et al 2010)
TRPM7	Sensory neurons	(Low et al 2011)

Recent research indicates that disruption of TRP channel functioning is implicated in a variety of pathological events associated with neurological and mental illnesses, including neurodegenerative disease, autism, epilepsy, and stroke (Griesi-Oliveira et al 2015, Takada et al 2013, Zhang et al 2014, Zhou & Roper 2014).

### 1.6.4.2 Piezo channel family

Piezo channels are prototypical mechanosensitive ion channels that are directly gated by mechanical forces leading to the opening of a non-selective cationic pore (Figure 1.13) (Coste et al 2010, Syeda 2021).

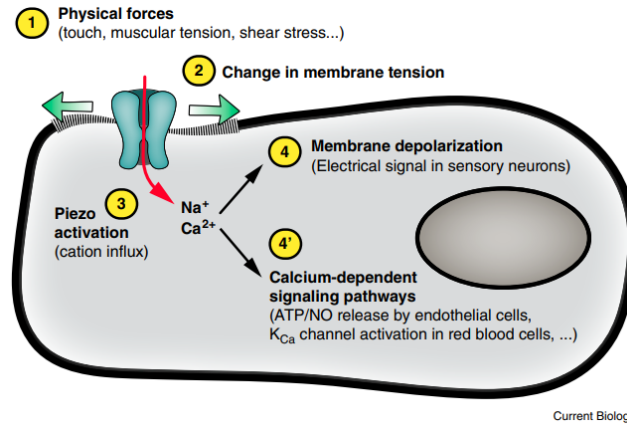


**Figure 1.13. Piezo-dependent mechanosensation.** The image is adopted from (Parpaite & Coste 2017).

The discovery of the Piezo ion channel gene family in 2010 (Coste et al 2010) has been considered the most significant breakthrough in the mechanobiology field, which led to a Nobel Prize in Physiology or Medicine in 2021 awarded to Ardem Patapoutian (jointly with David Julius). Diverse mechanical stimuli in different cell types can generate a response from Piezo channels such as shear stress, compression, membrane tension, cell swelling, and ultrasounds (Cox et al 2016, Jiang et al 2021b, Passini et al 2021, Qiu et al 2019).

Despite some small variations, the fast activation and inactivation features of these channels are mostly comparable across many cell types (Lewis & Grandl 2020). Piezo1 and Piezo2 expression is found in a wide range of tissues and organs, including the CNS, PNS, and capillaries (Coste et al 2010, Harraz et al 2022, Nakamichi et al 2022, Wang et al 2019). Therefore, Piezo proteins have been connected to a variety of physiological functions in animals, including touch, proprioception, blood-pressure sensing, immunity, stem cell differentiation, and cognitive function (Assaraf et al 2020, Chi et al 2022, Harraz et al 2022, Jantti et al 2022, Pathak et al 2014, Wang et al 2019).

### 1.7 Piezo1 structure

Piezo1 ion channels are evolutionarily conserved and functionally diverse mechanosensitive cation channels in which global knockouts of Piezo1 and Piezo2 in mice are lethal (Li et al 2014). Piezo1 and related Piezo2 are uncommonly large size proteins with approximately 2500 amino acids long. They are multipass transmembrane proteins that are bioinformatically predicted to have 30–40 transmembrane (TM) domains (Figure 1.14).

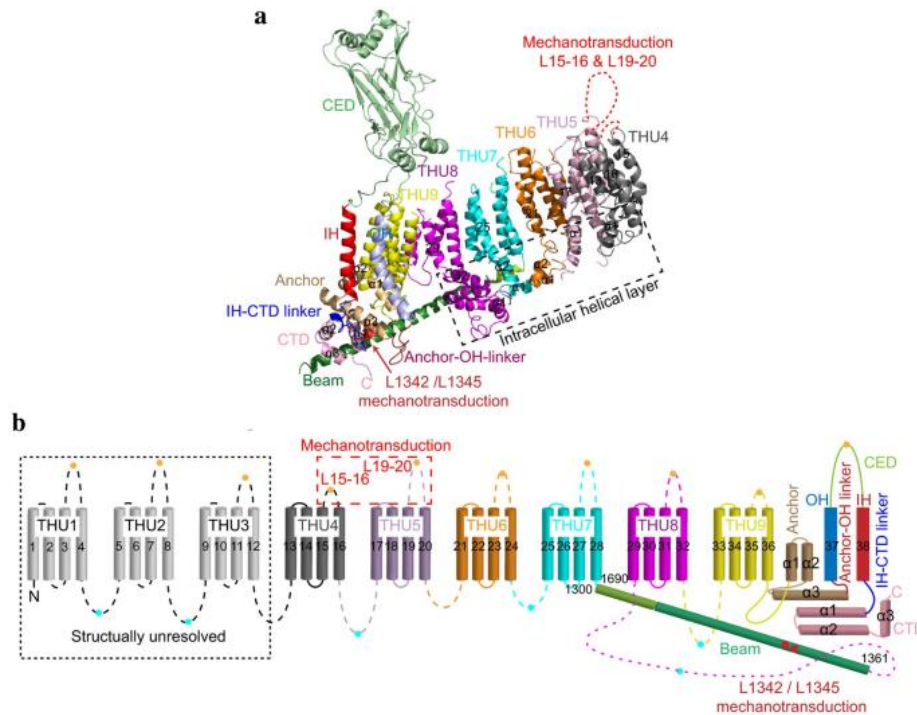


**Figure 1.14 Piezo1 predicted structure** (A) Model illustrating the cylindrical helices of Piezo1 with individual domains. (B) Topology model of the full-length mPiezo1 protein with 38 transmembrane domains. The image is adopted from (Zhao et al 2018).

Using a single-particle approach and cryo-electron microscopy, Ge and colleagues could map the trimeric structure of mouse Piezo1 with three blades and a central cap permeable to monovalent and most divalent ions (Ge et al 2015). High-resolution structure of mouse Piezo1, revealing a distinct 38-TM topology in each subunit (Zhao et al 2018). The two TM sections (TM37 and TM38) closest to the protein's core are known as the inner helix (IH) and outer helix (OH), respectively, and enclose the central pore module's transmembrane pore. The remaining 36 TM regions (TM1-36) create a curved blade-like structure with nine repeated folds, each comprising four TM regions, which are referred to as transmembrane helical units (THUs).

The C-terminal extracellular domain of Piezo1 protein consists of the residues 2210-2457, which are considered the central cap of the channel following the last transmembrane region of the protein. These residues form a trimeric complex of the central cap (Figure 1.15). The region-specific deletion in these residues would result in a mutant (mPiezo1 $\Delta$ 2218-2453) with negative staining in electron microscopy. The structure of the cap is consistent with a potential permeation pathway. It has been shown that Piezo1 inactivation kinetics and mechanical gating are dependent on small subdomains within the cap (Lewis & Grandl 2020). By sequence alignment analysis, six cap subdomains have been identified with a special secondary structure that accounts for the distinct inactivation kinetics of Piezo channels (Lewis & Grandl 2020).

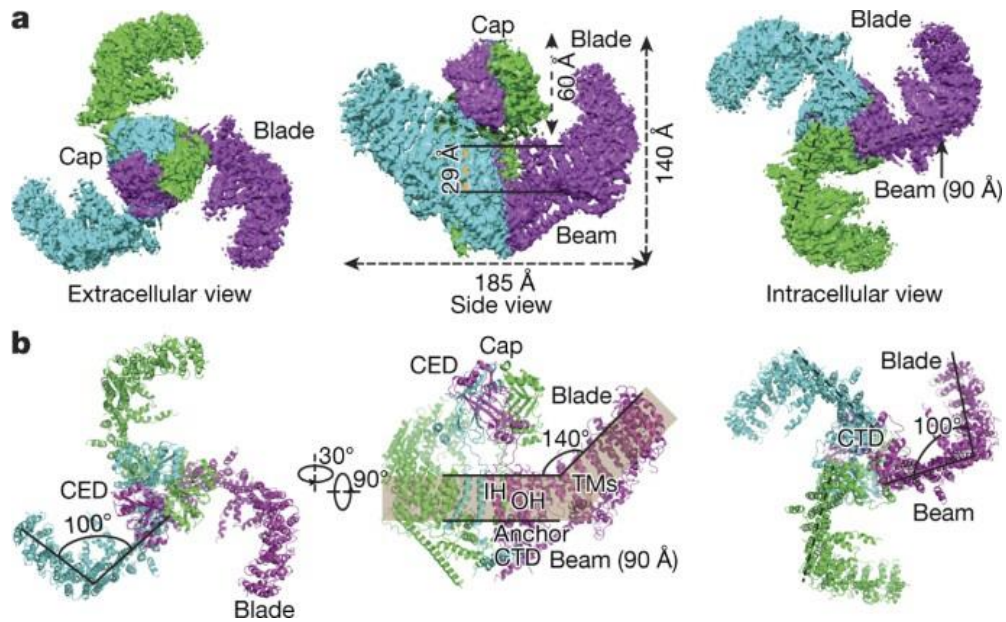


**Figure 1.15 Structure of Piezo1.** (A) High-resolution illustration of extracellular, side, and intracellular views showing different components of the Piezo1 structure. (B) color-coded Piezo1 subunits. The image is adopted from (Zhao et al 2018).

A hairpin structure, referred to as the anchor, connects the transmembrane domains 37 and 38 (inner and outer helix) to the C-terminal domain. This anchor domain of Piezo1 could be mapped to residues around 2100 to 2190, a region with highly evolutionarily conserved sequence motifs (Ge et al 2015). A disease in humans, dehydrated hereditary stomatocytosis, is a result of a mutation in this region, which supports the functionally important role of anchor in Piezo structure (Andolfo et al 2013).

Three beamlike structures generate the intracellular surface which contains the residue 1300-1362 of the Piezo protein. The length of the beams is 90 nm and organized at a 30° angle relative to the membrane plane (Wang & Xiao 2018). The absence of mutant protein coming from the deletion of this region showed the functional importance of this region in the protein structure (Ge et al 2015). The organization of the beams provides a distinct structure for mechanical gating from the distal transmembrane helical units to the central ion-conducting pore (Zhao et al 2018).

In the Piezo protein structure, each of the 24 peripheral subunits of TM helices are arranged into 12 parallel pairs, spreading to generate a highly curved pattern of blades from the core outer helices-inner helices pair to the periphery. When seen from a line parallel to the plasma membrane plane, the proximal TM25-TM36 and peripheral TM13-24 interact at a 100° angle and a 140° angle, respectively (Figure 1.15). Both mechanosensation and the induction of local membrane curvature seem to benefit from this distinct structural property. It's interesting to note that the membrane plane, in which the peripheral TM13–24 looks to be very curved, suggests that the Piezo1 channel can bend the membrane in which it is located. This is

in line with other research suggesting that the mechanical-forced unfolding, tension, and curvature of cellular membranes can control Piezo1 ion channel function.

Six transmembrane helices are arranged triangularly in the Piezo1 channel's membrane-based core. At the innermost position, three IHs appear to line a central pore and are most likely extensions of the C termini of the CEDs. The three IHs are further enclosed by three OHs that are extended from the CEDs' N termini. The IH-OH pairs, CEDs, and CTDs found in this middle area most likely make up the pore module of Piezo1 (Ge et al 2015).

### **1.8 The kinetics of Piezo channels**

Both vertebrates and invertebrates have piezo ion channels, which are biological mechanical sensors that are activated by a variety of mechanical stimuli. Three stages—open, closed, and inactivated—can be used to describe the normal Piezo channel kinetics; together, these states have become a key mechanism for Piezo channel function (Bae et al 2015). According to previous studies, the Piezo1 channel directly responds to lateral membrane tension in cells (Lewis & Grandl 2015).

Cryo-EM structure of the mouse Piezo1 proposed a membrane dome mechanism to explain the activation mechanisms of Piezo channels. Membrane tension will modify gating energetics quantitatively in proportion to the change in the anticipated area beneath the dome. In the context of a tiny, cation-selective pore, this process can account for extraordinarily sensitive mechanical gating (Guo & MacKinnon 2017). Heterologous expression of Piezo channels in HEK cells has provided detailed information on their kinetics; notably, these channels don't need cofactors or accessory subunits (Coste et al 2010). The transfected cells can be stimulated repeatedly in a cell-attached, outside-in patch, and whole cell configurations (Figure 1.16). Piezo currents have unique kinetic characteristics, such as fast activation and voltage-dependent inactivation (Wu et al 2017b), that set them apart from endogenous currents. In addition, compared to Piezo2 channel inactivation, Piezo1 channel inactivation is slower.

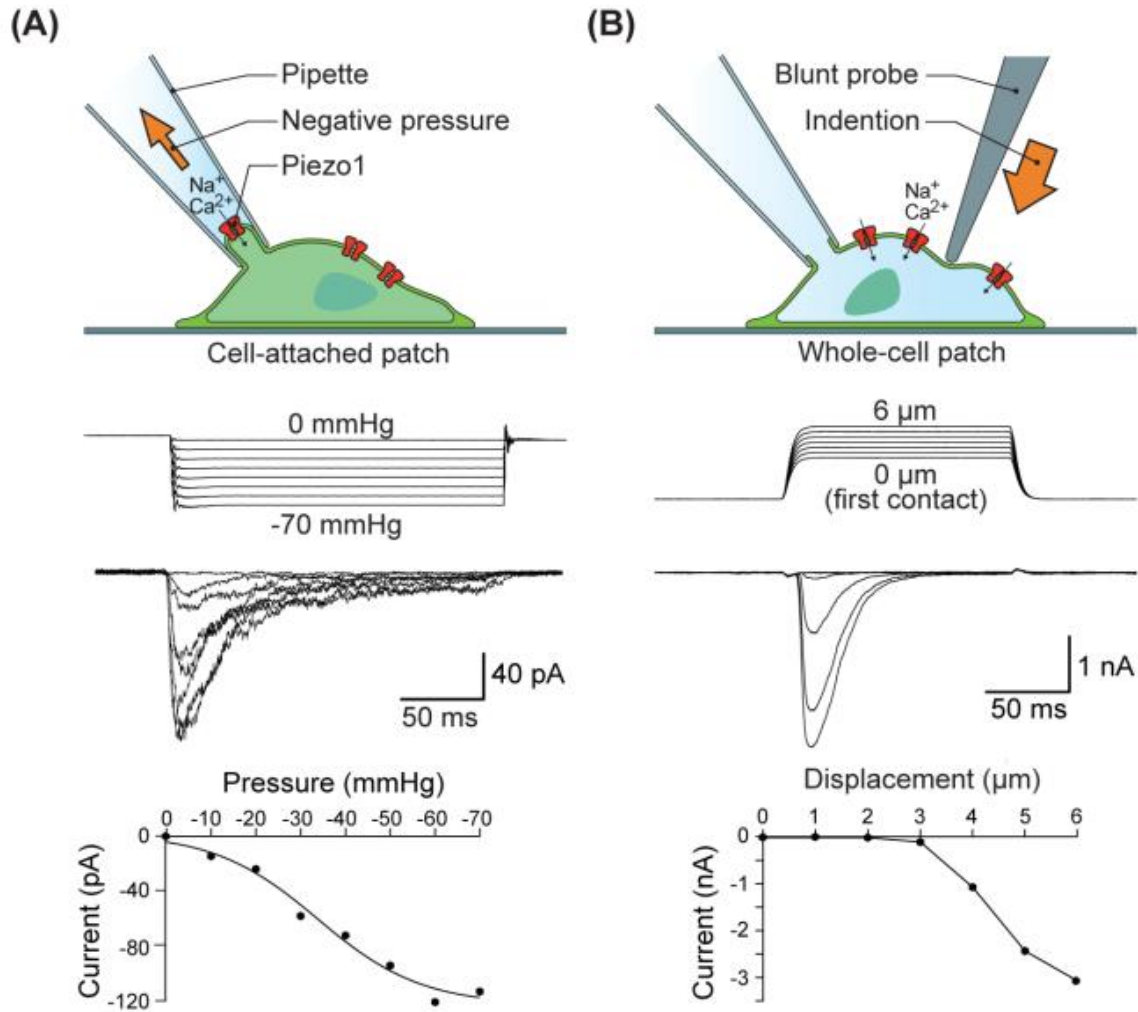


**Figure 1.16 Piezo1 can be studied in different configurations of patch-clamp recording.** (A) “stretch” setup with cell-attached configuration. (B) “poke” setup with whole-cell recording configuration. The text and image are modified from (Wu et al 2017a).

There have been reports of several point mutations in Piezo channels slowing the inactivation process, which results in greater cation fluxes and causes several human disorders. In red blood cells, Piezo1-mediated  $\text{Ca}^{2+}$  influx promotes  $\text{K}^+$  efflux through the Gardos channel (KCa3.1), leading to water loss and RBC dehydration (Cahalan et al 2015).

Recent years have seen advancements regarding Piezo1 small-molecule modulators. Yoda1 and Jedi1/2 are two Piezo1 chemical activators that can open Piezo1 ion channels in the absence of mechanical stimulation. Using a cell-based fluorescence assay, Syeda and colleagues screened around 3.25 million compounds and discovered a synthetic small molecule we named Yoda1 (Figure 1.17) that functions as an agonist for the Piezo1 (Syeda et al 2015). Yoda1 influences the sensitivity and the inactivation kinetics of mechanically generated responses. Yoda1 has been studied in artificial droplet lipid bilayers and it was discovered that

in the absence of other biological elements, Yoda1 can activate purified Piezo1 channels. Their research shows that Piezo1 can be chemically activated and suggests that endogenous Piezo1 agonists may exist. Yoda1 become a crucial research tool for examining Piezo1 regulation and operation (Syeda et al 2015).

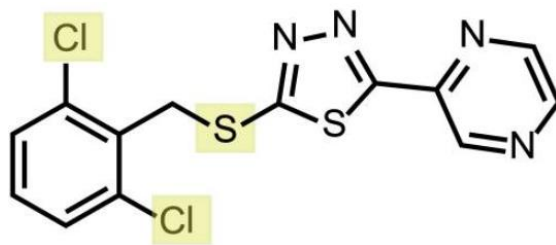


**Figure 1.17 Chemical structure of Yoda1 with chlorines and thioether as the functional groups.** The image is adopted from (Syeda et al 2015).

Jedi1/2, a novel hydrophilic Piezo1 chemical activator, gates the core ion-conducting pore by acting through the periphery blades and using a periphery lever-like device made up of the blades and a beam (Wang et al 2018b).

Gadolinium and ruthenium red have also been demonstrated to block mouse Piezo1 channels as non-specific inhibitors of the ion pore in stretch-activated ion channels (Caldwell et al 1998). It was discovered that GsMTx4, a toxin inhibitor of mechanosensitive channels, also inhibited the Piezo1 channel (Bae et al 2011). Dooku 1 reversibly inhibits the activity of Yoda1 with the IC<sub>50</sub>=1.5 M. It has no impact on constitutive Piezo1 channel activity, but it suppresses Yoda1-induced Piezo1 activation in endothelial cells and Yoda1-induced Ca<sup>2+</sup> entry *in vitro* (Evans et al 2018). Figure 1.18 illustrates potential activators and inhibitors of the Piezo1 channel used in different studies.

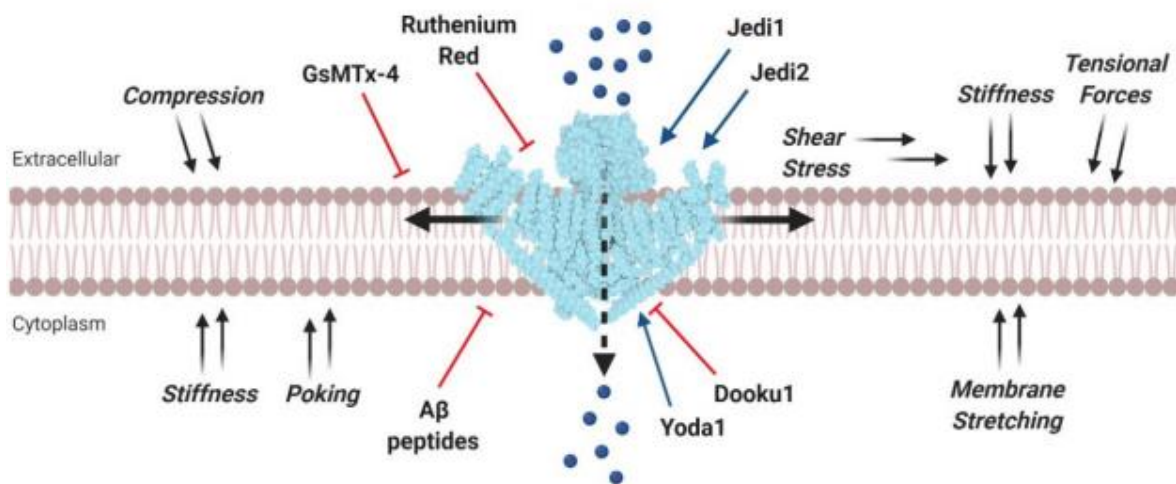


**Figure 1.18 Schematic view of some activators and inhibitors of the Piezo1 channel and their places of action.** The image is adopted from (De Felice & Alaimo 2020).

## 1.9 Cellular pathways activated by Piezo channels

### 1.9.1 HIPPO (YAP/TAZ) pathway

Mechanotransduction molecular control remains unclear. One of the well-studied and key pathways in mechanosensing is the HIPPO pathway. The Hippo signaling pathway is the most recent addition to the family of signaling pathways known to be involved in controlling organ size and development (Pan, 2010; Halder and Johnson, 2011). The Hippo pathway is a serine/threonine kinase signaling cascade that was discovered first through a genetic screen for cell size control in *Drosophila melanogaster* (Harvey et al., 2003; Wu et al., 2003). The Hippo pathway's activity is reliant on cell-cell junctions, cell polarity, cellular architecture, cellular metabolism, and mechanical inputs from the surrounding microenvironment (Figure 1.19). The alternative name of the HIPPO pathway is Yes-associated protein 1 (YAP/TAZ) pathway because of the two key components involved in this pathway.

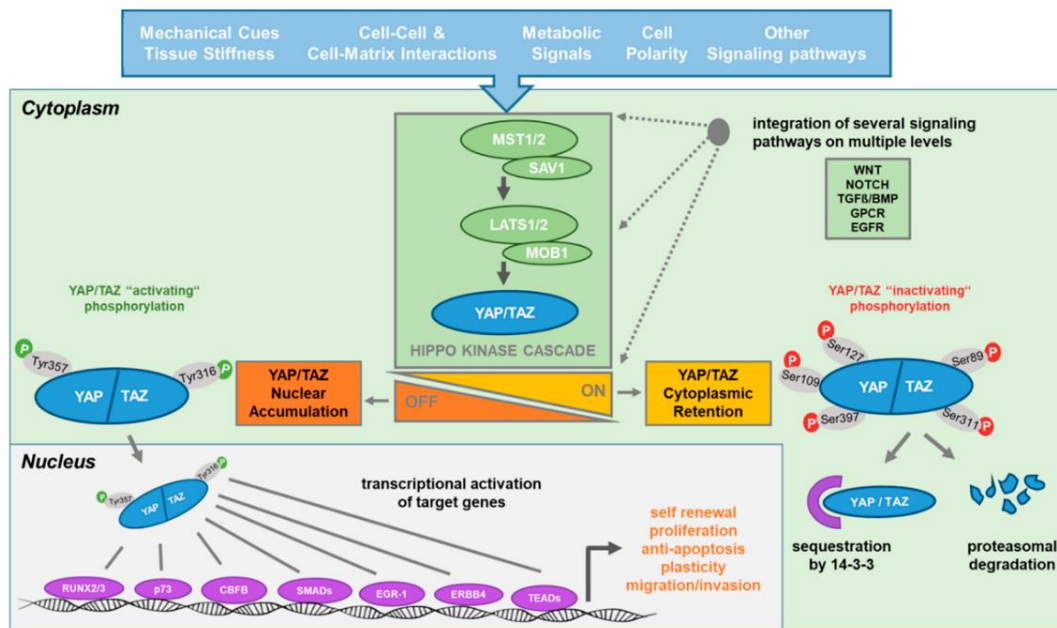


**Figure 1.19 Schematic view of the main component and related stimulator of the YAP/TAZ pathway.** The image is adopted from (Kovar et al 2020).

In mammals, the primary Hippo pathway signaling cascade consists of a serine/threonine kinase cascade composed of mammalian sterile20-like 1 and 2 (MST1/2) and large tumor suppressor kinase 1 and 2 (LATS1/2). MST1/2 interacts with Salvador homolog-1 (SAV1) and phosphorylates LATS1/2, which are activated and phosphorylate YAP on five and TAZ on four conserved serine residues. These YAP and TAZ inhibitory phosphorylation provide a signal for cytoplasmic retention and YAP/TAZ binding to 14-3-3 protein or YAP/TAZ destruction. MST1/2 and LATS1/2 activity indicate that the Hippo pathway is ON, whilst YAP/TAZ are inactive. Indeed, in the presence of different cellular stimuli including mechanical

cues and tissue stiffness, cell-cell and cell-matrix interaction LATS1/2 is not able to phosphorylate YAP/TAZ anymore and drives nuclear translocation and recruitment of YAP/TAZ as a transcriptional co-activator to a target site to regulate expression of genes involved in cellular homeostasis with a certain transcription factor, most importantly, the TEA domain family (TEAD) of transcription factors (Heng et al 2021).

Piezo1-dependent YAP expression has been studied recently. In osteoblastic cells, Piezo1 regulates the YAP-dependent production of type II and IX collagens, which is required for influencing osteoclast differentiation in response to mechanical stresses. The findings point to Piezo1 as the primary skeletal mechanosensor that regulates bone homeostasis (Wang et al 2020).

Furthermore, in recent studies, abnormal Piezo1 expression has been linked to a poor prognosis in some forms of cancer coupled with the YAP/TAZ pathway (Hasegawa et al 2021, Xiong et al 2022, Zhu et al 2021).

### 1.9.2 Mitogen-activated protein (MAP) kinases

MAP kinases are a diverse family of protein-serine/threonine kinases that engage in signal transduction pathways governing intracellular processes in response to extracellular responses. Three sequentially active protein kinases are essential components of the network that can be activated by distinct extracellular inputs and result in the activation of a specific MAPK after the activation of a MAPK kinase kinase (MAPKKK) and a MAPK kinase (MAPKK) (Figure 1.20).

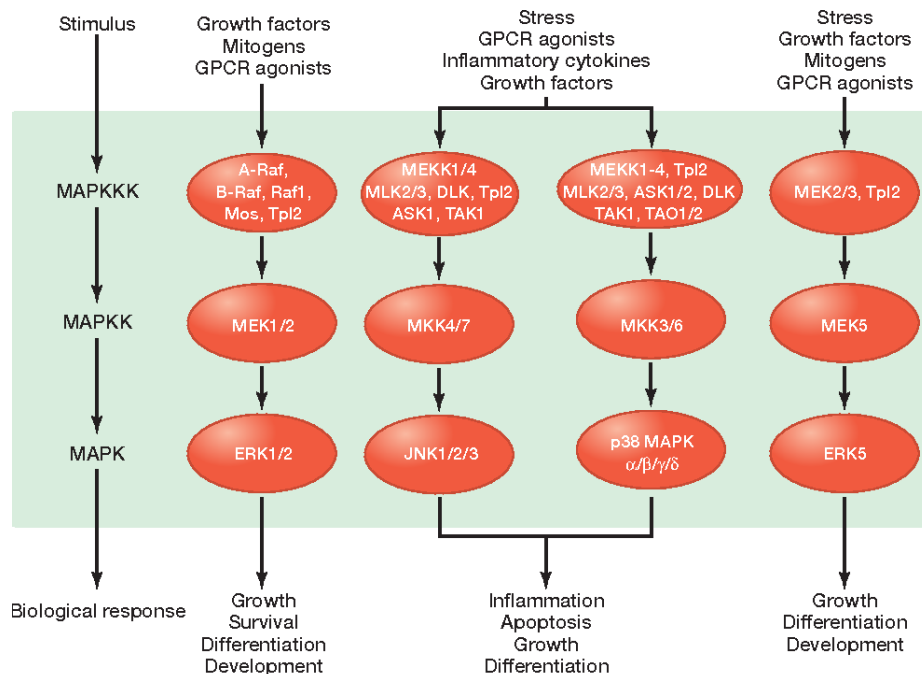


**Figure 1.20 Activation of the MAPK pathway in response to different stimuli results in different biological responses.** The image is adopted from (Morrison 2012).

Recent studies reported that Piezo1 activation by its specific activator, Yoda1, results in enhanced IL6 gene expression via the p-38 MAPK pathway in cardiac fibroblast. It seems that this effect is specific to p38 as the inhibitors of other MAPKs like ERK1/2/5, c-Jun N-terminal kinases (JNK1/2/3) do not rescue the effect but SB203580, a specific inhibitor for p38 MAPK does (Blythe et al 2019). In a separate study, it has been shown that Piezo1 activation by Yoda1 results in the activation of MAPK in a dose and time-dependent manner coupled with the YAP/TAZ pathway in hepatocellular tumor cells (Liu et al 2021b).

P-38 MAPK is especially important, as this is one of the most essential signaling pathways in inflammation. P38 MAPK is highly expressed in brain areas associated with learning and memory (Brust et al 2006, Perea et al 2022), and it is increasingly becoming recognized as a major factor in synaptic regulation and function.

In microglia, p38 MAPK is an important regulator of proinflammatory pathways induced by beta-amyloid and tau proteins (Bachstetter et al 2011, Perea et al 2022). An increase in neuronal p38 MAPK activity has been reported with aging in mice as well (Moreno-Cugnon et al 2019).

It has been reported that p38 activation in Alzheimer's disease in neurons is associated with neurofibrillary tangles and paired helical filaments in the hippocampus (Hensley et al 1999). In pathological conditions, p38 MAPK seems to impair LTP. Reduced p38 MAPK activity, for example, increased synaptic plasticity in angiotensin II-dependent hypertensive rats via either genetic knockdown or pharmacological inhibition in the hippocampal slices (Dai et al 2016). In the entorhinal cortex (EC), specific pharmacological inhibition of p38 MAPK inhibited the reduction of synaptic plasticity caused by the injection of amyloid-beta (Origlia et al 2008).

Inhibiting extrasynaptic NMDA receptors that include GluN2B-containing receptor trafficking is a function of the polysialylated neural cell adhesion molecule (polySia-NCAM). Aging can lead to deficiencies in the expression of this molecule, which in turn may promote the activity of extrasynaptic GluN2B-NMDA receptor, Ras-GFR1 activation, and ultimately decrease LTP levels through increasing phosphorylation of the p38 MAPK (Kochlamazashvili et al 2010b). Neuronal Ca<sup>2+</sup>-dependent activation of Ras via calmodulin binding to an IQ motif in Ras-GRF has been reported previously (Farnsworth et al 1995). Indeed, p38 MAPK is consistently engaged in synaptic long-term depression (Bolshakov et al 2000).

### **1.9.3 Calpain protease**

Calpains are a kind of non-lysosomal cysteine proteases that have been linked to a variety of calcium-dependent biological processes. Calpain 1 and 2 are the most common isoforms of calpain found in the brain and are widely and consistently distributed in both neurons and glial cells. Calpain hyperactivity has

been associated with both apoptotic and necrotic neuronal death in a variety of *in vitro* and *in vivo* neurodegenerative models (Camins et al 2006). Calpain-1 activation is essential for the formation of LTP and is neuroprotective in general, but calpain-2 activation restricts the degree of potentiation and is neurodegenerative (Baudry & Bi 2016).

Piezo1-mediated calpain activation has been recently reported in a few studies. In cardiomyocytes, Piezo1 disrupted calcium homeostasis by mediating external  $\text{Ca}^{2+}$  inflow and  $\text{Ca}^{2+}$  intracellular overload, activating  $\text{Ca}^{2+}$ -dependent signaling, calcineurin, and calpain. *In vitro*, calcineurin or calpain inhibition prevented Yoda1-induced induction of hypertrophy markers and hypertrophic development (Zhang et al 2021). In pulmonary endothelial cells, enhanced Piezo1 expression following ionizing radiation was associated with increased  $\text{Ca}^{2+}$  influx and calpain activity. Radiation effects on endothelial cell ferroptosis were partially mitigated by inhibiting Piezo1 activity with the specific inhibitor GsMTx4 or inhibiting downstream calpain signaling (Guo et al 2021). Liu and colleagues proposed that membrane stretch during immunological synapse formation activates Piezo1 and causes  $\text{Ca}^{2+}$  influx, which activates calpain. The activation of calpain contributes to the cleavage of spectrin and the reorganization of the actin scaffold, leading to an enhancement in human T cell activation (Liu et al 2018a). Interestingly, inhibition of Piezo1/calpain signaling in the rat basal forebrain rescues fear memory impairment induced by sleep deprivation (Ma et al 2022b).

Extrasynaptic NMDA receptors particularly activate calpain-2, which degrades Striatal-Enriched protein Phosphatase (STEP) and eventually causes neurotoxicity (Xu et al 2009). Calpain also has been demonstrated to cleave GluN2B and disrupt its association with synapse-associated protein 102 (SAP102), impairing NMDA receptor trafficking (Briz et al 2012). The interaction of GluN2A and GluN2B with the scaffold proteins postsynaptic density 95 (PSD95) and SAP102 controls the synaptic location and trafficking of NMDA receptors (Chen et al 2012). Given that aberrant calpain activity was seen in age-dependent pathological conditions like AD (Saito et al 1993), Therefore, Piezo1-mediated calpain activation might be one of the pathways leading to synaptic plasticity and cognitive function impairment in the aged brain.

### **1.10 Role of Piezo1 in the CNS immunomodulation**

High mechanical sensitivity allows both central neurons and glial cells to quickly respond to changes in the stiffness of their environment (35, 36). Piezo1 expression in reactive cortical astrocytes is amplified by peripheral infection and aging (Velasco-Estevez et al 2018). In line with this, non-AD brains do not exhibit increased Piezo1 expression while in reactive astrocytes exposed to  $\text{A}\beta$ , the expression of Piezo1 is upregulated both in the human and animal model of AD (Satoh et al 2006, Velasco-Estevez et al 2018). In

the AD brain, astrocytes are more reactive and release pro-inflammatory cytokines, therefore, Piezo1 might be able to control the signal transduction of reactive astrocytes and changing their phenotype (Figure 1.21).

According to evidence, Piezo1 is expressed in human MO3.13 oligodendrocytes and mouse Schwann cells and actively contributes to myelination as a negative regulator by regulating the YAP/TAZ pathway (Acheta et al 2022, Velasco-Estevez et al 2020). Channel blockage utilizing GsMTx4 may attenuate demyelination while pharmacological stimulation accelerates demyelination (Acheta et al 2022, Velasco-Estevez et al 2020). Piezo1 also limits axonal regrowth and impairs regeneration (Song et al 2019).

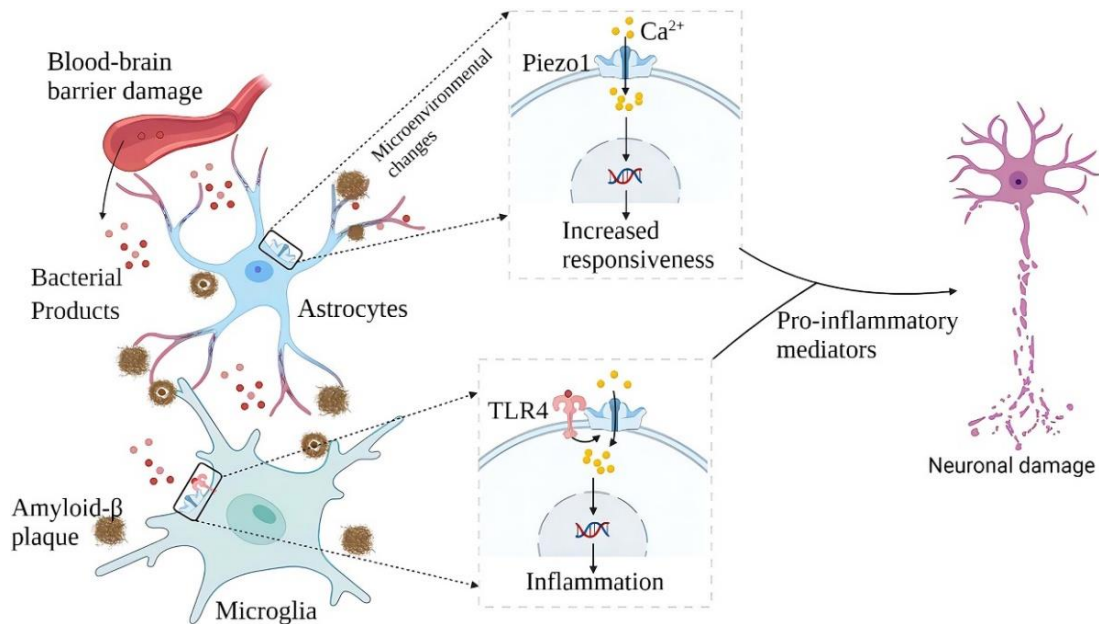


**Figure 1.21 Schematic illustration of the role of cell-type specific of Piezo1 in AD pathology.** The image is adopted from (Liu et al 2022).

Previously, the high expression of Piezo1 in human microglia has been confirmed. Induced pluripotent stem cell (iPSC)-derived microglia-like cells (iMGL) from human iPSC-lines that mimic human microglia in terms of their morphology, marker expression, functional characteristics, and ability to react to ATP and ADP with  $Ca^{2+}$  transients was created in order to examine human microglia. Piezo1 was expressed by human iMGLs and the human microglial SV40 cell line. In addition to this, Piezo1 expression is detected in murine trigeminal neurons, astrocytes, microglia, and microglial cell line (BV2), whereas Piezo2 was only found in the SV40 cell line and main mice microglia (Jantti et al 2022).

Interestingly, Yoda1 treatment of 5xFAD mice for two weeks via intracranially lateral ventricle administration showed that Yoda1-treated mice had a higher immunoreactive area of IBA1-positive microglia in the hippocampus and cortex (Jantti et al 2022).

Piezo1 might also be a viable target for treating hyperglycemia-related brain injury as Liu and colleagues showed that Piezo1 is required for microglia-mediated damage in acute hyperglycemia. Piezo1 inhibition reduced acute hyperglycemia-induced cell damage and elevated phosphorylation of JNK1 and mTOR, indicating that the latter alteration represents a possible Piezo1 downstream pathway (Liu et al 2021a).

## 2. AIMS AND OBJECTIVES

With the data outlined in the Introduction section, it seems plausible to hypothesize that increased brain stiffness in combination with the increased expression of genes involved in mechanosensation may lead to impaired synaptic plasticity and cognitive function in both aged and 5xFAD model. The molecular mechanism involved in this alteration is not clear. The primary aim of this study, therefore, was to identify the age-dependent changes in the mechanosensitive-dependent pathways in the hippocampus of the aged and 5xFAD mice, and dissect the underlying molecular mechanism and target it to rejuvenate the aged brain.

Therefore, this thesis work includes the following objectives:

1. To investigate the expression of mechanosensitive ion channels and related genes using q-PCR, western blot, and immunohistochemistry.
2. To mimic activation of the Piezo1 mechanosensitive channel in the aged brains by its pharmacological activation in the young brains and study the effects of this activation on synaptic plasticity in hippocampal slices by electrophysiological approach.
3. To rescue the synaptic plasticity in the young mice after Piezo1 activation by targeting downstream signaling pathways.
4. To rescue the synaptic plasticity in the aged brain by knockdown of Piezo1 in the hippocampus.
5. To unravel the possible cellular and molecular mechanisms behind the age-dependent mechanosensation.

### **3. MATERIALS AND METHODS**

#### **3.1 Animals**

All animal experiments were performed in strict conditions following the ethical animal research standards defined by German law and approved by the Ethical Committee on Animal Health and Care of the State of Saxony-Anhalt, Germany (license 42502-2-1322 DZNE). Animals were from the Deutsches Zentrum für Neurodegenerative Erkrankungen e.V. (DZNE) animal facility (Pawlow Haus). We used C57BL6/J mice that were 2-4 months old and >30 months old as young and healthy aging conditions, respectively. For pathological conditions, we used a mouse model 5xFAD (B6SJL) mice as an Alzheimer's disease model. These mice express human *APP* and *PSEN1* transgenes with a total of five AD-linked mutations: The Swedish (K670N/M671L), Florida (I716V), and London (V717I) mutations in *APP*, and the M146L and L286V mutations in *PSEN1*. Basal synaptic transmission and LTP in the CA1 area of 5xFAD mice begin to decline between 4 and 6 months (Kimura & Ohno 2009).

#### **3.2 Hippocampal tissue isolation, RNA, and protein purification**

To isolate the hippocampi, animals were anesthetized with isoflurane and transcardially perfused with ice-cold phosphate-buffered saline (PBS). Animals were decapitated, brains were removed and hippocampi were dissected quickly and flash-frozen on dry ice and kept at -80°C freezer until the next use for the RNA and protein purification.

Total RNA and protein from the frozen hippocampi have been purified by using GeneMATRIX DNA/RNA/Protein Purification Kit (EUR<sub>x</sub> Cat. No. E3597) according to the manufacturer's recommended protocol. With this kit, I was able to purify both total RNA and total protein simultaneously from a single sample. To inactivate DNases, RNases, and proteases, samples are first homogenized in the presence of lysis and denaturing solutions. Then, DNA fragments are bound to DNA binding spin columns in the subsequent stage. Following the application of the sample to an RNA-binding spin column, all RNA molecules are adsorbed. Then, high-quality RNA is eluted in water devoid of RNase. The follow-through from the RNA binding step is used to purify the protein. Proteins are centrifuged into pellets and finally, protein dissolving PLB buffer dissolves the protein pellet for the final SDS-PAGE analysis.

#### **3.3 cDNA synthesis and quantitative real-time PCR**

The purified RNA from the previous step was converted to cDNA by using a High-Capacity cDNA Reverse Transcription Kit (Applied Biosystems™, Cat.4368814). I used this kit to convert 0.5-1 µg of total RNA to single-stranded cDNA for further quantitative PCR (qPCR) analysis. Table 3.1 describes the mixture of the reaction for cDNA synthesis.

**Table 3.1** Components of a reaction for the cDNA synthesis

cDNA synthesis reaction components	Volume for 1 reaction
10X RT buffer	2 $\mu$ l
25X dNTP mix (100 mM)	0.8 $\mu$ l
10X random primers	2 $\mu$ l
Reverse transcriptase	1 $\mu$ l
RNase-free H <sub>2</sub> O	4.2 $\mu$ l
Volume of the sample	10 $\mu$ l
Total volume	20 $\mu$ l

Gene expression analysis has been done by using the TaqMan gene expression array (Cat. 4331182) from Thermo-Fisher Scientific and the Quant-Studio-5 device from Applied Biosystems. PCR reaction components were prepared using TaqMan™ Fast Universal PCR Master Mix (2X) kit (Applied Biosystems™ Cat. 4352042) (Table 3.2).

**Table 3.2** Components of a reaction for the qPCR analysis

qPCR reaction mix component	Volume for 1 reaction
2X TaqMan™ gene expression mater mix	5 $\mu$ l
20X TaqMan™ gene expression probe	0.5 $\mu$ l
RNase-free H <sub>2</sub> O	2 $\mu$ l
cDNA sample	2.5 $\mu$ l
Total volume	10 $\mu$ l

Based on the Ct value observed for each transcript, I used the  $2^{-\Delta\Delta C_t}$  method to calculate the relative fold gene expression of target genes in different experimental groups. Table 3.3 lists all Taqman probes used for qPCR analysis in this study.

**Table 3.3** Taqman qPCR probes used in this thesis

Gene	Species	Reference Sequence
<i>Gapdh</i>	Mus musculus	NM_001289726.1
<i>Piezo1</i>	Mus musculus	Mm01241549_m1
<i>Piezo2</i>	Mus musculus	Mm01265861_m1

<i>YAP</i>	Mus musculus	Mm01143263_m1
<i>TAZ</i>	Mus musculus	Mm04239390_g1
<i>CTGF</i>	Mus musculus	Mm01192933_g1
<i>CYR61</i>	Mus musculus	Mm00487498_m1
<i>ANKRD1</i>	Mus musculus	Mm00496512_m1
<i>TRPV1</i>	Mus musculus	Mm01246300_m1
<i>TRPV2</i>	Mus musculus	Mm00449223_m1
<i>TRPV4</i>	Mus musculus	Mm00499025_m1
<i>TRPC1</i>	Mus musculus	Mm00441975_m1
<i>TRPC3</i>	Mus musculus	Mm00444690_m1
<i>TRPC4</i>	Mus musculus	Mm00444280_m1
<i>TRPC5</i>	Mus musculus	Mm00437183_m1
<i>TRPC6</i>	Mus musculus	Mm01176083_m1
<i>TRPM3</i>	Mus musculus	Mm01210379_m1
<i>TRPM7</i>	Mus musculus	Mm00457998_m1
<i>TRPA1</i>	Mus musculus	Mm01227437_m1
<i>TNF</i>	Mus musculus	Mm00443258_m1
<i>IL1<math>\beta</math></i>	Mus musculus	Mm00434228_m1

### 3.4 SDS-PAGE and western-blot

The concentration of the pellet containing total protein from the purification step has been determined by using Pierce™ BCA Protein Assay Kit (ThermoFisher Cat. 23225) and NanoDrop™ 2000/2000c Spectrophotometers (ThermoFisher). Protein samples were boiled for 5 minutes at 95°C then 10  $\mu$ g loaded per lane and analyzed by 10 % SDS gels (Table 3.4).

**Table 3.4** Chemical component for SDS-PAGE gel preparation

Separating gel (10%) - 10 ml	
H <sub>2</sub> O	4 ml
Acrylamide/bis	3.3 ml
Tris-HCl (1.5 M, pH 8.8)	2.5 ml
SDS, 10%	100 µl
TEMED	10 µl
Ammonium persulfate (APS), 10%	50 µl
Stacking gel (4%) - 5ml	
H <sub>2</sub> O	3.05 ml
Acrylamide/bis	0.650 ml
Tris-HCl (0.5 M, pH 6.8)	1.25 ml
SDS, 10%	50 µl
TEMED	10 µl
Ammonium persulfate (APS), 10%	100 µl

Samples were separated in the electrophoresis tank containing cold separating 1X TGS (Tris/Glycine/SDS) buffer for 2 hours at 90 V. Separated proteins were blotted on nitrocellulose membranes by using the Trans-Blot Turbo transfer system (Bio-Rad).

The blocking step was done using tris-buffered saline with 0.1% tween20 (TBST) supplemented with 5% skim milk (SERVA) for 1 hour at room temperature. Primary antibodies were diluted in TBST/1% milk and applied to the membranes overnight at 4°C on a shaker. Next, blots were washed three times for 10 min with TBST and incubated for one hour with secondary antibodies conjugated with Horseradish Peroxidase (HRP) in 1/10000 dilution (Table 3.5). After another three steps of washing in TBST, blots were developed by using the SuperSignal® West Pico Chemiluminescent Substrate (ThermoScientific Cat. 34078). The membranes were incubated with a working solution containing one to one volume of peroxide solution and luminol enhancer for 5 minutes at room temperature. Excess reagent was drained and the blots were covered with clear plastic wrap and imaged by the chemiluminescence Imager (Azure Biosystems C300).

**Table 3.5** Secondary antibodies used for western-blot in this thesis

Antibody	Dilution	Provider	Cat. No
HRP Goat anti-Rabbit	1:10000	Jackson ImmunoResearch	111-035-144
HRP Goat Anti-Guinea pig	1:10000	Jackson ImmunoResearch	106-035-003
HRP Goat Anti-Mouse	1:10000	Jackson ImmunoResearch	115-035-146

### 3.5 Immunohistochemistry

Brain samples were fixed with 4% PFA in PBS overnight and then immersed in 30% sucrose in PBS for 48 hours overnight. Finally, brains were frozen in 100% 2-methyl butane at -80°C before sectioning into coronal sections. For 350 µm hippocampal slices, tissue was kept in 4% PFA for 2 hours and then 30% sucrose until further sub-sectioning. All tissue samples were cut into 50 µm-thin sections for immunostaining and kept in a floating solution (Table 3.6) at 4°C until further use.

I permeabilized the sections in a permeabilization solution (Table 3.6) for 10 minutes at room temperature after washing the sections three times with 120 mM PB solution pH of 7.2 (Table 3.6). I blocked the sections for an hour at room temperature using a blocking solution (Table 3.6). Following blocking, I incubated the sections with primary antibodies (Table 3.7) at 37 °C overnight, washed them three times in PB for 10 minutes, then incubated them with secondary antibodies (Table 3.8) at room temperature for 3 hours, followed by a third three-hour incubation at room temperature, and finally washed them three times in PB for 10 minutes. Finally, I used Fluoromount (Sigma, F4680) to mount the slices on Superfrost glasses so that confocal pictures could be captured.

**Table 3.6** Buffers and solutions for IHC

Buffer	Composition
4% paraformaldehyde (PFA) (w/v)	4 % PFA in PBS, pH 7.4
Phosphate buffer (PB)	0.1 M sodium phosphate dibasic; 0.1 M sodium phosphate monobasic
Permeabilization solution	0.4 % Triton-X 100 in PB
Blocking Solution	10 % normal goat serum (NGS) in PB, 0.4 % Glycine, 0.4 % Triton-X 100
Floating solution	Ethylene glycol, glycerin, PBS in the ratio 1:1:2

**Table 3.7** Primary antibodies used for the IHC in this thesis

Antibody/Reagent	Dilution	Species	Provider	Cat. No
Piezol	1:200	Rabbit	Novus Biologicals	NBP1-78537
NeuN	1:500	Guinea pig	Synaptic Systems	266004
Phospho-CaMKII (Thr286)	1:300	Mouse	Cell signaling	12716
GFAP	1:500	Chicken	Millipore	AB5541
IBA1	1:500	Guinea pig	Synaptic Systems	234004
YAP	1:500	Mouse	Cell Signaling	12395
p- YAP	1:500	Rabbit	Cell Signaling	13008
P38	1:300	Rabbit	Cell Signaling	9212S
Phospho-p38	1.300	Rabbit	Cell Signaling	4511S

**Table 3.8** Secondary antibodies used for the IHC in this thesis

<b>Antibody (Alexa Fluor)</b>	<b>Dilution</b>	<b>Species</b>	<b>Provider</b>	<b>Cat. No</b>
Anti-Rabbit	1:1000	Goat	Invitrogen	A11034
Anti-Guinea pig	1:1000	Goat	Invitrogen	A11074
Anti-Mouse	1:1000	Goat	Invitrogen	A11029
Anti-Chicken	1:1000	Goat	Invitrogen	A-11040

### **3.6 Generation, and characterization of Adeno-associated viruses (AAV) containing Piezo1 shRNA**

To knock down the Piezo1 protein, we used short hairpin RNA (shRNA) strategy. Production, purification, and titration of the viral particles were done in collaboration with Mrs. Katrin Boehm (DZNE, Magdeburg). The shRNA plasmid was created by inserting siRNA sequences (Sigma) which were previously shown to be effective against Piezo1 mRNA (Coste et al 2010) with a target sequences CACCGGCATCTACGT CAAATA into AAV U6 GFP backbone (Cell Biolabs Inc.) using BamH1 (New England Biolabs) and EcoR1 (New England Biolabs). The shRNA universal negative control (scramble) (Sigma, Control shRNA) was employed as a non-targeting control. Following bacterial transformation, positive clones were selected and plasmid was purified with a mini-prep kit to confirm further by sequencing approaches.

After doing maxi-prep plasmid purification to have a high yield of the plasmid, HEK 293T cells were transfected with an equal amount combination of the shRNA-encoding AAV U6 GFP, pHelper (Cell Biolabs Inc), and RapCap DJ plasmids (Cell Biolabs Inc) by using PEI (1ng/ul). Freeze-thaw cycles were used 48-72 hours after transfection to lyse cells, followed by 1 hour at 37 °C with benzonase (50 U/mL; Merck Millipore, Burlington, MA, USA). Lysates were centrifuged at 8000 g for 4 minutes at 4 °C, supernatants were collected, and a 0.2-micron filter was used to filter the supernatants. We then purified the filtrates using pre-equilibrated HiTrap Heparin HP affinity columns (GE HealthCare, Chicago, IL, USA), followed by washing with the following buffers in order: Wash Buffer 1 (20 mM Tris, 100 mM NaCl, pH 8.0; sterile filtered) and Wash Buffer 52 (20 mM Tris, 100 mM NaCl, pH 8.0; sterile filtered) (20 mM Tris, 250 mM NaCl, pH 8.0; sterile filtered). The viral particles were then eluted using elution buffer (20 mM Tris, 500 mM NaCl, pH 8.0; sterile filtered).

To further purify viral particles, we used the Amicon Ultra-4 centrifugal filters with 100,000 Da molecular weight cutoff (Merck Millipore, Burlington, MA, USA) along with 0.22 µM Nalgene® syringe filter units (sterile, PSE, Sigma-Aldrich, St. Louis, MO, USA) to further purify viral particles before being aliquoted and stored at -80 °C.

### **3.7 Primary neural culture preparation**

To validate the knockdown efficiency of the AAV, I used primary hippocampal neurons. The hippocampal cells were isolated from embryonic C57BL6/J mice (E18) as described previously (Kaech & Banker 2006). The pregnant mouse was killed by breaking the neck. The babies were carefully removed with tweezers and scissors and put in a Petri dish filled with 50ml ice-cold HBSS. The heads were transferred in the Petri dish on ice under the sterile bench and fixed with forceps (in the eyes area) and with scissors 3 small cuts were made in the skull of the head (from behind to midline, to down left, and to downright). The brain was removed and cut into 2 halves using a scalpel. The hippocampus was isolated and transferred to in 15ml tube filled with HBSS. When all of the hippocampi have been extracted, we put them in a 15 ml conical centrifuge tube and dilute them with HBSS to 4.5 ml. In a water bath at 37 °C, we added 0.5 ml of 2.5% trypsin and incubated for 15 minutes. Trypsin solution was gently removed, leaving the hippocampi at the bottom of the tube then 5 ml of HBSS was added and left at room temperature for 5 minutes twice to allow the remaining trypsin to disperse from the tissue. Pipet the hippocampi up and down repeatedly in a Pasteur pipet to dissociate them. After harvesting, I seeded the cells with a density of 500,000 cells per well in a 6-well plate coated with PLL/laminins in 1ml DMEM+ (DMEM supplemented with 2% B27, 1% L-glutamine, and 1% Pen-Strep) for 4 hours. After 4 hours, the DMEM+ medium was replaced with NB+ media, which had the same composition as DMEM+ but contained Neurobasal medium instead of DMEM. Cells were infected with either Piezo1\_shRNA or control shRNA at 7 days *in vitro* (DIV). Cells were fed every three other days up to DIV-21. Virus efficiency was monitored by observing the GFP signal in each well. Total RNA purification and quantitative real-time PCR analysis have been done as described above.

### **3.8 Injection of AAV encoding control and Piezo1 shRNA into the dorsal hippocampus**

The injection of the virus into the dorsal part of the hippocampus is a commonly used procedure in neuroscience research, particularly for the study of learning and memory. This precise localization is crucial because the hippocampus exhibits functional specialization along its longitudinal axis. The dorsal portion is primarily associated with spatial navigation, cognitive mapping, and declarative memory. When AAV vectors are introduced into this region, they enable the targeted manipulation of specific genes or proteins within neurons, facilitating the investigation of their roles in memory processes. To this, same AAV suspension from control and Piezo1 shRNA was injected bilaterally into the CA1 region of the hippocampus (2 mm posterior, 1.5 mm lateral to the bregma, 1.3 mm depth; 1 µL/side). All injections were carried out with a 10 µl NanoFil syringe (World Precision Instrument, USA) and a UMP3 pump (World Precision Instrument, USA) at a rate of 0.2 µL/min. The needle was remained in place for 5 minutes after each

injection. Following the procedure, the animals were placed in a recovery chamber with red light for 15 minutes.

### **3.9 Behavioral experiments**

Behavioral studies were conducted in collaboration with David Baidoe-Ansah (DZNE, Magdeburg). For behavioral tests, 5 mice aged 2-4 months (1 mouse died a few days after injection) and 6 mice aged >30 months were employed. All mice were transported from the DZNE animal breeding house to the DZNE research facility and kept separately for at least 72 hours before tests under a reversed 12/12 light/dark cycle (light on 9 P.M.). All trials were carried out during the dark part of the cycle when mice were active and at constant temperature and humidity. The Anymaze 4.99 (Stoelting Co., Wood Dale, IL, USA) software was used to record and evaluate animal activity during behavioral experiments. Following that, animals were subjected to the open field test, the novel object location test (NOLT), and the novel object recognition test (NORT). All behavior trials, particularly following injection, were carried out by a trained observer who was blinded to the treatment circumstances.

#### **3.9.1 Open field**

Animals from each experimental group were placed in an open field arena (50 x 50 x 30 cm) and permitted to walk freely for 10 minutes while being recorded with an above camera. The arena was divided into two sections: the core (30 x 30 cm) region and the periphery (30 x 30 cm) area (the 10 cm area adjacent to the wall of the recording chamber). I estimated the animal's general activity and anxiety based on the total distance traveled and time spent in the central/peripheral region.

#### **3.9.2 Novel object location and recognition tests**

In the same open-field arena, we conducted the novel object location test. During the encoding phase, we let animals explore the area for 10 minutes with a pair of identical items. During the retrieval phase, we let the animals explore the arena again for 10 minutes with identical items, except one of them was placed in a different position. To assess animal behavior, we utilized the time spent investigating items in familiar (F) and novel (N) locations, as well as the discriminating ratio  $[(N-F)/(N+F)] \times 100\%$ . Following that, 24 hours after the NOLT retrieval phase, we conducted the NORT in the open field arena, which included the previously stated encoding and retrieval phases. We allowed animals to explore the arena with a pair of identical items throughout the encoding phase, but during the retrieval phase, one of the objects was replaced by a novel object that the animal had never seen before. The encoding and retrieval phases each took 10 minutes (Figure 3.1). We measured animals' recognition memory using a manner identical to the one described before.

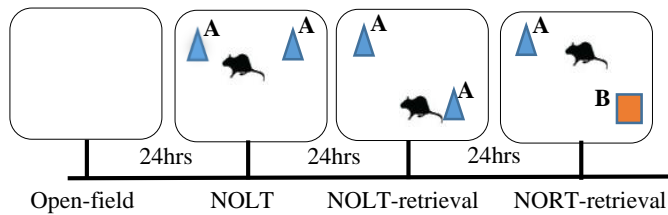


**Figure 3.1 Timeline for NOLT and NORT tests**

### 3.10 Preparation of acute hippocampal slices

Hippocampal slices were prepared from 2- to 4-month-old C57BL6/J male mice. Animals were deeply anesthetized with isoflurane and then immediately decapitated. The brain was removed and cut into two hemispheres. 350  $\mu\text{m}$ -thick transverse slices were cut by a Vibroslicer (Leica, Nussloch, Germany) in an ice-cold sucrose-based solution (Table 3.9). Slices were transferred and kept at room temperature in a large chamber (500 ml) filled with carbogen-bubbled storage solution (Table 3.9) containing drugs for at least three hours before recording. The final concentration of DMSO (0.1%), Yoda1 (10  $\mu\text{m}$ ), p38 inhibitor SKF86002 (5 $\mu\text{m}$ ) and calpain inhibitor E64 (2 $\mu\text{m}$ ) were used in our experiments. Finally, acute slices were transferred into a submerged-type recording chamber for recordings of fEPSPs in artificial cerebrospinal fluid (ACSF) (Table 3.9). All solutions were saturated with 95%  $\text{O}_2$  and 5%  $\text{CO}_2$  with osmolality maintained at  $300 \pm 5$  mOsm.

**Table 3.9** Solutions used for the electrophysiology experiment on hippocampal slices

<b>Solution</b>	<b>Composition (in mM)</b>
Slice cutting solution	240 sucrose, 2 KCl, 2 $\text{MgSO}_4$ , 1.25 $\text{NaH}_2\text{PO}_4$ , 25 $\text{NaHCO}_3$ , 1 $\text{CaCl}_2$ , 1 $\text{MgCl}_2$ , and 10 D-glucose. (pH 7.3, adjusted with NaOH)
Storage solution	113 NaCl, 2.38 KCl, 1.24 $\text{MgSO}_4$ , 0.95 $\text{NaH}_2\text{PO}_4$ , 24.9 $\text{NaHCO}_3$ , 1 $\text{CaCl}_2$ , 1.6 $\text{MgCl}_2$ , 27.8 D-glucose (pH 7.3, adjusted with NaOH)
ACSF	120 NaCl, 2.5 KCl, 1.5 $\text{MgCl}_2$ , 1.25 $\text{NaH}_2\text{PO}_4$ , 24 $\text{NaHCO}_3$ , 2 $\text{CaCl}_2$ and 25 D-Glucose

### 3.11 Analysis of synaptic transmission and plasticity

For stimulation and recording of fEPSPs, glass electrodes filled with ACSF were employed. Monopolar stimulating glass electrodes with a fractured tip and resistance less than 1  $\text{M}\Omega$  were used to deliver 0.2 ms stimulation current pulses. The stimulus-response curve was generated by applying increasing current pulses and monitoring the slope of evoked responses. For recordings of paired-pulse facilitation (PPF) and

LTP, the stimulation intensity was selected based on the stimulus-response curve to elicit fEPSPs with a slope of 30% and 50% of the supramaximal fEPSPs, respectively.

PPF was defined as the ratio of the slopes of the fEPSPs elicited by the second and first pulses given with 20, 50, 100 ms intervals. For LTP induction in young and aged animals, TBS protocol has been used which includes 5 trains of stimuli delivered with 20 sec intervals. Each train is composed of 8 stimulus bursts delivered at 5 Hz (200 ms interval) with each burst consisting of four pulses given at 100 Hz (Figure 3.2). The LTP value was computed by comparing the mean slope of fEPSPs obtained 50-60 minutes after TBS to the mean slope of fEPSPs recorded 10 minutes before TBS.

All recordings were obtained at  $30 \pm 1$  using an EPC-10 amplifier (HEKA Elektronik, Germany). The recordings were filtered at 1 kHz and digitized at 10-20 kHz.

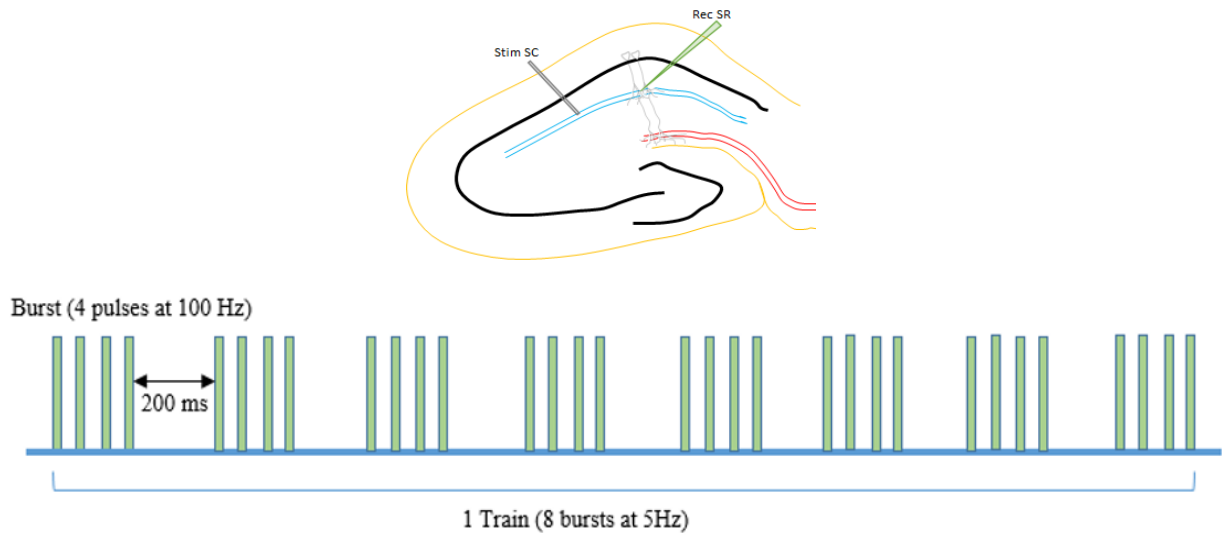


**Figure 3.2 TBS pattern for LTP induction in hippocampal slices**

In the TBS analysis, for each burst-induced fEPSP, I analyzed the area of the curves which correspond to fast component AMPA (50 ms) and slow component NMDA (90 ms) receptors activity normalized to baseline area, 20 ms before the beginning of the burst (Figure 3.3).

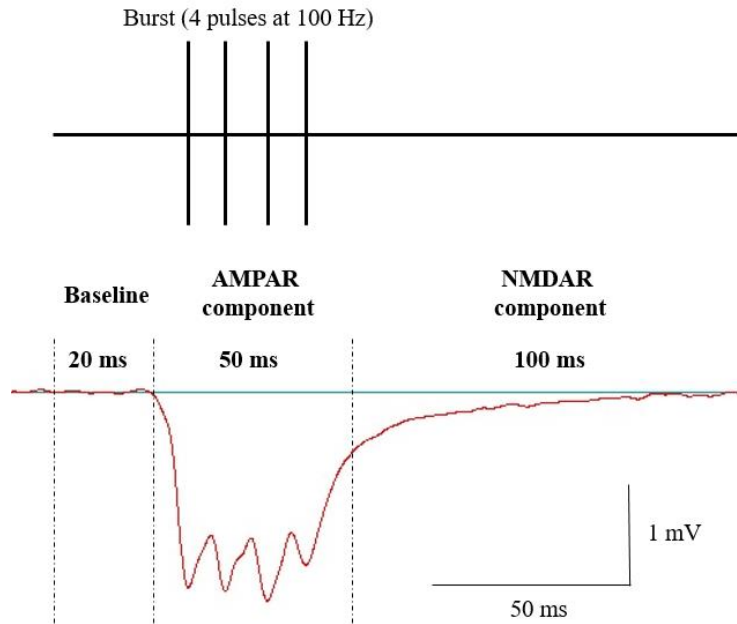


**Figure 3.3** Burst-induced fEPSPs were measured as the fEPSPs area corresponding to AMPA and NMDA components.

### 3.12 Chemical LTP induction

Chemical LTP was induced as described previously (Kopec et al 2006). Hippocampi are dissected from the young brain and acute 350  $\mu\text{m}$  thick slices are prepared in ice-cold ACSF. Before stimulation, slices were incubated in ACSF at  $30 \pm 1^\circ\text{C}$  in a submerged chamber containing drugs (DMSO, Yoda1) for 3 hours. Then they are transferred into new beakers containing rolipram (100 nM), forskolin (50  $\mu\text{M}$ ), and picrotoxin (100  $\mu\text{M}$ ) dissolved in ACSF lacking  $\text{Mg}^{2+}$  at  $31 \pm 1^\circ\text{C}$  for induction of chemical LTP for 15 minutes. Basal control slices are incubated in the same buffer without stimulation. The LTP value was calculated by comparing the mean slope of fEPSPs obtained 80-90 minutes after chemical induction to the mean slope of fEPSPs recorded 10 minutes before induction.

### 3.13 Statistical analysis

For data administration and statistical analysis, I utilized GraphPad Prism 7.0. (GraphPad Software Inc., La Jolla, USA). Figures with asterisks imply statistical significance. The Kolmogorov-Smirnov test was used to verify for normal distribution of the data before subjecting it to one-way ANOVA or the t-test. The data in the text is all mean values  $\pm\text{SEM}$ . I used the Student's t-test for pairwise comparisons when the samples qualified for the normality test; otherwise, I used the Mann-Whitney test. In addition, for paired comparisons that failed the normality test, the Wilcoxon matched-pairs test was applied. To account for multiple comparisons, the Holm-t-test Sidak's was utilized. When suitable, one- and two-way ANOVA with uncorrected Fisher's LSD, as well as Brown-Forsythe and Welch ANOVA tests, were utilized. Additionally,

cumulative frequency distribution analysis was employed before post hoc testing when the p-value for one-way ANOVA showed a tendency toward significance. To compare cumulative frequency distributions, the Kolmogorov-Smirnov test was utilized. Unless otherwise noted, the p-values represent the degree of significance as shown in the figures by asterisks (\*p < 0.05, \*\*p < 0.01, \*\*\*p < 0.001, and \*\*\*\*p < 0.0001).

### 3.14 List of chemicals and equipment

The following tables 3.10 and 2.11 show the chemicals and equipment used in this thesis.

**Table 3.10** Lis of chemical used in this thesis

Chemical	Provider	Cat. No
2-mercaptoethanol	Roth	4227-3
2-Propanol	Roth	6752.4
4% PFA	Roth	P087.1
Acrylamide/bis	Sigma	A3574
Agarose	Roth	3810.2
Ammonium persulfate	MP biomedicals	802811
B27	Gibco	17504044
CaCl <sub>2</sub>	Roth	31307
DMEM	Gibco	41965039
DMSO	Roth	A994.1
E-64	Sigma	E3132
Forskolin	Tocris	1099
Glucose	Sigma	49139
Glycine	Sigma	50046
KCl	Roth	P017.2
L-glutamine	Gibco	25030024
MgCl <sub>2</sub>	Roth	A537.4
MgSO <sub>4</sub>	Roth	31307
NaCl	Sigma	S7653
NaH <sub>2</sub> PO <sub>4</sub>	Roth	T879.2
NaHCO <sub>3</sub>	Sigma	S5761
Neurobasal medium	Gibco	10888022
PBS	Gibco	10010056
Penicillin/Streptomycin	Gibco	15140122
Picrotoxin	Tocris	1128
Rolipram	Tocris	0905
SDS	Sigma	<u>151-21-3</u>
SKF-86002	Sigma	S0193
Sucrose	Roth	4661.2
TEMED	MP biomedicals	110-18-9
Tris	Sigma	A411.2
Triton X-100	Sigma	9036-19-5
Tween-20	Scy Tek	62620
Yoda1	Tocris	5586

**Table 3.11** List of equipment used in this thesis

Equipment	Provider
Vibroslicer	Leica
EPC-10 Patch Clamp Amplifier	HEKA
Micromanipulators	Scientifica
Stimulus Isolator	WPI
Azure c300 Gel Imaging System	Azure Biosystems
Osmometer	VAPRO
pH meter	METTLER TOLEDO
Pipet puller	Zeitz
LSM 700 confocal microscope	Carl Zeiss
NanoDrop™ 2000/2000c Spectrophotometers	ThermoScientific
Mini-PROTEAN Tetra Vertical Electrophoresis Cell	BioRad
Trans-Blot Turbo Transfer System	BioRad
QantStudio 5 Real-Time PCR Systems	ThermoFisher
Mastercycler® Nexus X2 Thermal Cyclers	Eppendorf®

## 4. RESULTS

### 4.1 Increased expression of some mechanosensitive ion channels in the hippocampus of aged mice

In the hippocampus of the aged brain, the increased protein level of some mechanosensitive channels such as Piezo1 and TRPV4 has been reported (Lee & Choe 2014, Velasco-Estevez et al 2018). As these changes coincide with the ECM accumulation, increased stiffness, and also impaired cognitive function and synaptic plasticity in the aged brain, first I investigated the expression levels of two main families of mechanosensitive genes such as Piezo and TRP channel families in two age groups, the 2-4 months, and the > 30 months old mice. I observed an upregulation in the mRNA levels of the Piezo family including *Piezo1* and *Piezo2* by more than 79% and 160%, respectively (Figure 4.1A). I also found that *Piezo2* expression is 88% less than the expression of *Piezo1* in young mice (Figure 4.1A). The inflammatory condition in the collected aged brains was confirmed by increased expression of the neuroinflammatory markers including *GFAP* (95%), *TNF $\alpha$*  (184%), and *IL1 $\beta$*  (247%) (Figure 4.1B). I also found that from the TRP channels family, the mRNA levels of *TRPV1*, *TRPV4*, *TRPM3*, and *TRPA1* were increased in >30 m mice compared to young mice (37%, 85%, 47%, and 92%, respectively). Additionally, the mRNA levels of *TRPC4* and *TRPC5* were slightly but significantly downregulated in >30M mice by 15% and 12%, respectively (Figure 4.1C).

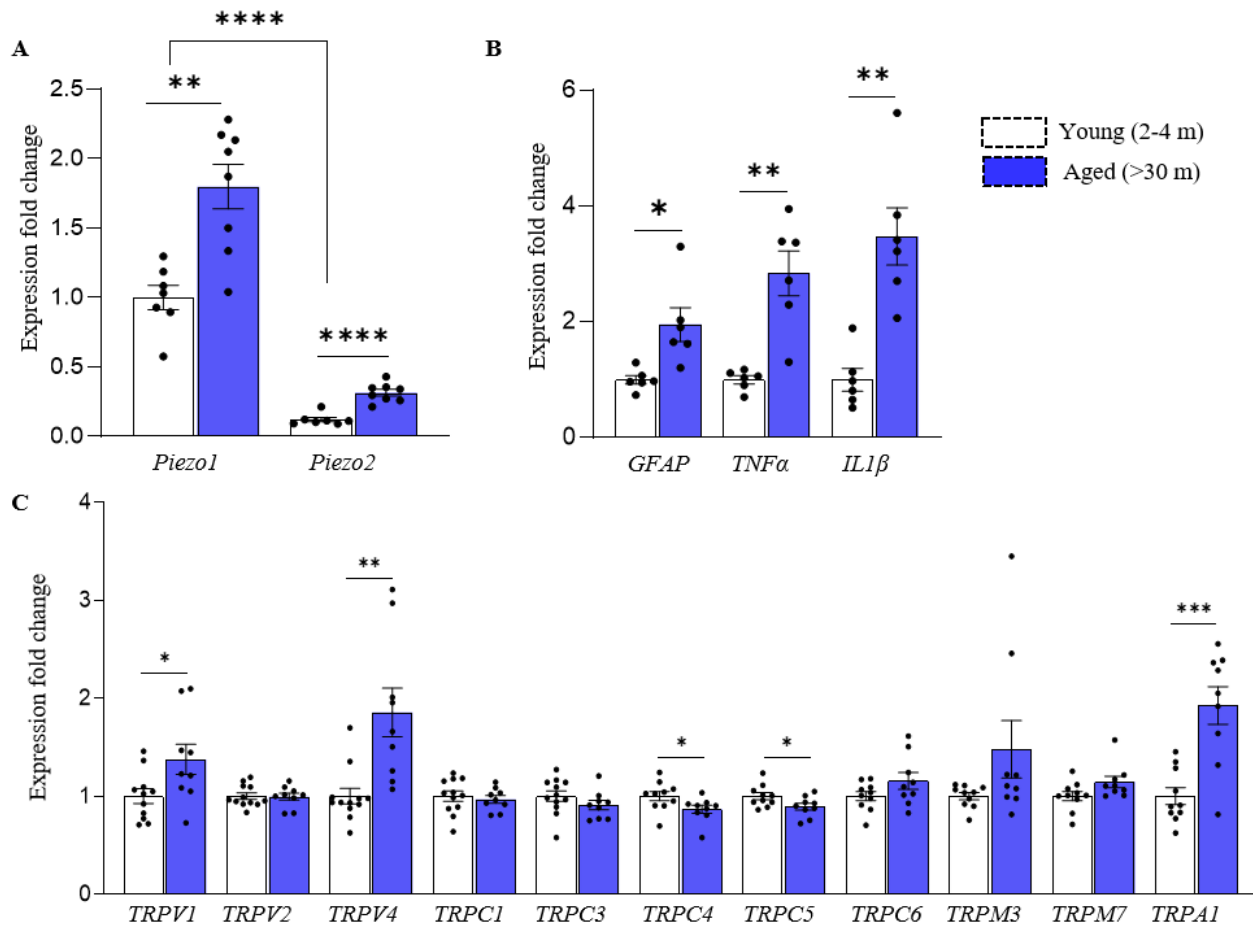


**Figure 4.1. mRNA expression levels of the Piezo family and some TRP mechanosensitive channel genes are increased in the aged hippocampus.** (A) The mRNA expression of the *Piezo1* and *Piezo2* were upregulated in >30 m old mice compared to 2-4 m old mice. The normalized levels are expressed relative to the mean level of *Piezo1* in young mice. Gene expression values were normalized using the mean value of gene expression in young mice, here and in all following panels (B) Inflammatory markers genes were upregulated in the aged hippocampus. (C) The mRNA levels of some TRP channel such as *TRPV1*, *TRPV4*, and *TRPA1* were increased in >30 m old mice relative to 2-4 m old mice while *TRPC4* and *TRPC5* expression was decreased. The bar graph shows mean  $\pm$  SEM values; Unpaired t-test with Welch's correction. For *TRPM3* gene, Mann-Whitney test was used: \* $p < 0.05$ , \*\* $p < 0.01$ , \*\*\* $p < 0.005$  and \*\*\*\* $p < 0.001$ .

Previously, it has been shown that the HIPPO pathway (YAP/TAZ) is downstream of Piezo1 in different cell types, therefore I utilized it as a marker for Piezo1 activation. I measured the expression levels of the main components of the HIPPO pathway, YAP and TAZ, and also two downstream targets of this pathway such as *CYR61* and *CTGF*. Upregulation of these two genes is correlated with YAP/TAZ dephosphorylation and translocation to the nucleus. I've found that *YAP1* expression showed a tendency to upregulation ( $p$  value= 0.06) while *TAZ* did not. *CYR61* mRNA levels were upregulated significantly (40%) but *CTGF* did not show a significant difference (Figure 4.2).

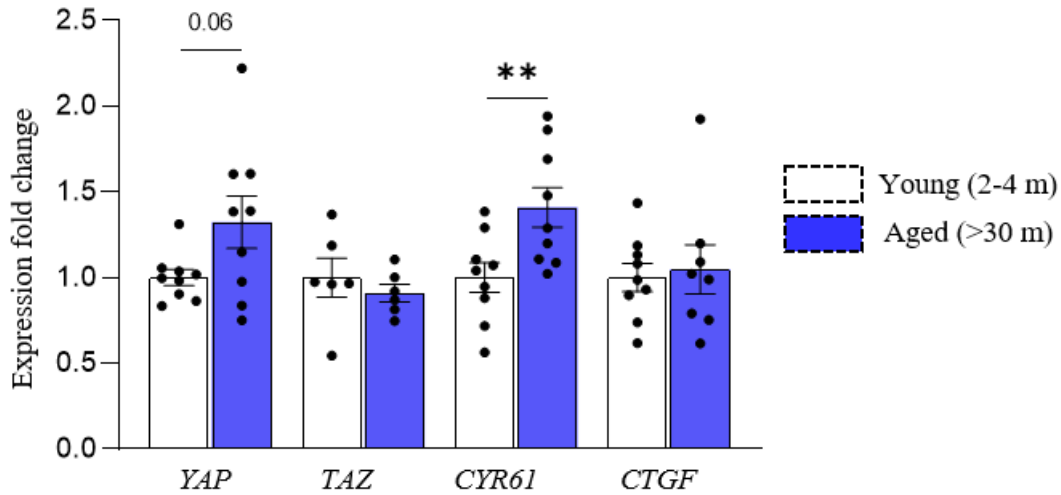


**Figure 4.2 mRNA fold changes of YAP/TAZ pathway components in aged mice.** The mRNA expression of the *YAP* and its downstream target gene *CYR61* are upregulated in >30 m old mice compared to 2-4 m old mice. Not a significant difference was seen in *TAZ* and *CTGF* expression. The bar graph shows mean  $\pm$  SEM values. Unpaired t-test with Welch's correction: \* $p < 0.05$ , \*\* $p < 0.01$ .

Piezo 1 is upregulated both in the human and animal models of AD compared to the control condition (Sato et al 2006, Velasco-Estevez et al 2018). To investigate the changes in the mRNA level for the Piezo channel family and also for TRP channels, I did a qPCR analysis of the hippocampi of 6-month-old 5xFAD mice and the littermate controls (Figure 4.3A). Interestingly, like in aged animals, *Piezo1* and *Piezo2* were upregulated in the mRNA level (by 75% and 70%, respectively). As expected, inflammatory gene expression also increased, *TNF $\alpha$*  (195%), *GFAP* (315%), *IBA1* (119%), and *IL6* (53%) compared to control mice (Figure 4.3B). Some members of TRP channels such as *TRPV1*, *TRPC1*, *TRPC3*, and *TRPM7* were also upregulated in 5xFAD mice (47%, 84%, 75%, and 72%, respectively) (Figure 4.3C).

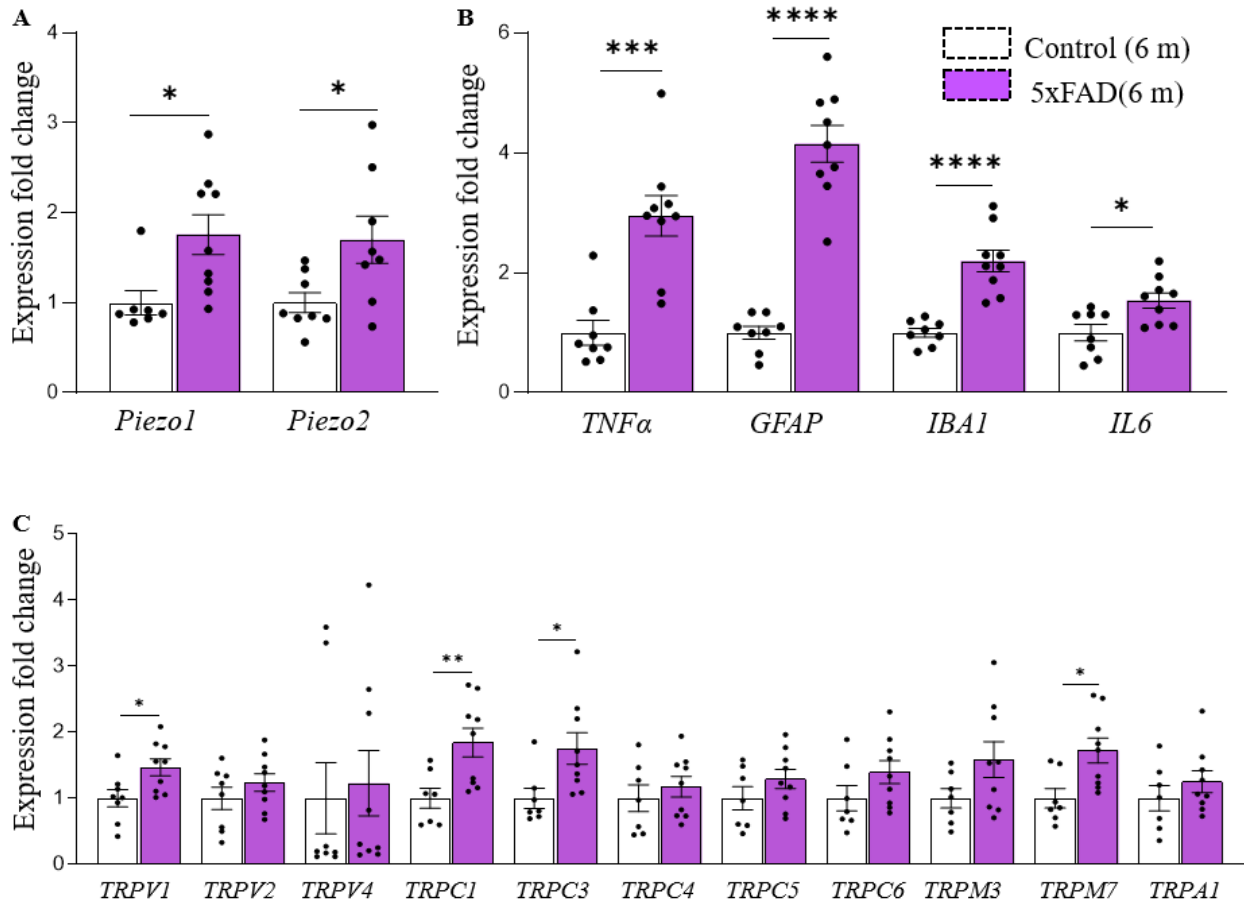


**Figure 4.3. mRNA expression levels of the Piezo family and some TRP mechanosensitive channels are increased in the 5xFAD hippocampus.** (A) The mRNA levels of the *Piezo1* and *Piezo2* were upregulated in 5xFAD mice compared to control mice. Gene expression values were normalized using the mean value of gene expression in young mice, here and in all following panels (B) The mRNA level of some TRP channels such as *TRPV1*, *TRPC1*, *TRPC3*, *TRPM7* was increased in 5xFAD mice relative to control mice. The bar graph shows mean  $\pm$  SEM values; Unpaired t-test with Welch's correction. For the *TRPV4* gene, Mann-Whitney test was used. \* $p < 0.05$ , \*\* $p < 0.01$ , \*\*\* $p < 0.001$ , \*\*\*\* $p < 0.0001$ .

Expression analysis of the YAP/TAZ pathway showed a significant increase in *YAP* and *TAZ* (61% and 60% respectively) and also in the downstream genes, *CYR61* and *CTGF* (141% and 52, % respectively) (Figure 4.4).

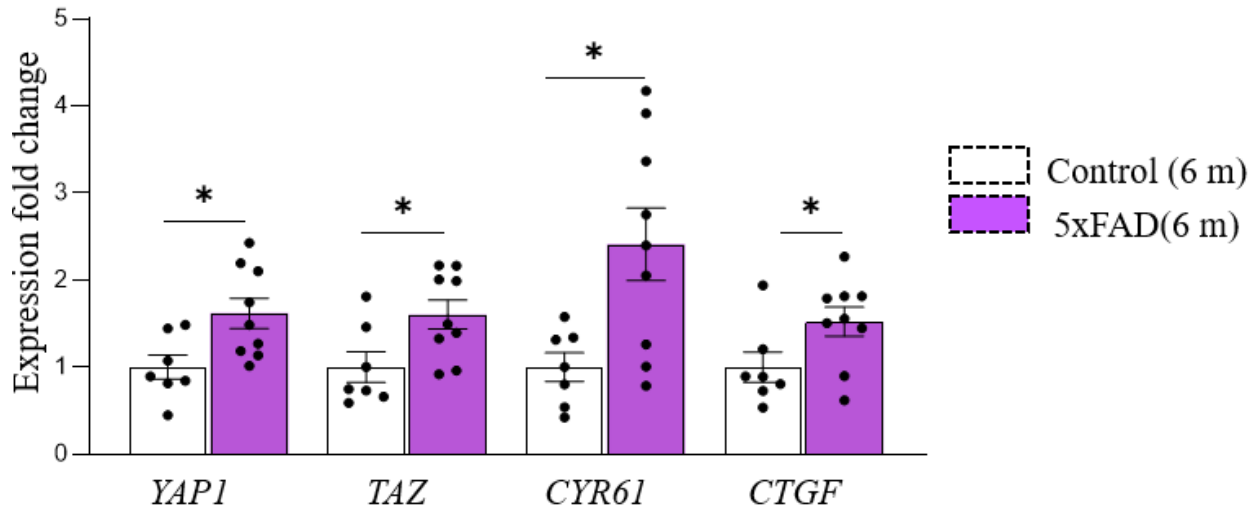


**Figure 4.4. The mRNA levels of YAP/TAZ pathway components are upregulated in 5xFAD mice.** Expression of the *YAP* and *TAZ* and its downstream target genes *CYR61* and *CTGF* is upregulated in 5xFAD mice compared to control mice. The bar graph shows mean  $\pm$  SEM values; Unpaired t-test with Welch's correction: \* $p < 0.05$ .

#### 4.2 Expression of Piezo1 channel is increased at the protein level in neurons but not in astrocytes of aged mice

To verify the significant upregulation of Piezo1 in the mRNA level, I quantified the protein levels of Piezo1 in the aged hippocampus. To reveal a source of increased upregulation of Piezo1, I did cell-type immunostaining for neurons and astrocytes. For this purpose, I used NeuN and GFAP as specific markers for neurons and astrocytes, respectively. With this staining, I found that Piezo1 and YAP proteins are upregulated in the aged neurons about by 20% and 44% in NeuN positive cells (Figure 4.5A, B) whereas no significant difference was seen for Piezo1 protein in aged astrocytes, but YAP protein was increased 33% in GFAP positive cells (Figure 4.6A, B). The antibody used for Piezo1 quantification was previously validated in Piezo1 knockout cells (Lee et al 2021). YAP upregulation implies the HIPPO pathway involvement, which has been previously reported for cells that reside in a stiff environment.

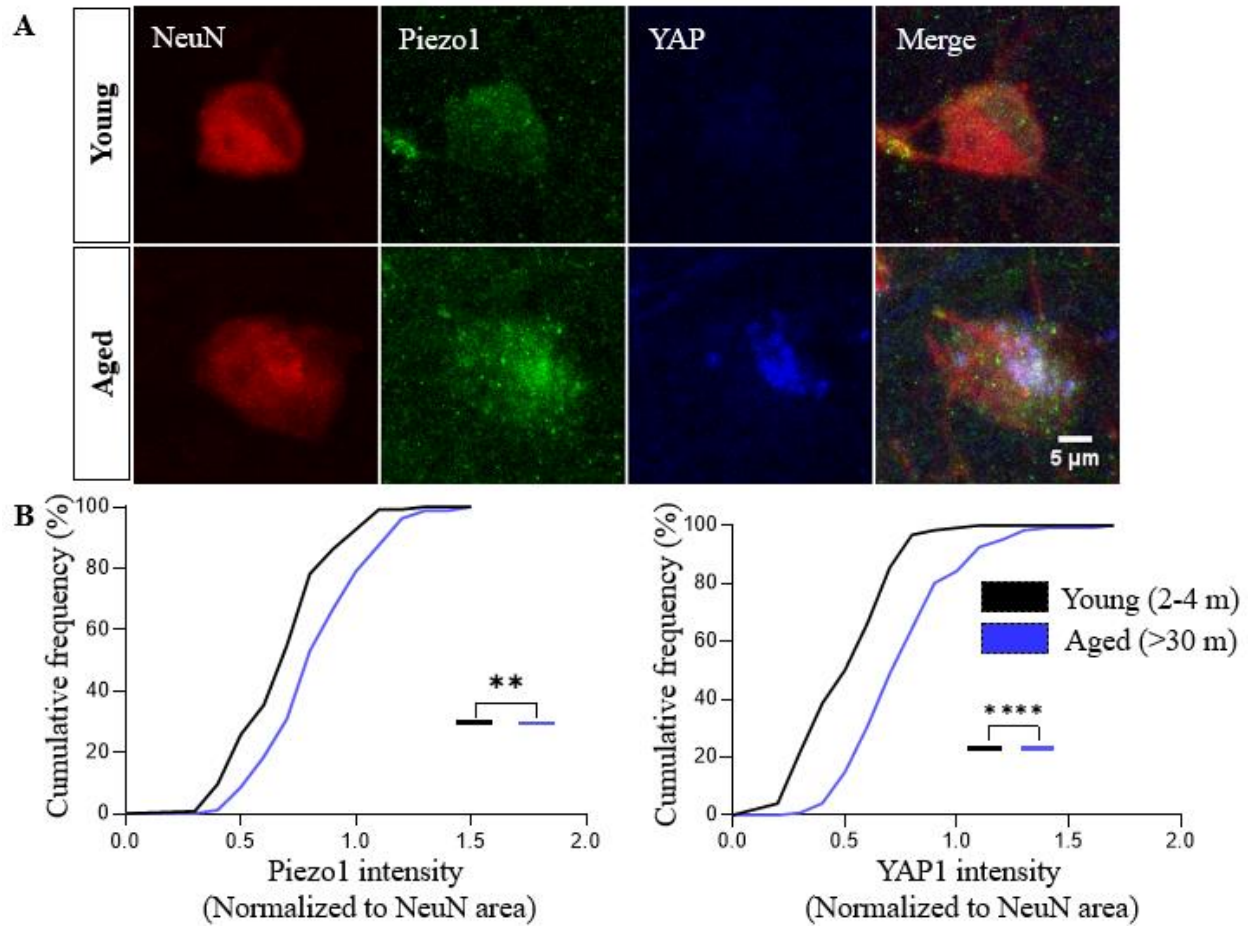


**Figure 4.5 Piezo1 protein is increased in aged neurons.** (A) Representative image of Piezo1 and YAP IHC in CA1 neurons of young and aged mice. (B) Cumulative probability functions for Piezo1 and YAP intensity values normalized to NeuN area. Kolmogorov-Smirnov's test for the comparison of cumulative frequency distributions: \*\*  $p < 0.01$ ; \*\*\*\*  $p < 0.0001$ . Young:  $n=150$ ,  $N=3$ , and aged:  $n=150$ ,  $N=3$ .  $n$  and  $N$  represent the numbers of cells and animals used for the analysis, respectively.

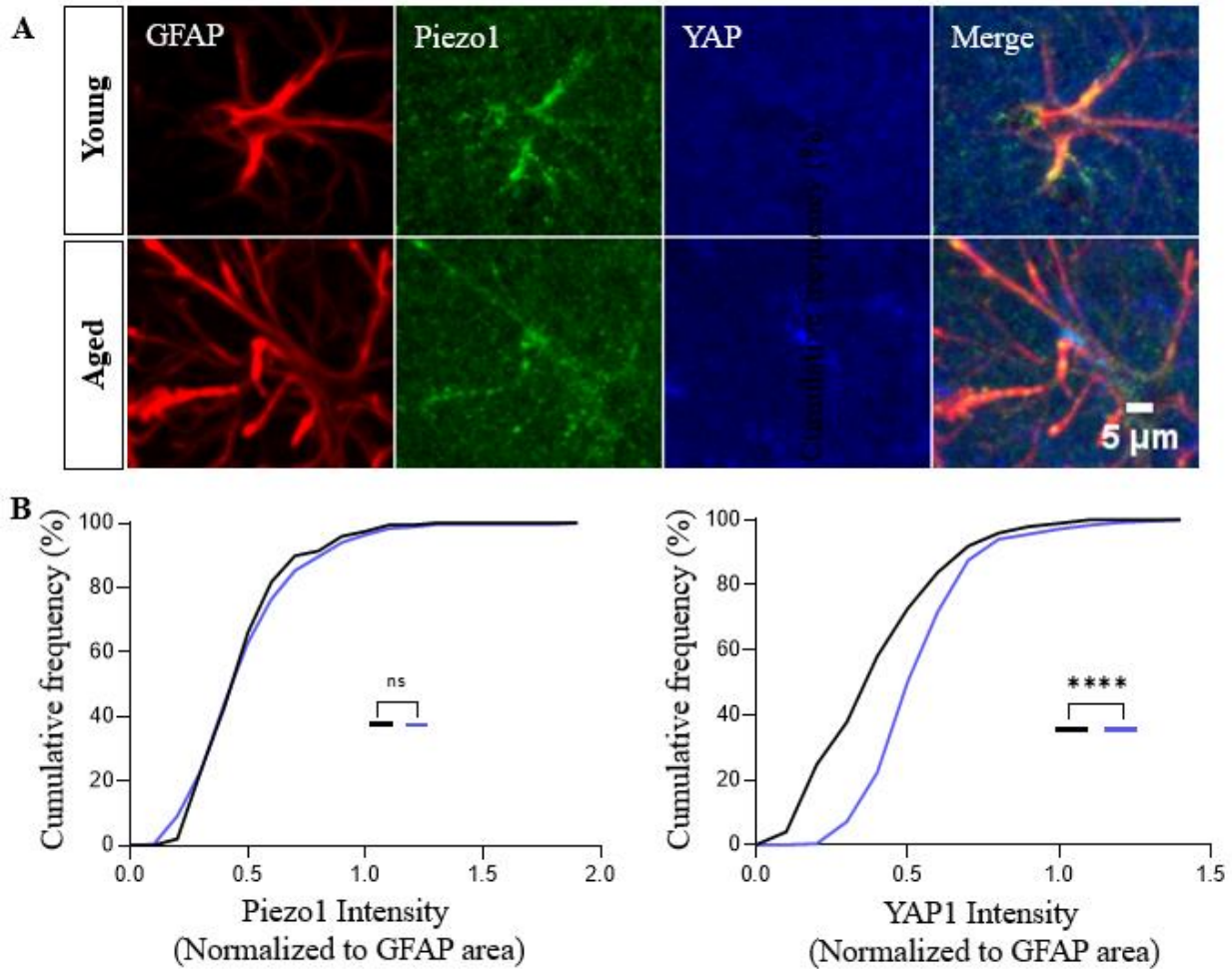


**Figure 4.6. Piezo1 protein was not increased in the aged astrocyte.** (A) Representative image of Piezo1 and YAP IHC in CA1 astrocytes of young and aged mice. (B) Cumulative probability functions for Piezo1 and YAP intensity values normalized to GFAP area. Kolmogorov-Smirnov's test for comparison of the cumulative frequency distributions: \*\*\*\*  $p < 0.0001$ . Young:  $n=200$ ,  $N=3$ , and aged:  $n=250$ ,  $N=3$ .  $n$  and  $N$  represent the number of cells and animals used for the analysis, respectively.

### 4.3 YAP/TAZ expression is decreased following Piezo1 knockdown *in vitro*

As synaptic plasticity and cognitive functions are impaired in both aged and 5xFAD mice, targeting the Piezo1 to rescue the phenotypes is reasonable. We used the shRNA approach to downregulate the *Piezo1* expression in the aged brain. For this, we generated an AAV carrying the shRNA for the *Piezo1* gene and validated it *in vitro* by qPCR in the mouse primary hippocampal cultures (Figure 4.7A). The qPCR result demonstrated that our shRNA is able to reduce the expression of *Piezo1* mRNA at least by 60% (Figure 4.7B). I also analyzed the YAP/TAZ pathway as a control for shRNA efficiency and realized that shRNA reduced the expression of the main components and downstream targets of the YAP/TAZ pathway. Downregulation for *YAP1*, *TAZ*, *CYR61*, and *CTGF* was approximately 49%, 25%, 33%, and 42%, respectively (Figure 4.7C).

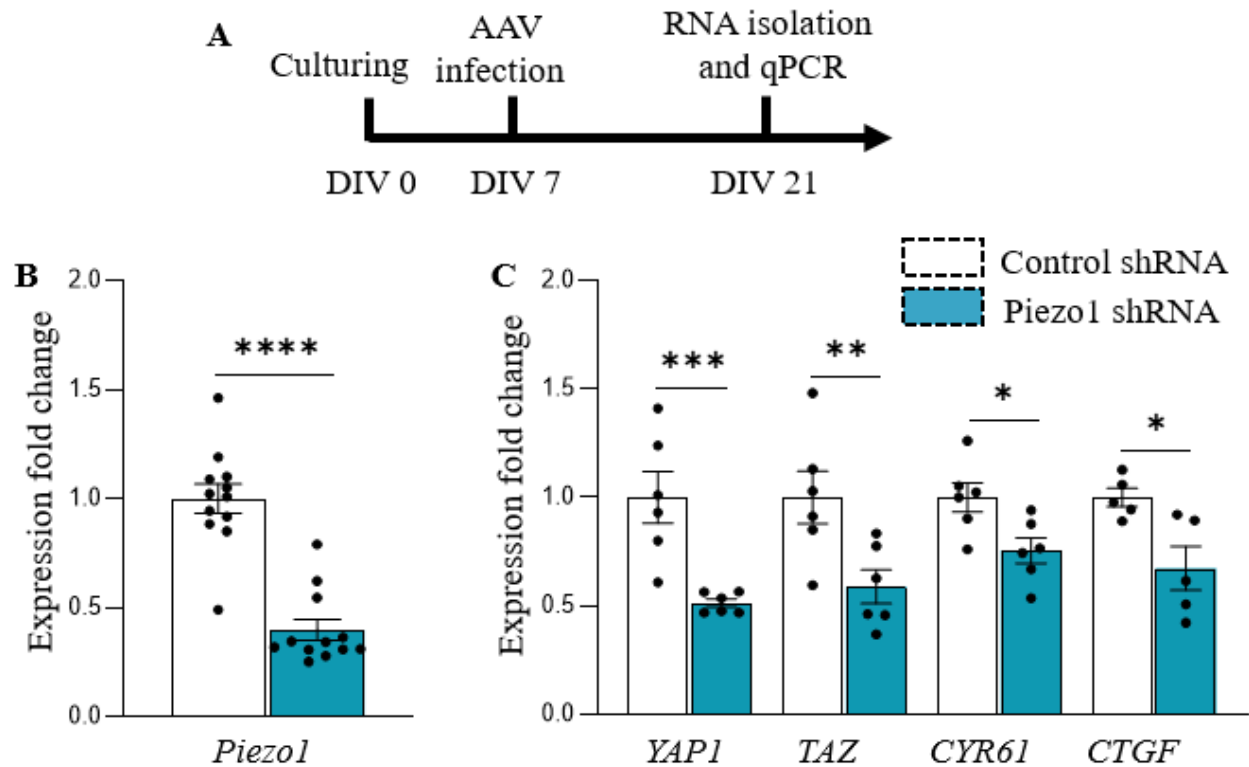


**Figure 4.7** *Piezo1* shRNA decreases mRNA levels of *Piezo1* and YAP/TAZ pathway components. (A) Timeline for the *in vitro* approach to validate the *Piezo1* shRNA. (B, C) Decreased mRNA level of *Piezo1*, *YAP*, *TAZ*, *CYR61*, and *CTGF* following shRNA treatment *in vitro*. The bar graph shows mean  $\pm$  SEM values; Unpaired t-test with Welch's correction: \* $p < 0.05$ , \*\* $p < 0.01$ , \*\*\* $p < 0.001$  and, \*\*\*\* $p < 0.0001$ .

#### 4.4 *Piezo1* knockdown changes the expression pattern of ECM molecules and ECM-related enzymes *in vitro*

Tissue homeostasis is kept by cells sensing and modifying the mechanical condition of the ECM via specialized cell-matrix interactions. To find out how *Piezo1* knockdown affects the ECM turnover, I analyzed the expression of ECM genes and genes involved in the regulation of ECM formation and remodeling like proteases (*MMP9*, *ADAMTS4*, and *ADAMTDS5*) and protease inhibitors (*TIMP1* and *TIMP3*). Interestingly, following shRNA treatment, upregulation of some ECM proteins such as *aggrecan* (197%), *brevican* (46%), and *TNR* (100%) was seen (Figure 4.8A). The qPCR results for *brevican* and *aggrecan* were further confirmed by western blot analysis from the protein lysate samples (Figure 4.8B). I also observed an increase for *HAS2* (179%), a key enzyme involved in the synthesis of hyaluronic acid, *ADAMTS5* (36%), and a decrease for *MMP9* (31%), *TIMP1* (35%), and *TIMP3* (53%) (Figure 4.8C).

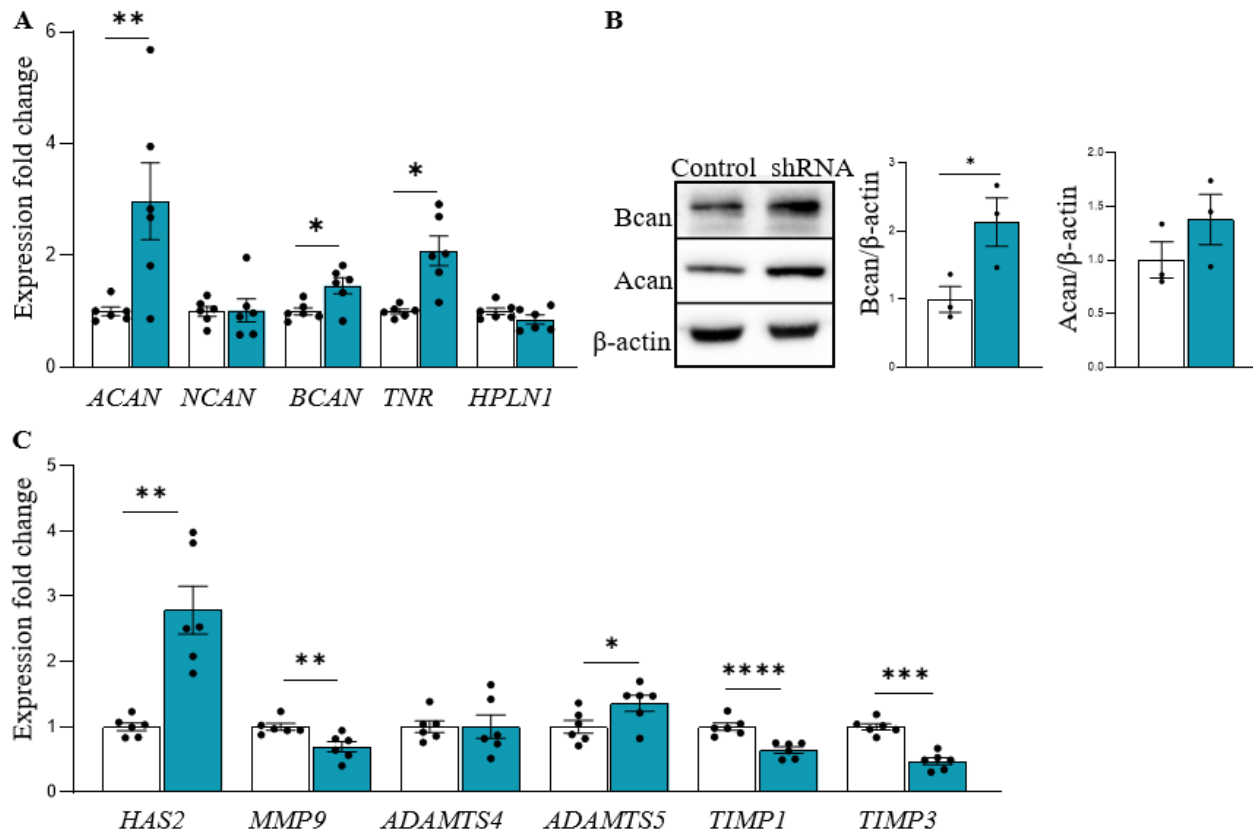


**Figure 4.8 Piezo1 knockdown changes the expression pattern of some ECM molecules and ECM-related enzymes *in vitro*.** (A) qPCR analysis revealed an elevated expression of ECM molecules after *Piezo1* knockdown. (B) Western blot analysis of two ECM proteins brevicane and aggrecan revealed an increase in the expression of brevicane. (C) The expression of several ECM-modifying enzymes was changed after *Piezo1* knockdown. Bar graphs show mean  $\pm$  SEM values; Unpaired t-test with Welch's correction: \* $p < 0.05$ , \*\* $p < 0.01$ , \*\*\*\* $p < 0.0001$ .

#### 4.5 Aging-mimicking activation of Piezo1 impairs synaptic plasticity in the young hippocampus

Following the upregulation of Piezo1 in the aged hippocampus, we hypothesized that Piezo1 chemical activation could mimic this aspect of aging and lead to synaptic dysfunction in young mice. To test this hypothesis, I incubated hippocampal slices with Yoda1, a specific Piezo1 chemical activator for at least 3 hours to simulate an aged condition accompanied by chronic activation of Piezo1 and did subsequent analyses using qPCR, western blot, IHC, and electrophysiology approaches. As Piezo1 is permeable for  $Ca^{2+}$ , it is plausible to expect that Yoda1 can increase the basal resting calcium level in the pyramidal neurons in the CA1. In collaboration with Prof. Christian Henneberger (Institute of Cellular Neurosciences, University of Bonn) we performed FLIM measurements of intracellular  $Ca^{2+}$ . The result shows that resting somatic calcium concentration significantly increased following incubation of hippocampal slices with Yoda1 (Figure 4.9A, B), demonstrating Piezo1's functional importance for neurons.

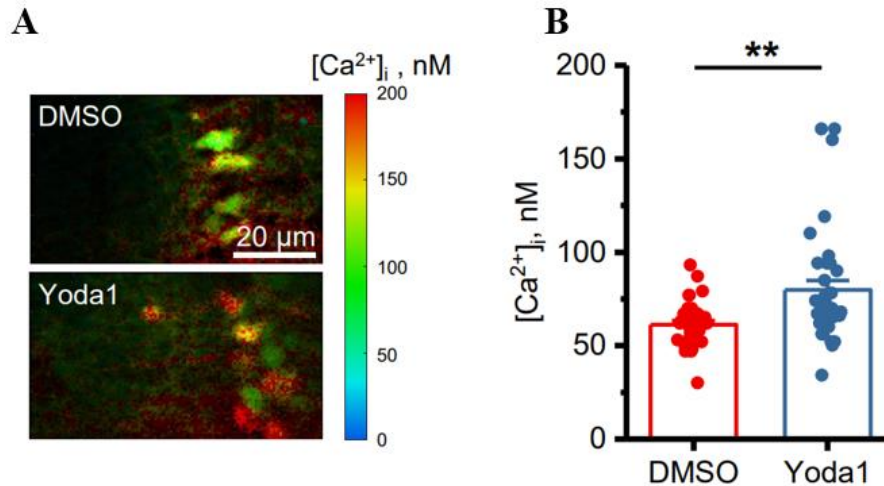


**Figure 4.9 Piezo1 activation increases the resting intracellular calcium level.** (A) Representative FLIM image of the pyramidal neuron in the CA1 treated with DMSO and Yoda1. (B) Calculated resting calcium in both groups. **\*\*** $p < 0.01$ , two-sample t-test. DMSO:  $n=30$ ,  $N=4$ ; Yoda1:  $n=36$ ,  $N=4$ .  $n$  and  $N$  represent the number of cells and animals used for the analysis, respectively.

Based on the previously published studies in non-neuronal cells (Blythe et al 2019, Fu et al 2021, Liu et al 2021b), we realized that potential pathways downstream of Piezo1 activation are the p38 MAPK and calpain pathways. P38 MAPK has a central role in both neuroinflammation and synaptic plasticity. Calpain also plays a fundamental role in synaptic plasticity by modifying a few targets including the spectrin-based cytoskeleton and Glun2A. Hence, we analyzed the synaptic plasticity using fEPSPs recordings (Figure 4.10A) to answer the questions of whether Piezo1 activation will lead to synaptic plasticity impairment and if the plasticity could be rescued by applying p38 MAPK and calpain inhibitors. First, I found that basal synaptic transmission is impaired in the Yoda1-treated slices compared to DMSO (Figure 4.10B). A positive tendency toward improvement was seen in the SKF86002 group, however, the impairment can not be rescued by SKF86002 and calpain inhibitor E64 (Figure 4.10B). No significant differences were seen following the PPF analysis between groups (Figure 4.10C).

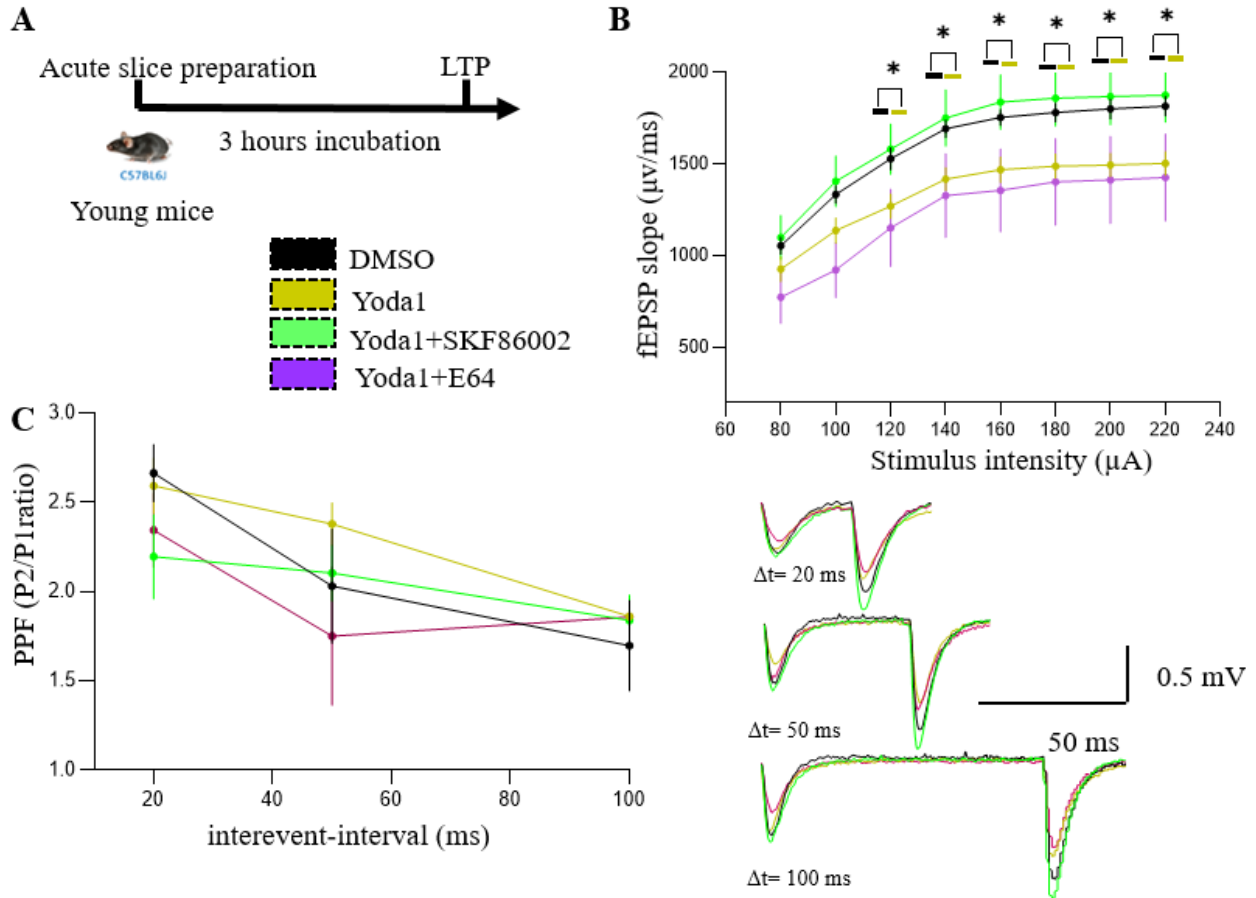


**Figure 4.10 Piezo1 activation impairs slightly basal synaptic transmission and does not change the PPF in the young hippocampus.** (A) Timeline for chemical treatment of the hippocampal slices and LTP recordings. (B) The stimulus-response curve was constructed by applying increasing current pulses and calculating the slope of evoked responses. Holm-Sidak's multiple comparisons after two-way RM ANOVA. (C) PPF calculation, as the ratio of the slopes of the fEPSPs elicited by the second and first pulses given with 20, 50, and 100 ms intervals and representative traces showing PPF in all conditions. Holm-Sidak's multiple comparisons after RM ANOVA. DMSO: n=9; Yoda1: n=9; Yoda1+SKF86002: n=6; Yoda1+E64: n=5. n represents the number of hippocampal slices used for the analysis.

Analyzing the burst-induced AMPA and NMDA receptor-mediated fEPSP components during TBS showed no significant difference between DMSO and Yoda groups, however, a slight increase in both components was observed in the SKF86002 and E-64 groups (Figure 4.11A, B). LTP analysis revealed a significant decrease in the normalized fEPSPs slope in the Yoda1-treated group compared to the DMSO group, which could be rescued by co-treatment with the p38 inhibitor SKF 86002, and also by the calpain inhibitor E-64 (Figure 4.11C, D).

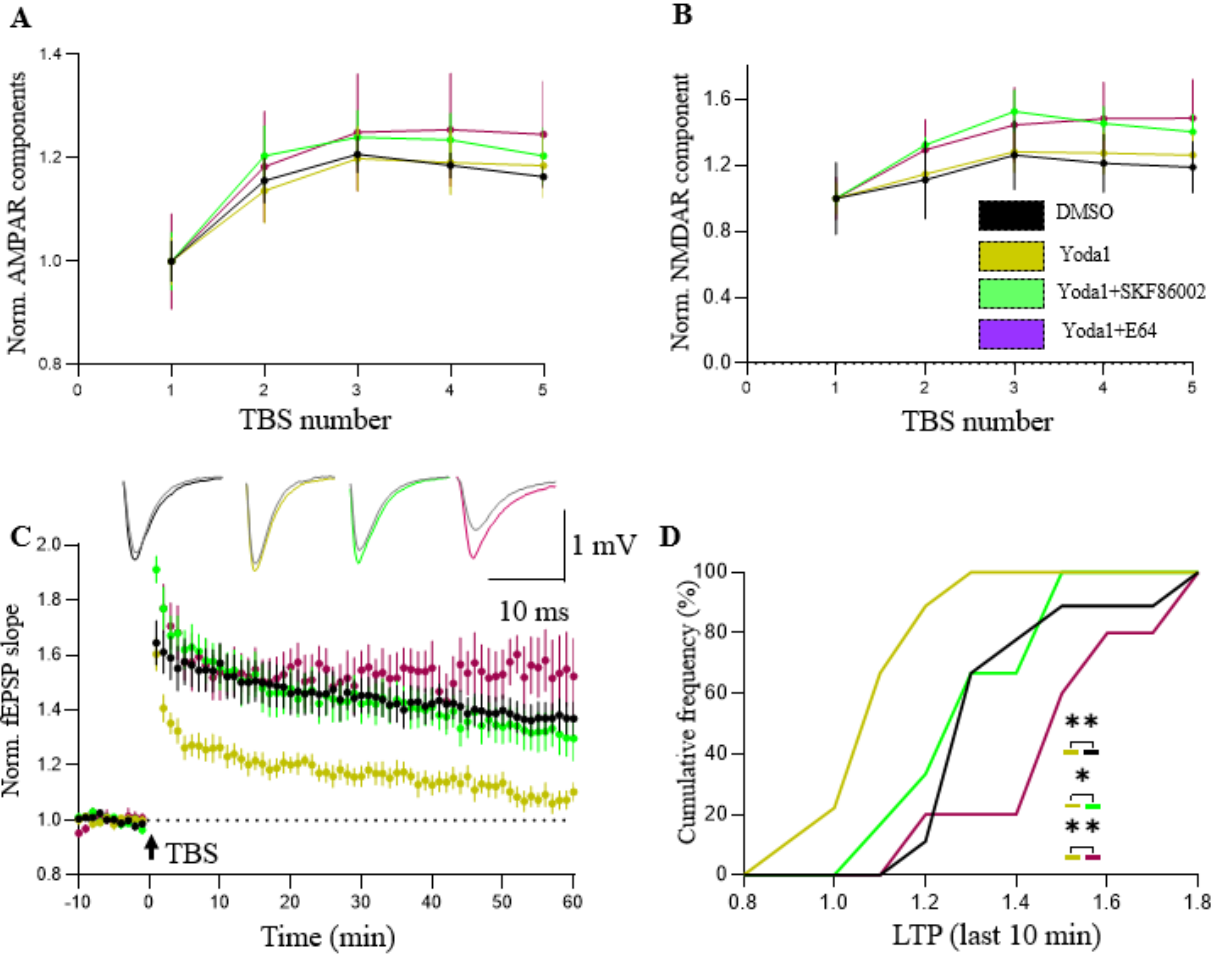


**Figure 4.11 Piezo1 activation impaired LTP which could be rescued by p38 and calpain inhibitors. (A, B)** Normalized burst-induced AMPA and NMDA receptors component during LTP induction. No significant differences were detected by Holm-Sidak's multiple comparisons two-way mixed ANOVA. **(C)** The LTP graph of normalized basal and post-TBS fEPSPs slope. LTP was calculated by comparing the mean slope of fEPSPs obtained 50-60 minutes after TBS to the mean slope of fEPSPs recorded 10 minutes before TBS. **(D)** Cumulative frequency graph of LTP values obtained in each group. Kolmogorov-Smirnov's test was used for the comparison of cumulative frequency distributions: \*  $p < 0.05$ . DMSO  $n=9$ , Yoda1  $n=9$ , Yoda1+SKF86002  $n=6$ , Yoda1+E64  $n=5$ .  $n$  represents the number of hippocampal slices used for the analysis.

#### 4.6 Piezo1 activation mimics the aged brain and stimulates the p38 MAPK pathway

To dissect the molecular mechanism underlying the synaptic impairment after Yoda1 treatment, I did a series of western blot and IHC experiments (Figure 4.12A). Some Piezo1-dependent molecular pathways were proposed previously in different cell types including p38 MAPK and calpain pathways (Blythe et al 2019, Zhang et al 2021). Western blot analysis following hippocampal slice incubation with Yoda1 demonstrated a 41% upregulation in the phosphorylated form of p38 when normalized to total protein (Figure 4.12B). Yap phosphorylation also decreased up to 55% when normalized to total protein (Figure 4.12C). I also observed degradation in the full length of  $\alpha$ II-spectrin which leads to an increased level of the spectrin breakdown products (SBDPs) up to 45% (Figure 4.12D).

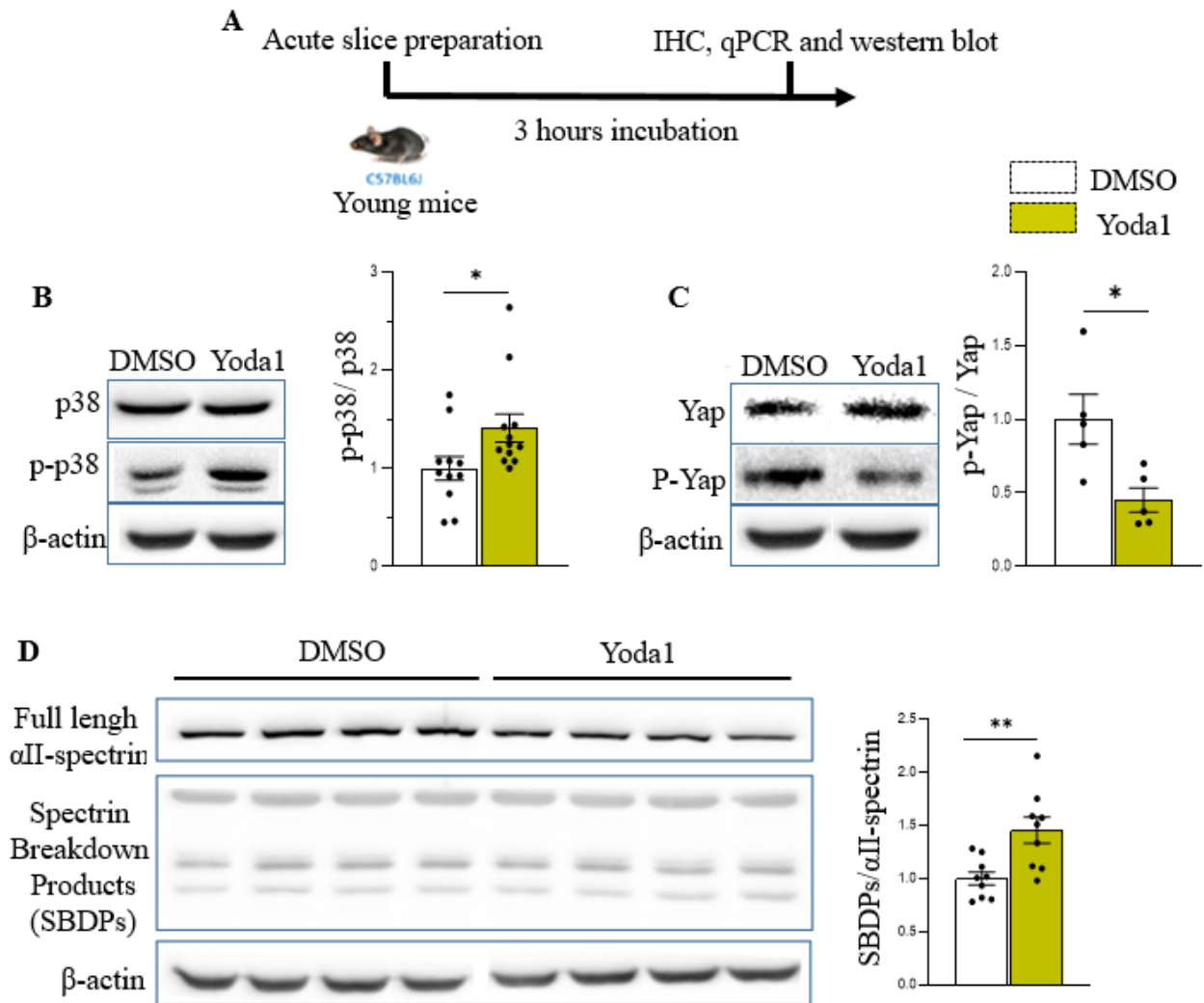


**Figure 4.12 Piezo1 activation increases p38 MAPK, decreases YAP phosphorylation, and cleaves αII-spectrin.** (A) Timeline for chemical treatment of the acute hippocampal slices and subsequent experiments. (B, C, D) Representative western blot images and subsequent analysis for the protein levels of p38, phosphorylated p38, YAP, phosphorylated YAP, αII-spectrin full length, and its breakdown products in acute hippocampal slices treated with DMSO and Yoda1. The bar graph shows mean ± SEM values; unpaired t-test \*p < 0.05, \*\*p < 0.01.

I further analyzed the mRNA level of the *YAP*, *TAZ*, and its downstream targets and also inflammatory markers *TNFα* and *IL1β*, which may increase as a consequence of p38 phosphorylation. At the mRNA level, there was no significant difference in *Piezo1*, *YAP*, *TAZ*, and *CTGF* expression, however, I observed a tendency for upregulation in the expression of *CYR61* (65%) (Figure 4.13A). Analysis of inflammatory markers showed a significant increase in *IL1β* (152%) but not in *TNFα* mRNA level (Figure 4.13B).

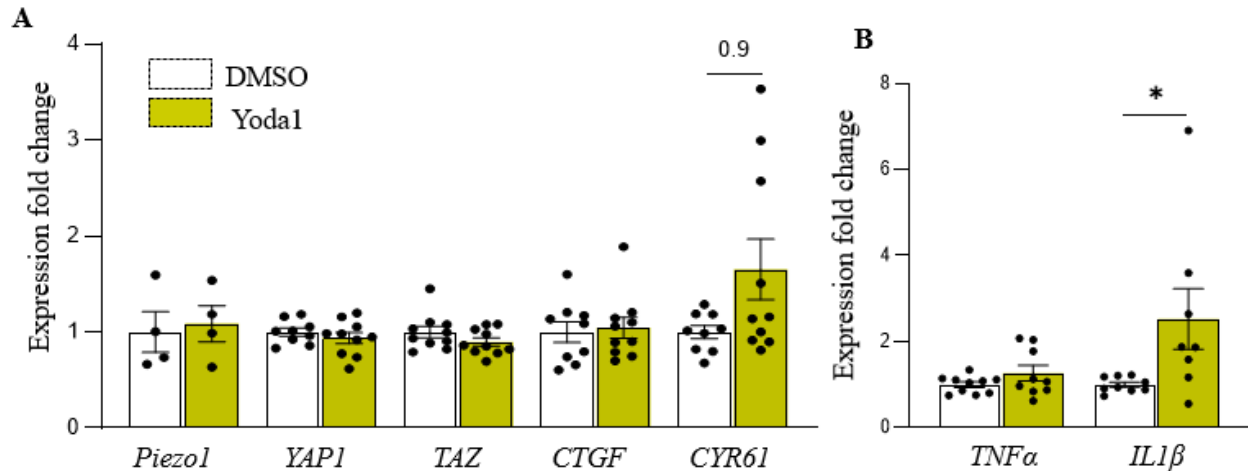


**Figure 4.13 Piezo1 activation by Yoda1 in hippocampal slices slightly increased expression of Yap1-downstream gene *CYR61* and inflammatory marker *IL1β*.** (A) A tendency in the upregulation of the mRNA level of the YAP downstream target gene, *CYR61* was seen after Yoda1 treatment. No significant difference was seen for other genes; Bar graph shows mean ± SEM values. Unpaired t-test with Welch's correction. For the *CYR61* gene, Mann-Whitney test was used. (B) *IL1β* mRNA level increased after acute Yoda1 treatment in the young hippocampus slices. The bar graph shows mean ± SEM values; Unpaired t-test with Welch's correction: \* $p < 0.05$ .

Next, I did immunostaining on the hippocampal tissues treated with Yoda1 and DMSO to further confirm the elevation of the phosphorylated p38 in both neurons and astrocytes. I detected an upregulation in the intensity of phosphorylated p38 in both neurons (75%) and astrocytes (20%) in the *striatum pyramidale* of the CA1 region (Figure 4.14A, B), as a confirmation of what I observed in the western blot before.

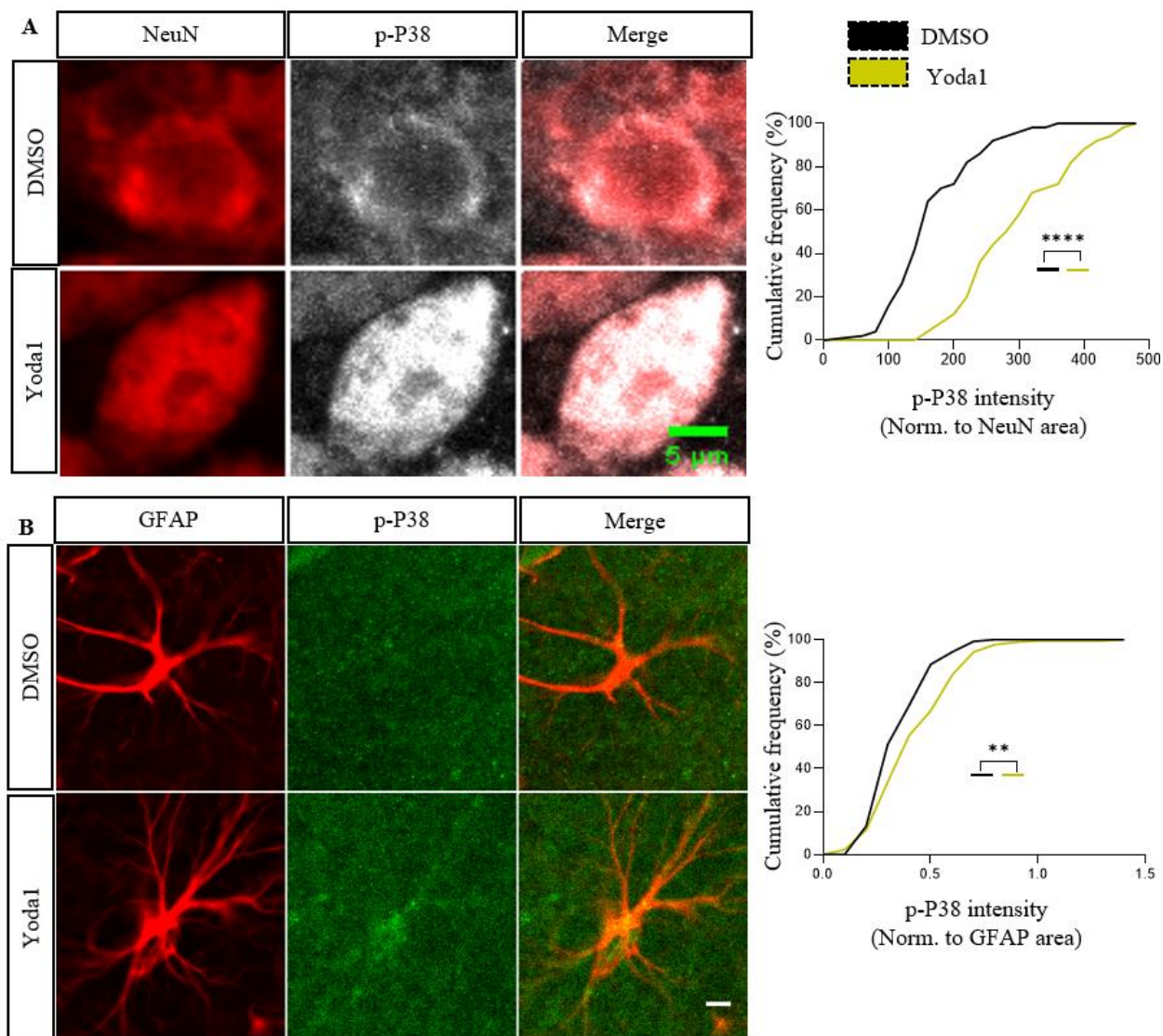


**Figure 4.14 Piezo1 activation increases p38 phosphorylation in both neurons and astrocytes.** (A) Representative 40 $\times$  images of NeuN $^{+}$  neurons in the *striatum pyramidale* of the young hippocampus treated with DMSO and Yoda1 with subsequent analysis showing an increase in the p-p38 intensity (Scale bar; 5  $\mu$ m). (B) P-p38 intensity is enhanced in the CA1 astrocytes marked by GFAP (Scale bar; 5  $\mu$ m). Kolmogorov-Smirnov's test was used for the comparison of cumulative frequency distributions: \*\*p < 0.01, and \*\*\*\*p < 0.0001. For each group, 3 hippocampal slices from 3 different animals were used for the staining, and from each slice, 2 images from the CA1 region were captured for final analysis.

#### 4.7 Piezo1 activation impairs chemical LTP (cLTP) induction in the young hippocampus

We employed chemical LTP in hippocampal slices to correlate the Piezo1 activity and changes in synaptic transmission. The cLTP was generated by perfusing the acute slices for 15 minutes with an Mg-free ACSF solution containing rolipram (100 nM), forskolin (50  $\mu$ M), and picrotoxin (100  $\mu$ M). This approach raises the amount of cAMP followed by increased network activity which ultimately results in a tetanic-like stimulation in the excitatory synapses in the hippocampus. Hippocampal slices treated with Yoda1 showed

an impaired potentiation in the mean slope of fEPSPs was recorded 80-90 minutes after the beginning of LTP induction when normalized to the averaged slope before stimulation (Figure 4.15A, B).

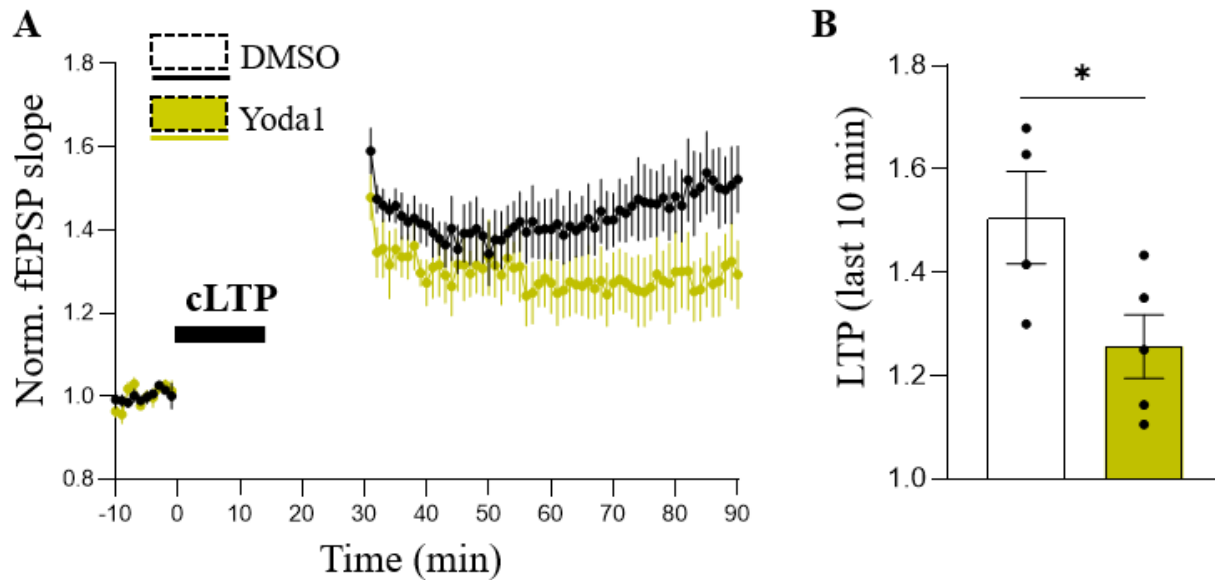


**Figure 4.15 Yoda1 application impaired chemical LTP in young hippocampal slices.** (A) The LTP graph of normalized basal and post-cLTP fEPSPs slopes. LTP was calculated by comparing the mean slope of fEPSPs obtained 80-90 minutes after the beginning of cLTP induction relative to the mean slope of fEPSPs recorded 10 minutes before cLTP. (B) The LTP level was calculated by comparing the mean slope of fEPSPs recorded 80-90 minutes after cLTP to the mean slope of fEPSPs recorded 10 minutes before cLTP. Unpaired t-test with Welch's correction: \*  $p < 0.05$ . DMSO:  $n=4$ , and Yoda1:  $n=5$ .  $n$  represents the number of hippocampal slices used.

#### 4.8 Piezo1 activation mimics aging in the brain and reduces the CaMKII phosphorylation

CaMKII is known as a central regulator of synaptic plasticity for a long time. It enhances synaptic transmission and is necessary for LTP induction and maintenance (Tao et al 2021). Acute CaMKII inhibition erases LTP, but transitory CaMKII inhibition promotes LTP. With this knowledge, I did immunostaining in the activated (phosphorylated at Thr286) form of CaMKII (p-CaMKII) in pyramidal neurons of the CA1 region as a marker for synaptic plasticity. I found that the intensity of the p-CaMKII decreased significantly (47%) in the slices treated with Yoda1 (Figure 4.16).

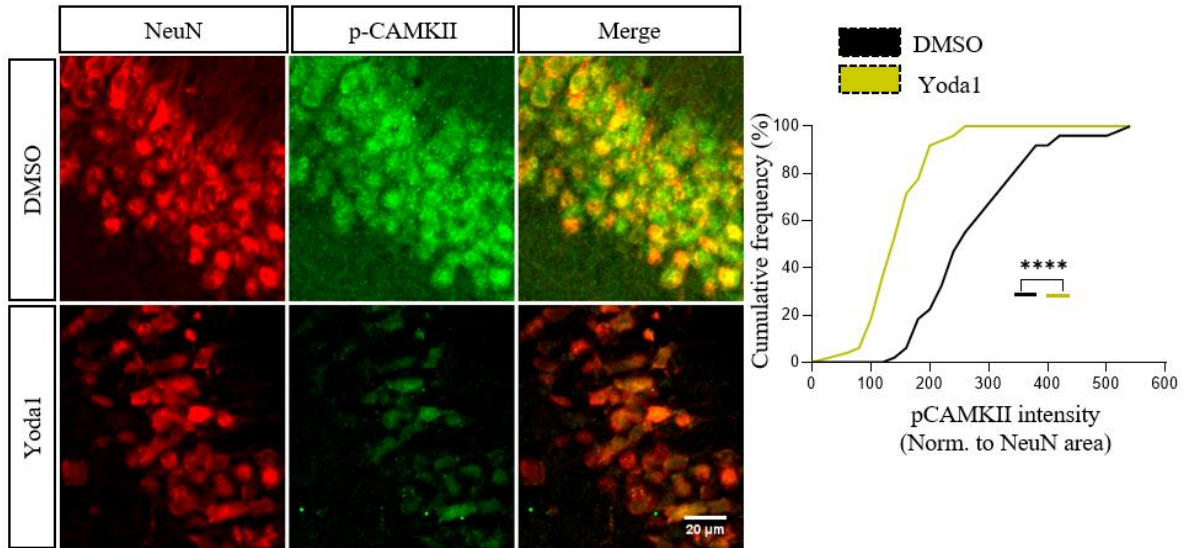


**Figure 4.16 Piezo1 activation decreased CaMKII phosphorylation (Thr286).** Young hippocampal slices treated with Yoda1 show decreased the p-CaMKII levels in the CA1 neurons marked by NeuN. Kolmogorov-Smirnov's test was used for the comparison of cumulative frequency distributions: \*\*\*\* p < 0.0001. For each group, 2 hippocampal slices from 2 different animals and 50 NeuN positive cells were used for the staining. (Scale bar 20  $\mu$ m).

#### 4.9 Synaptic plasticity is impaired in the aged mice compared to the young mice

To establish analysis of synaptic plasticity in aged mice, I did a series of fEPSPs recordings in the *stratum radiatum* of the CA1 region of >30 M old mice. I measured both pre- and postsynaptic changes by analyzing the paired-pulse facilitation and fEPSPs changes during LTP induction, respectively. Interestingly, no significant difference was seen in basal synaptic transmission (Figure 4.17A). This indicates no changes in synapse numbers in both young and aged groups. However, analysis for PPF showed a significant decrease in the ratio of second to first fEPSPs slopes for 20 ms inter-event interval (Figure 4.17B). TBS-induced activation of AMPA and NMDA receptors did not show a significant difference when the area of the AMPA and NMDA receptor-mediated components was analyzed (Figure 4.17C, D). LTP levels were analyzed using the normalized mean slope of fEPSPs recorded 50 to 60 min after induction of LTP relative to the mean baseline slope. In this case, an impairment in the LTP value (14.7% vs. 34.6 %) was seen in the aged mice as compared to young mice (Figure 4.17E, F).

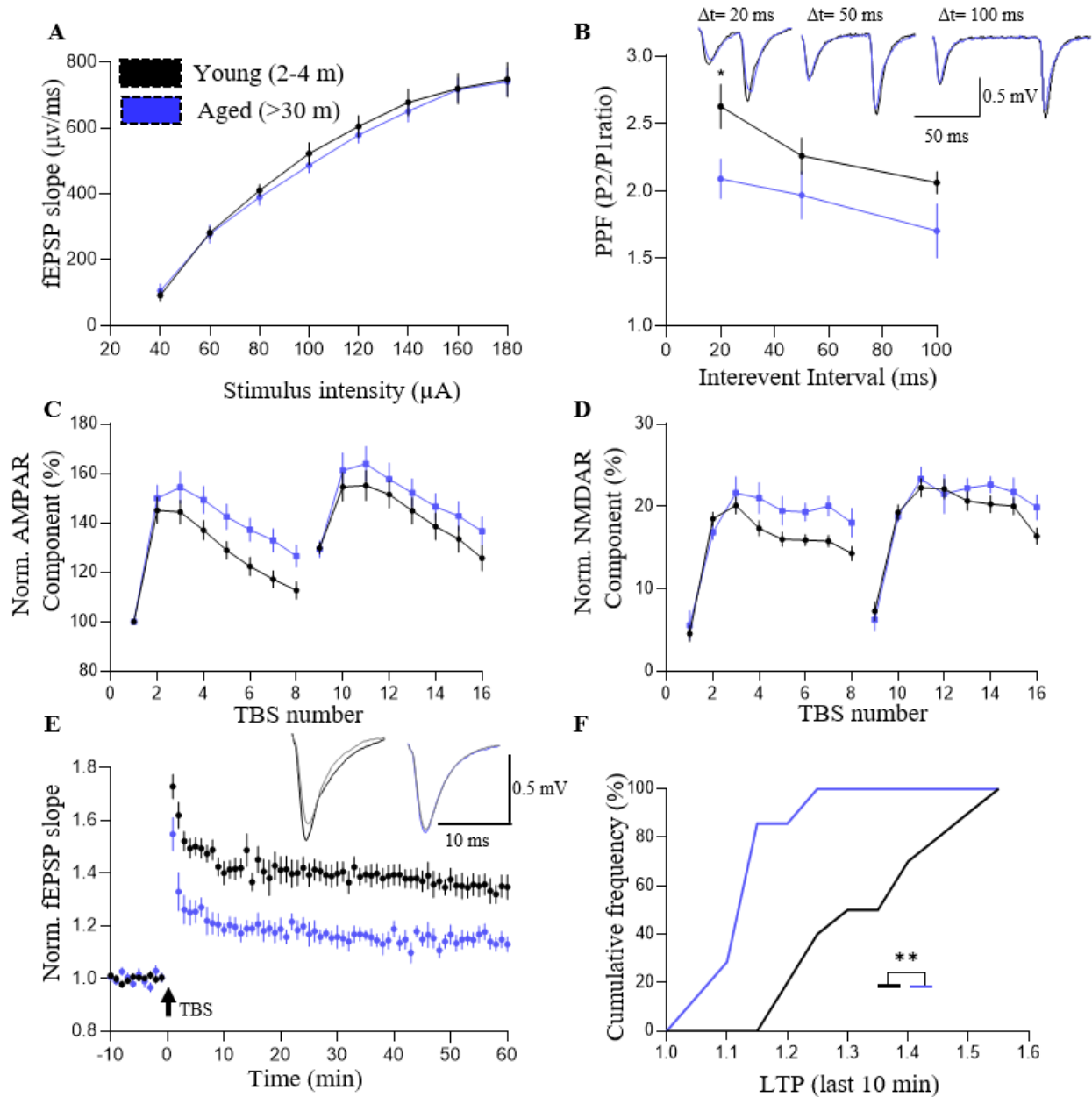


**Figure 4.17** (A) The stimulus-response curve was computed by applying increasing current pulses and calculating the slope of evoked responses. Holm-Sidak's multiple comparisons two-way RM ANOVA. (B) PPF calculation, as the ratio of the slopes of the fEPSPs elicited by the second and first pulses given with 20, 50, and 100 ms intervals. Holm-Sidak's multiple comparisons after RM ANOVA. (C, D) Normalized burst-induced AMPA and NMDA receptor activity during LTP induction. No significant differences were observed when analyzed by two-way RM ANOVA. (E) The LTP graph of normalized fEPSPs slope. The LTP level was calculated by comparing the mean slope of fEPSPs recorded 50-60 minutes after TBS to the mean slope of fEPSPs recorded 10 minutes before TBS. (F) Cumulative probability of LTP values obtained in each group. Kolmogorov-Smirnov's test was used for the comparison of cumulative frequency distributions: \*\*  $p < 0.01$ . Young mice:  $n=10$ ; aged mice:  $n=7$ ,  $n$  represents the number of hippocampal slices used.

#### **4.10 Piezo1 knockdown tends to improve the impaired cognitive function in aged mice**

Spatial memory and navigation are notably linked to the dorsal portion of the hippocampus (Lee et al 2019). The dorsal hippocampus plays a significant role in NOLT, which assesses an individual's capacity to recall the location of a novel object in a setting they are acquainted with (Asgeirsdottir et al 2020). This area stores and retrieves spatial information, enabling mammals to detect changes in the locations of objects within a specific environment. Spatial memory and the capacity to perform NOLT can be hampered by disturbances in the dorsal hippocampus (Broadbent et al 2004).

To investigate the beneficiary effects of Piezo1 knockdown in the aged hippocampus, we performed behavioral analysis in the aged mice injected with control and Piezo1 shRNA (Figure 4.18A). We used the NOLT together with the NORT to study spatial memory, object discrimination, and recognition memory. We have previously published that there is a difference in the hippocampus-dependent NOLT assay between young and aged mice (Baidoe-Ansah et al 2022). We initially analyzed mice for motor or emotional changes by using the open-field test. The results of this test in two groups of aged mice showed no significant differences between Piezo1 shRNA and control groups. No statistical distinction suggests that the locomotor activity and exploratory behavior of these two groups of aged mice are comparable (Figure 4.18B). Additionally, I did not find any difference in time spent in the central area between groups (Figure 4.18B).

Then, I compared the discrimination ratio for groups after injection and noticed a tendency toward improvement in the aged Piezo1\_shRNA mice compared to aged control mice ( $p = 0.1$ ) (Figure 4.18C). This suggests that the Piezo1 knockdown may enhance hippocampus-dependent spatial discrimination and memory, but more data should be collected for the final conclusion. Next, I performed the NORT test and observed no difference in time spent exploring both familiar and novel objects between groups (Figure 4.18D). It is noteworthy to mention that whereas the NOLT test has a clear hippocampal dependency that is well documented, the NORT is perirhinal cortex-dependent and less hippocampus-dependent (Aggleton et al 2010). This needs to be considered while interpreting the NORT data after hippocampal injection of Piezo1 shRNA.

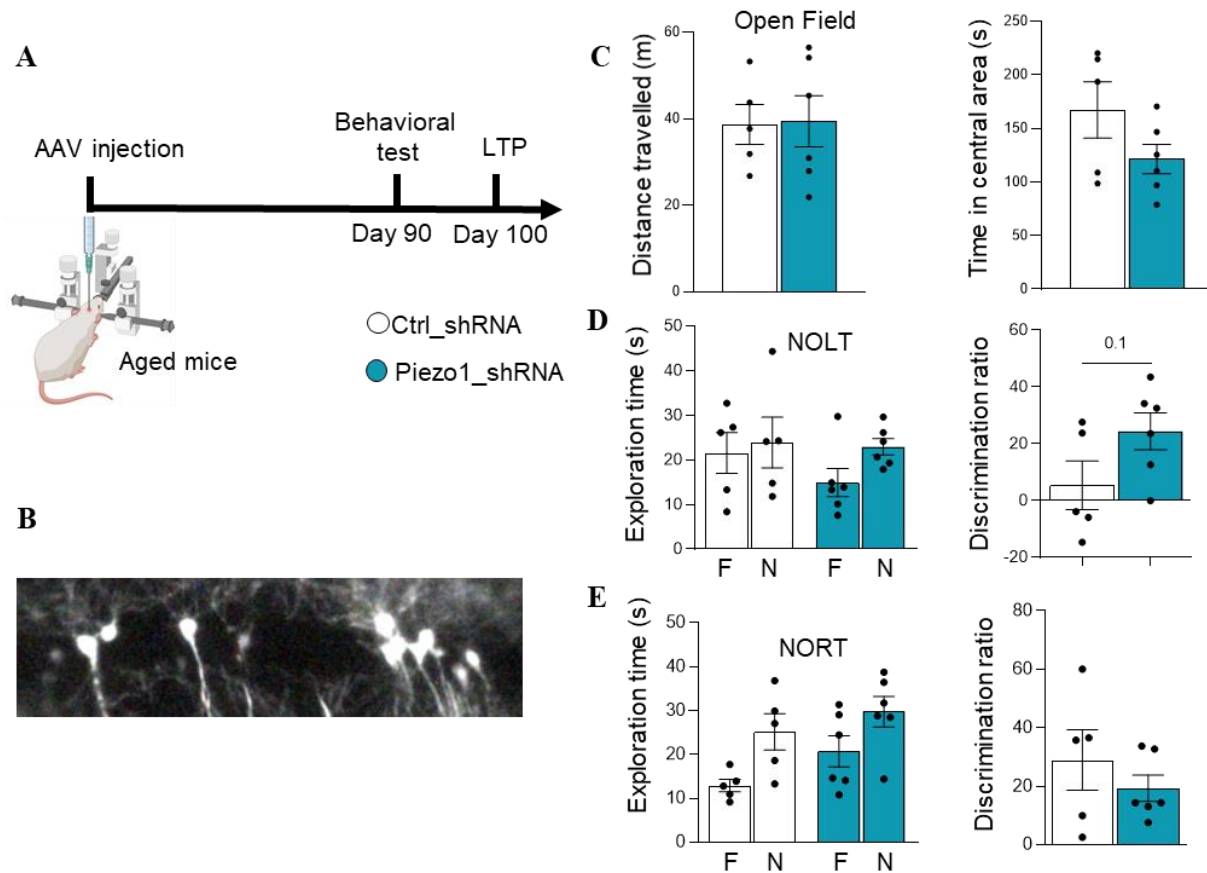


**Figure 4.18 Piezo1 knockdown tends to improve hippocampal function in aged mice.** (A) Timeline of experiments and paradigm used for the behavioral analysis. (B) A representative epifluorescent image of GFP expression in the dorsal CA1 region of injected mice. (C) Open-field test graphs showing distances traveled and time spent at the central areas for both groups. The bar graph shows mean  $\pm$  SEM values, t-test. (D) The exploration time spent in both familiar and non-familiar locations and the calculated discrimination ratio in NOLT. The bar graphs show mean  $\pm$  SEM values, unpaired t-test was used for statistical analysis. (E) The exploration time spent in both familiar and non-familiar objects and the calculated discrimination ratio in NORT. The bar graphs show mean  $\pm$  SEM values, unpaired t-test was used for statistical analysis. Aged control mice: n=5; aged Piezo1 shRNA mice: n=6.

After performing the behavioral test and seeing a tendency for improvement in cognitive function, I did fEPSPs recording in the CA1 region to study the synaptic plasticity changes in aged mice treated with Piezo1 shRNA (Figure 4.19A). There was no significant difference between the groups in the basal synaptic transmission (Figure 4.19B). TBS-elicited AMPA and NMDA receptor-mediated components also were not statistically significant (Figure 4.19C, D). However, the fEPSPs slope calculated for the last 10 minutes of the 1-hour recording after TBS showed a significant difference in aged mice injected with Piezo1 shRNA (Figure 4.19E, F).

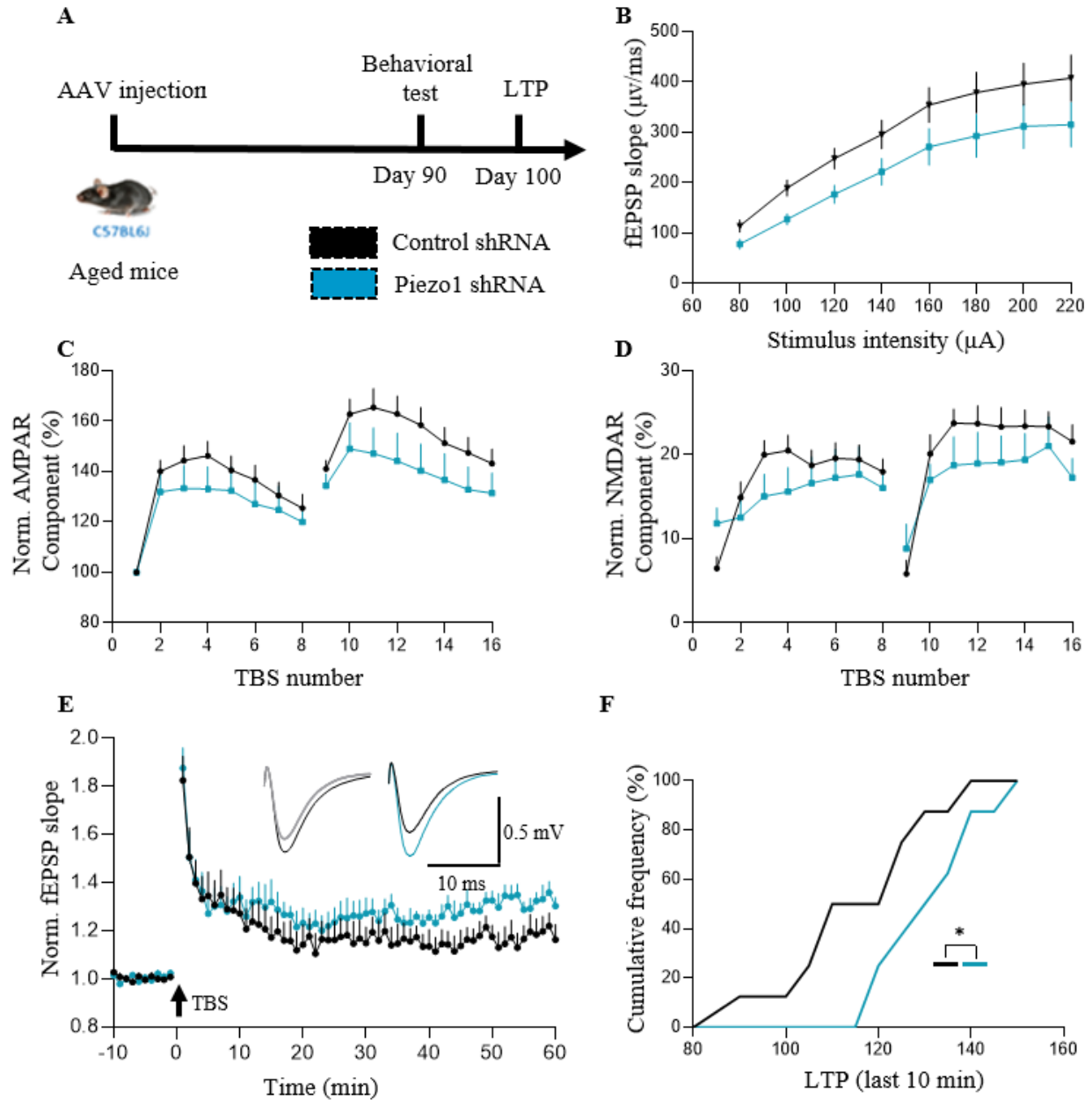


**Figure 4.19 Piezo1 knockdown rescues impaired synaptic plasticity in the aged mice.** (A) Timeline for AAV injection into hippocampal CA1 and LTP experiments. (B) The stimulus-response curve was computed by applying increasing current pulses and calculating the slope of evoked responses. No significant difference was seen after Holm-Sidak's multiple comparisons two-way RM ANOVA. (C, D) Normalized TBS-induced AMPA and NMDA receptors components during LTP induction. No significant difference was detected by two-way RM ANOVA. (E) The LTP graph of normalized fEPSPs slopes. LTP was calculated by comparing the mean slope of fEPSPs recorded 50-60 minutes after TBS to the mean slope of fEPSPs recorded 10 minutes before TBS. (F) Cumulative probability of LTP values obtained in each group. Kolmogorov-Smirnov's test was used for the comparison of cumulative frequency distributions: \*  $p < 0.05$ . Aged control mice:  $n=8$ ; aged Piezo1 shRNA mice:  $n=8$ .  $n$  represents the number of hippocampal slices used.

#### 4.11 ECM cleavage downregulates Piezo1 expression *in vitro* and rescues synaptic plasticity deficits in aged mice *ex vivo*

To analyze the ECM accumulation effects on the mechanotransduction and Piezo 1 function, we cleaved the mature ECM in the primary hippocampal culture by overexpressing ADAMTS 5 enzyme (Figure 4.20A). We chose this enzyme for several reasons. ADAMTS-5 has a stronger aggrecanase activity than other proteoglycanases. Under physiological conditions, ADAMTS-5 aggrecan-cleaving activity is more than 1,000 times that of ADAMTS-4. ADAMTS-5 also cleaves additional lecticans such as versican and brevican, although it has little effect on fibronectin. I found that *ADAMTS5* overexpression results in *Piezo1* (36%) and *Piezo2* (60%) downregulation (Figure 4.20B) and was accompanied by decreased expression of the main and downstream components of the YAP/TAZ pathway (Figure 4.20C).

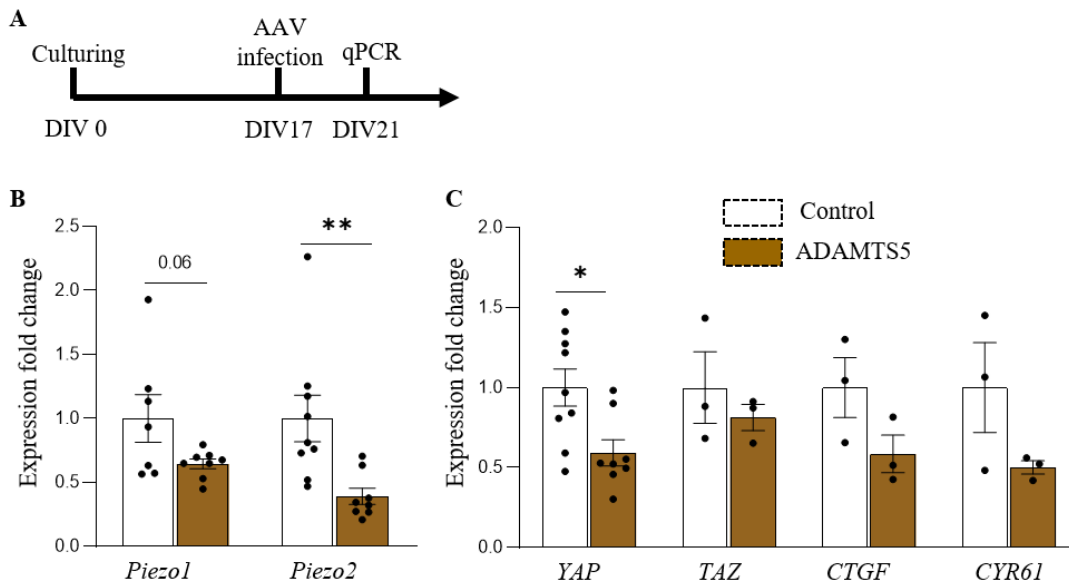


**Figure 4.20 Gene expression analysis after *ADAMTS5* overexpression in hippocampal primary cultures.** (A) Timeline for AAV infection of hippocampal cultures and subsequent experiment. (B, C) The mRNA expression of the *Piezo1*, *Piezo2*, *YAP1* and *TAZ* and its downstream target genes *CYR61* and *CTGF* are decreased after *ADAMTS5* overexpression in the primary hippocampal cultures compared to the control condition. The bar graph shows mean  $\pm$  SEM values; Holm-Sidak's multiple comparisons test: \* $p < 0.05$ , \*\* $p < 0.01$ .

To test whether ECM cleavage will rescue the synaptic plasticity impairment in the aged mice, in collaboration with David Baidoe-Ansah (DZNE, Magdeburg), we injected AAV for overexpression of ADAMTS5 in the CA1 region of the hippocampus (Figure 4.21A). Two weeks post-injection, I did fEPSPs recordings to analyze basal synaptic transmission, PPF, TBS, and LTP. No significant differences in basal transmission, PPF, and activation of AMPA and NMDA receptors during TBS were seen (Figure 4.21B-E). However, the average fEPSPs slope of the last 10 minutes of 1-hour recording after induction of LTP

was significantly increased in the ADAMTS5 injected aged mice as compared to control aged mice (Figure 4.21F, G).

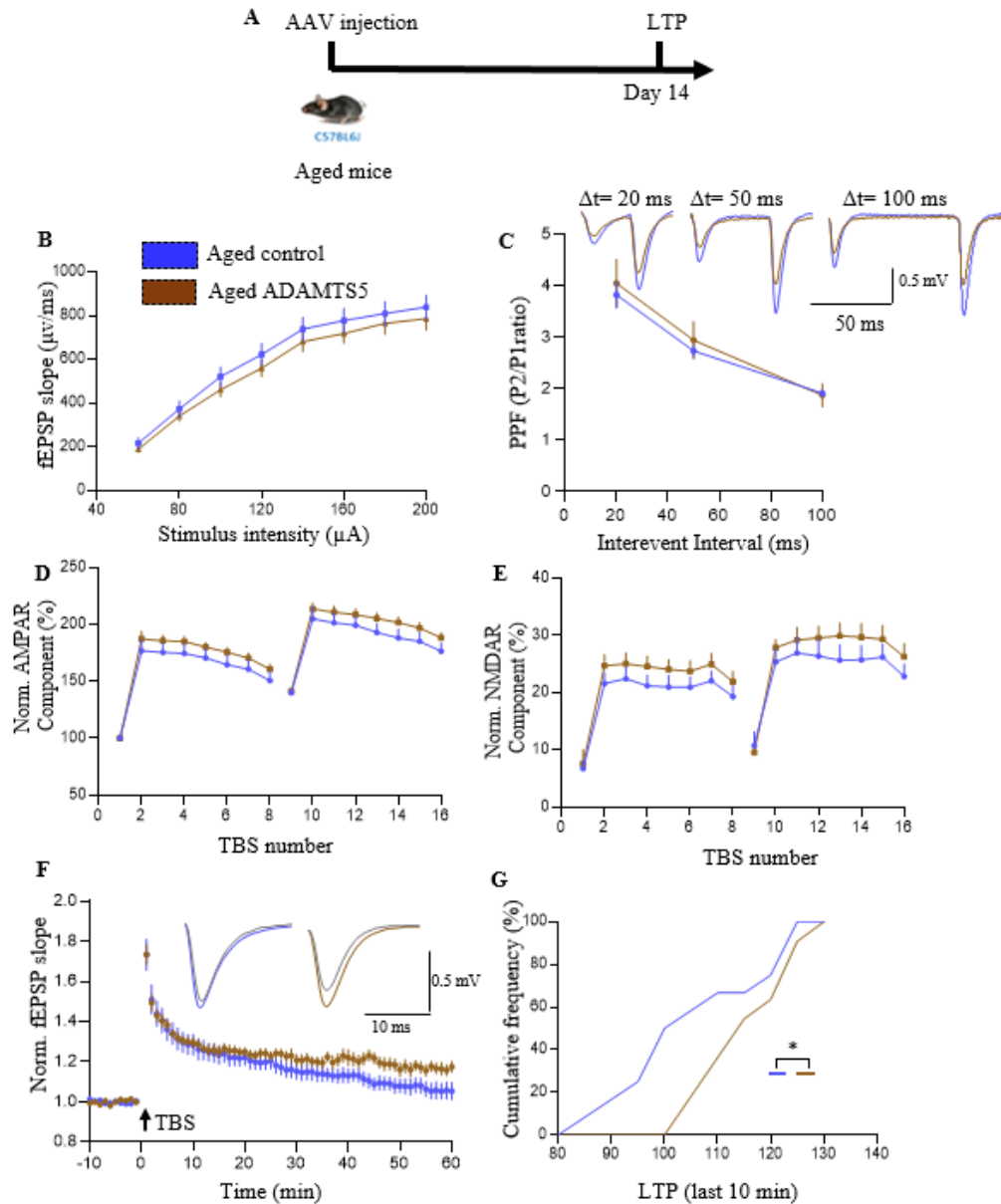


**Figure 4.21 ADAMTS5 overexpression improved the synaptic plasticity in aged mice.** (A) Timeline for AAV injection into the hippocampal CA1 and LTP experiments. (B) The stimulus-response curve by increasing current pulses and calculating the slope of evoked responses. No differences were detected by two-way RM ANOVA. (C) PPF calculation, as the ratio of the slopes of the fEPSPs elicited by the second and first pulses given with 20, 50, and 100 ms intervals. Multiple comparisons were done after RM ANOVA and significant differences were detected. (D, E) Normalized TBS-induced activation of AMPA and NMDA receptors during LTP induction. No difference was detected by two-way RM ANOVA. (F) The LTP graph of normalized fEPSPs slopes. LTP was calculated by comparing the mean slope of fEPSPs recorded 50-60 minutes after TBS to the mean slope of fEPSPs recorded 10 minutes before TBS. (G) Cumulative probability plot of LTP values obtained in each group. Kolmogorov-Smirnov's test was used for the comparison of cumulative frequency distributions: \*  $p < 0.05$ . Aged mice:  $n=13$ ; aged ADAMTS-5 mice:  $n=12$ ,  $n$  represents the number of hippocampal slices.

## 5. DISCUSSION

The functions of mechanosensitive ion channels in the CNS are getting increased attention following the initial studies on these channels performed in other systems. Cell-cell and cell-ECM adhesion systems couple cells together and to the microenvironments to generate physically coherent tissues capable of resisting and responding to mechanical forces (McMillen & Holley 2015). Tissue mechanics arises from the mechanical properties of cells interacting with the extracellular matrix, thereby governing tissue homeostasis through a bidirectional exchange of information between cells and the matrix. Cells regulate the ECM mechanics by degrading, synthesizing, and organizing it (Humphrey et al 2014). Cells' ability to sense and exert stresses on their environment is essential for growth, differentiation, and morphogenesis during development (Vining & Mooney 2017). Dynamic changes in how cells take in and react to pressures in their surroundings are necessary for the coordinated morphogenetic cellular movements that characterize embryonic development (Fernandez-Sanchez et al 2015). In addition to interacting with the ECM, cells can respond to force by causing an immediate change in their membrane structure, which makes them able to convert mechanical inputs, such as tension, compression, shear forces, and stretch into biochemical signals via transmembrane and intracellular molecular signaling cascades. This eventually results in modified gene transcription outcomes (Pruitt et al 2014).

The brain as a heterogeneous tissue is made up of a variety of cell types with different shapes and morphology, including neurons and glial cells. They reside in the ECM, which is composed of filamentous proteins such as fibronectin and collagens, as well as proteoglycans of the lecticans family. Although in recent decades, neuroscience research has focused on electrophysiological, pharmacological, and biochemical investigations, new data indicate that mechanobiology plays an important role in regulating brain function (Tyler 2012). Embryonic development demands precise cell and tissue patterning, which is driven by integrated signals to respond to physical and chemical cues. It is well understood that substrate stiffness impacts neural progenitor cell proliferation and differentiation, as well as axonal development, branching, and maturation (Leipzig & Shoichet 2009).

In the field of brain mechanobiology, the most important outstanding question is how neurons detect nano-scale mechanical stimulation. Data from electron microscopy revealed that the neurites are in close contact with the underlying topographical cues (Blumenthal et al 2014). Changes in membrane tension which affect the shape and distribution of mechanosensitive ion channels should occur as a result of intimate contact between neurites and surrounding areas (Blumenthal et al 2014). In terms of the brain, it remains unknown how tension interacts with other factors to govern cell activity and regulate morphology. However, animal models together with the gene editing approach targeting the potential genes, have provided valuable information to dissect the precise mechanical-dependent molecular pathways in the CNS (Cota-Coronado

et al 2019). As noted in the introduction part, brain tissue progressively stiffens with age and also in pathological conditions like A $\beta$  deposition in AD (Segel et al 2019). Interestingly, this phenomenon is accompanied by the accumulation of certain ECM molecules in the hippocampus (Vegh et al 2014b). Little to no information exists regarding the mechanisms behind the age-dependent changes in mechanotransduction pathways coupled to synaptic function in the CNS. Therefore, in this study, I investigated how age-dependent changes in mechanotransduction may lead to impairments in synaptic function during healthy aging and in the diseased brain.

### **5.1 mRNA levels of mechanosensitive ion channels and YAP/TAZ are upregulated in the aged and 5xFAD mice**

With immunoblotting, Velasco-Estevez and colleagues showed that Piezo1 expression increased from 12- to 18 months in wild-type rats in the DG and CA1 area (Velasco-Estevez et al 2018). However, they failed to dissect the underlying mechanism and did not investigate the relevance of these changes to synaptic alterations. This thesis, to my knowledge, is the first study to provide a shred of evidence that relates the increased mechanosensitivity of the cells in the aged hippocampus to impaired synaptic plasticity. First, as expected, I showed that mRNA levels of some inflammatory markers including GFAP, TNF $\alpha$ , and IL1 $\beta$  are increased in the hippocampus of aged animals, which is consistent with our previous data from a different batch of animals (Baidoe-Ansah et al 2022). Then I observed that the mRNA level of the main families involved in the mechanotransduction including Piezo and TRP channels are upregulated in an age-dependent manner. Interestingly the expression levels of the main components of the YAP/TAZ pathway were upregulated as well in the hippocampus of both healthy aging and 5xFAD mice. YAP translocation to the nucleus is an indicator of the mechanotransduction process in the cell and plays an important role in regulating responses to mechanical cues (Elosegui-Artola et al 2017, Mohri et al 2017). This event coincides with the increased protein levels of PNN components in the aged hippocampus as reported previously by our laboratory and others (Baidoe-Ansah et al 2022, Vegh et al 2014b). Several factors contribute to determining the stiffness of the environment, including ECM, cell density, and the cell's capacity to respond to mechanical forces. As noted before, changes in the microenvironment stiffness due to ECM overloading can be sensed by cells via mechanosensitive channels (Wang et al 2018a). Mechanosensitive receptors mainly are known from studies of sensory organs. Physical stimulation of sensory receptors in vertebrates causes a wide range of feelings, including touch, pressure, proprioception, and pain. The stimulation of specialized mechanoreceptors in sensory nerves initiates a neural signal to the CNS for the following motor responses (Cho et al 2002). However, our results suggest that mechanosensitive channels also are responsible for the nano-scale mechanical changes and signaling in the CNS in an age-dependent manner. Meanwhile, we also observed changes in the expression levels of some mechanosensitive channels,

especially Piezo1 and also YAP/TAZ pathway components in the 5xFAD model of AD which is consistent with the previously published finding of upregulation for Piezo1 in all subregions of the hippocampus of TgF344-AD rats (Velasco-Estevez et al 2018). Similar to 5xFAD mice, this transgenic rat expressing human *APP* with the Swedish mutation and human *PSEN1* with the  $\Delta$  exon 9 mutation. At 6 months, the number of neurons in the hippocampus and cortex of TgF344-AD rats is comparable to that of wild-type animals, but by 16 months, there is a 40 % loss of neurons (Cohen et al 2013). In 5xFAD mice, neuronal loss occurs at 6 months of life in the regions with the most severe amyloidosis—the subiculum and cortical layer V (Eimer & Vassar 2013). Therefore, it is reasonable to hypothesize that impaired cognitive function in both healthy aged and AD brains might be at least in part due to the upregulation of mechanosensitive receptors and downstream pathways.

## **5.2 Piezo1 activation mimics the aged brain by increasing p38 MAPK phosphorylation**

As a first step, to confirm that synaptic plasticity is impaired in the aged hippocampus, I recorded LTP in the CA1 region. As expected, the analysis showed that PPF and LTP are impaired in the aged mice compared to young controls. This is consistent with the previous published results (McGregor et al 2018). Since I observed an upregulation of Piezo1 expression in the aged brain, I hypothesize that similar to the aged brain, Piezo1 over-activation leads to synaptic dysfunction in the young hippocampus. To test this hypothesis, first, I incubated acute hippocampal slices with Yoda1, a widely used chemical to induce Piezo1 activation (Syeda et al 2015). As expected, Yoda1 treatment induced impairment in the LTP after 3-hour incubation in comparison to slices treated with vehicle (DMSO). To my knowledge, it is the first time that LTP impairment due to Piezo1 activation has been reported. However, the adverse effects of Piezo loss or gain of function on cellular functions in the CNS have been reported previously. Piezo1 deficiency in *Drosophila melanogaster* promotes axonal regrowth in both PNS and CNS (Song et al 2019). Moreover, conditional ablation of its mammalian counterpart promotes regeneration *in vivo*, while pharmacological activation with Yoda1 lowers regeneration (Song et al 2019). In a separate study, Yoda1-mediated demyelination of CNS axons was proposed, which can be reversed by Piezo1 inhibitor GsMTx4 that mitigated the adverse effects of Piezo1 overactivation (Velasco-Estevez et al 2020). This study proposed that enhanced  $Ca^{2+}$  influx via Piezo1 triggers calcium-induced calpain signaling in the neurons, which ultimately leads to axonal demyelination (Velasco-Estevez et al 2020). Yoda1 also generates a shear stress-induced TRAIL sensitization, increased mitochondrial outer membrane permeability (MOMP), mitochondrial depolarization, activated Bax, and finally apoptosis induction in some cell lines *in vitro* (Hope et al 2019). Based on previous knowledge of activated pathways following Piezo1 activation in different cell types, I analyzed involved potential pathways in the hippocampal slices by different approaches. Yoda1 activation raises both mRNA levels and protein release of IL-6, a pro-hypertrophic and

profibrotic cytokine in human cardiac fibroblasts (Blythe et al 2019). Furthermore, Piezo1 knockdown lowered baseline IL-6 expression. Subsequent analysis from multiplex kinase activity profiling revealed that Piezo1 activation increases IL-6 secretion via the p38 mitogen-activated protein kinase, a downstream target following  $Ca^{2+}$  influx (Blythe et al 2019). I observed similar findings in the young hippocampus treated with Yoda1. Phosphorylation of p38 MAPK was increased in both IHC and western blot analysis. P38 MPAK can induce biosynthesis of IL-1 $\beta$  and IL-6 in microglia and astrocytes (Asih et al 2020). My subsequent analysis of the inflammatory cytokines revealed an increased expression of *IL1 $\beta$*  following Yoda1-mediated Piezo1 activation. Interestingly, IL-1 $\beta$  can stimulate the synthesis of a variety of other proinflammatory chemicals (nitric oxide and IL-6) by astrocytes and microglia (Basu et al 2002). One possible explanation for impaired LTP observed following Yoda1 could be mediated by IL-1 $\beta$ , as the adverse effect of IL-1 $\beta$  on synaptic plasticity is well documented (Hoshino et al 2017, Prieto et al 2019). IL-1 $\beta$  has been demonstrated to impact  $Ca^{2+}$  conductance via NMDARs in a dose-dependent manner, improving or inhibiting  $Ca^{2+}$  influx at low and high concentrations, respectively (Viviani et al 2003). Moreover, p38-mediated *IL1 $\beta$*  overexpression inhibits BDNF-dependent Arc regulation as well as phosphorylation of cofilin and CREB through phosphorylation of insulin receptor substrate 1 (Tong et al 2012). Furthermore, it has been shown that following cLTP, IL-1 $\beta$  lowers the amount of newly generated proteins in proximal dendrites by suppressing Akt/mTOR signaling as well as the activation of GluA1, and LIM Domain Kinase 1 (LIMK1), an actin polymerization-promoting kinase (Prieto et al 2019).

Expectedly, in my experiment, impaired LTP observed in the hippocampal slices treated with Yoda1 was rescued by coincubation of slices with Yoda1 and p38 inhibitor SKF86002. Given that p38 can be activated by cellular stressors such as inflammatory cytokines, there is a feedforward loop in which changes in tissue mechanics either in aged mice or after agonist treatment in young mice can be sensed by Piezo1 to promote p38 activation, cytokine release, and further increase p38 activity.

There are several examples of association between ECM remodeling, tissue stiffness, and activated inflammatory pathways. The best and most well-known example is cancer. Dysregulated matrix production and remodeling occur during different types of cancer (Giussani et al 2019). Tumors are generally stiffer than normal tissue as a result of ECM changes which causes abnormal mechanosignaling (Winkler et al 2020). Interestingly, increased expression and activity of p38 MAPK are reported in cancer including brain cancer glioblastoma which is correlated with poor prognosis (Goldsmith et al 2018). Interestingly, p38 MAPK inhibition in cancerous cells reduces tumor invasiveness (Goldsmith et al 2018). That is why p38 MAPK inhibitors have attracted significant attention for use in chemotherapy. It is noteworthy to mention that increased Piezo1 activity in tumor cells has been reported recently in several studies (Dombroski et al 2021, Sun et al 2020). Piezo1 also regulates macrophage responses within varying stiffness environments

and its hyperactivity promotes interferon- $\gamma$  and LPS-induced inflammatory response and suppresses IL4 and IL13-induced healing responses (Atcha et al 2021). P38 activation also impairs the activity-dependent trafficking of AMPA receptors as the key mechanism of LTP expression (Krapivinsky et al 2004).

### **5.3 Piezo1 activation dephosphorylates YAP**

I also observed an increase in dephosphorylation of YAP following Yoda1 treatment. The role of the HIPPO pathway and downstream targets in synaptic plasticity and cognitive function is not clear yet. Our results clearly showed upregulation in both mRNA and protein levels of YAP in healthy aged and 5xFAD mice as well as an increase in dephosphorylation state (nuclear translocations) in young slices treated with Yoda1. In line with these findings, data from old and young fibroblasts, and young fibroblasts cultured on stiff silicone gel substrates showed a significant increase in the nuclear translocation of both YAP and TAZ (Stearns-Reider et al 2017). Moreover, age-mediated muscle stiffness promotes YAP/TAZ-mediated pathogenic production of extracellular matrix proteins by fibroblasts (Stearns-Reider et al 2017).

However, a recent study showed that in the cortical neurons of 5xFAD mice, nuclear YAP is decreased due to cytoplasmic co-segregation with A $\beta$  before the onset of cognitive impairment (Tanaka et al 2020). The analysis also found a comparable decrease in YAP in temporal and occipital tip tissues from AD patients, which was consistent with the lower nuclear YAP (Tanaka et al 2020). It is not clear, however, if the YAP activity alone can be involved in the impaired LTP phenotype. Further experiments are warranted to investigate the effects of YAP inhibitors in the acute hippocampal slices to answer this open question.

### **5.4 Piezo1 activation mediated calpain-dependent spectrin cleavage**

Our western blot result showed an increased cleavage of  $\alpha$ II-spectrin mediated by Piezo1 hyperactivity. Resting intracellular cytosolic Ca<sup>2+</sup> concentration is generally 100 nM, which is substantially lower than the extracellular concentration. Ca<sup>2+</sup> homeostasis is a critical cellular function, especially for Ca<sup>2+</sup>-dependent molecules like calpains which are tightly regulated and their aberrant activity can have negative consequences, resulting in the cleavage of multiple targets (Metwally et al 2021). The considerable portion of calpain-cleaved spectrin observed in the cerebrospinal fluid of AD patients indicates hyperactivation of calpains in the AD brain (Higuchi et al 2012). It is noteworthy to mention the subcellular localization of calpain 2 in the aged synapse is extrasynaptic. Contrary to calpain 1, which is localized in the synaptic density and is required for the LTP induction (Baudry & Bi 2016), Calpain 2 activity in the extrasynaptic region leads to STEP inhibition and finally p38 activation and neurotoxicity (Xu et al 2009). This may explain the higher LTP value observed in our experiments when the hippocampal slices were treated with calpain inhibitor E64 when compared to the p38 inhibitor. A hallmark of calpain activity is the spectrin cleavage. A substantial body of evidence indicates that calcium dysregulation and increased proteolysis of spectrin are processes that occur in the brain during both normal aging and Alzheimer's disease (AD)

(Benuck et al 1996, Garg et al 2011). Atypical spectrin labeling appeared in neuronal processes and axon terminals in the AD human brain, which may indicate an accumulation of SBDPs in the atrophic neurons. These findings support evidence of calpain overexpression and activation in AD. In addition to AD, enhanced SBDPs levels in aged brains were reported previously (Bernath et al 2006). Furthermore, as mechanoresponsive protein, spectrin influences cell surface physiology and shape, thus its partial degradation would be predicted to result in severe and long-lasting changes in synapses (Duan et al 2018, Nestor et al 2011, Pielage et al 2005).

### **5.5 Piezo1 activation mimics an aged brain and reduces the CaMKII phosphorylation**

CaMKII is the most prominent signaling molecule in the postsynaptic density (PSD) and a key mediator and effector in the early stages of LTP.  $\text{Ca}^{2+}$ /CaM binding stimulates CaMKII and Thr-286 autophosphorylation, resulting in an autonomously active version of CaMKII that facilitates transitory  $\text{Ca}^{2+}$  signals. My IHC results showed that there is a reduced level of phosphorylation in Thr-286 residue for CaMKII. This result is consistent with the previously published data showing that Piezo1 knockdown results in a tendency toward increased phospho-CaMKII (Thr286) and pCREB in the mouse hippocampal cell line mHippoE-18 (CLU199) (Qiu et al 2019). In the aging context, CaMKII is also reduced in elderly rats, which corresponds with worse spatial memory and presynaptic release probabilities since it is required for the phosphorylation of key vesicular proteins such as the SNARE complex (VanGuilder et al 2011). In 5xFAD mice, relative to wild-type mice, the level of p-CaMKII $\alpha$ /CaMKII $\alpha$  in both the hippocampus and cortex was decreased significantly (Zeng et al 2015).

### **5.6 Piezo1 knockdown tends to improve impaired cognitive function and enhances synaptic plasticity in aged mice**

Previous findings suggest that the CA1 region of the hippocampus, especially the dorsal CA1 region, plays a critical role in spatial memory (Yu et al 2018). It is also acknowledged that other subregions of the hippocampus, including CA3 and the dentate gyrus, may potentially contribute to spatial memory processing (Broadbent et al 2004). Our behavior analysis showed an improved tendency for NOLT but not NORT in the aged mice injected with Piezo1 shRNA1 in the dorsal CA1 area. There is not much information regarding the role of Piezo1 in cognitive function so far. However, a recent study showed that Piezo1 activation by Yoda1 injection into the rat basal forebrain mimicked sleep deprivation-induced effects followed by TrkB full-length cleavage and reduced short- and long-term fear memory (Ma et al 2022b). This phenotype was ameliorated further by Piezo1 inhibitor GsMTx4 which partially restored short- and long-term fear memory deficits (Ma et al 2022b). Furthermore, sleep deprivation resulted in a lower pain threshold than the control condition, which could be partially corrected by injections of GsMTx4 or calpain inhibitor PD151746. These findings suggest that Piezo1/calpain signaling is involved in sleep

deprivation-induced TrkB signaling disruption and fear memory deficits in rats (Ma et al 2022b). My data demonstrated an increase in LTP in the aged mice injected with Piezo1 shRNA. This is consistent with the impaired LTP after Piezo1 activation with Yoda1 in the young hippocampus. In a recent study in young mice, astrocytic Piezo1 knockout mice have impaired hippocampus LTP and learning and memory behavior (Chi et al 2022). While overexpression of Piezo1 in astrocytes, on the other hand, significantly improved LTP, and learning and memory function, presumably through the facilitation of gliotransmitter release (Chi et al 2022). However, in the aging context, the condition is different because of low-grade inflammation and the involvement of other factors like ECM upregulation and changes in tissue stiffness. Further studies in aged mice and cell type-specific knockdown or overexpression strategies are needed to address this issue.

### **5.7 ECM cleavage downregulates *Piezo1*, *2*, *YAP*, and *TAZ* expression *in vitro* and rescues synaptic plasticity deficits in aged mice *ex vivo***

Many cell types respond to the elastic characteristics of the microenvironment they reside. Stiffness properties can influence several biological processes in neurons and non-neuronal cells including cell motility, cell proliferation and differentiation, and even neural axon guidance (Nichol et al 2019). ECM stiffness mainly depends on fibrillar collagens, glycosaminoglycans, and proteoglycans. To explore the link between ECM mechanical properties and mechanotransduction pathways in neurons, we cleaved ECM by overexpressing ADAMTS-5, which has a strong aggrecanase activity, and observed that ECM cleavage leads to decreased expression of *Piezo1*, *Piezo2* and downstream YAP/TAZ signaling pathway components. Interestingly, similar to Piezo1 knockdown, aged mice with ADAMTS5 overexpression in the CA1 region exhibited an increased LTP. According to previously published data in the 3xTg-AD model and our unpublished data in the aged mice, ADAMTS5 protein levels and activity are lower in comparison to control and young mice, respectively (Krstic et al 2012).

### **5.8 Limitations and outlook**

In this study, I found that the mechanosensitive channel Piezo family and some of the TRP channels are upregulated in an aged-dependent manner. I used total hippocampal mRNA samples and protein lysate. Hence, I was not able to determine which cell types specifically are sensitive and more responsive to the age-dependent changes in tissue mechanics. As different cell types sense and respond to the mechanical cues in different strengths and intensities, single-cell RNAseq or cell-sorting approaches to screening the expression profile of these genes in different cell types is necessary for future studies. In this case, it would be easier to understand which specific cell types mediate impaired synaptic plasticity in the aged condition due to increased Piezo1 expression. In a similar vein, the knockdown method employed in this study was founded on a universal promoter and the AAV-DJ system, which utilizes a hybrid capsid composed of eight distinct AAV serotypes. This design significantly enhances infectivity rates across a broad spectrum of cell

types and tissues. Recently, a few cell-specific approaches using a synthetic specific promoter and specific AAV serotyping have been introduced to target specific cell types within a tissue (Challis et al 2022, Hoshino et al 2021).

While the knockdown of Piezo1 yielded limited effects on behaviour in our experimental paradigm, it is essential to consider the context in which these results were obtained. Notably, the sample size employed for this study was relatively small, and as such, the statistical power to detect significant differences may have been insufficient. To draw more definitive conclusions regarding the behavioural consequences of Piezo1 knockdown, future studies with larger sample sizes and more comprehensive behavioural assessments may be necessary to provide a more robust and accurate characterization of its effects.

Another constraint in this study was the absence of commercially accessible, specific Piezo1 inhibitors. Fortunately, Yoda1 represents a highly specific agent for Piezo1 activation. However, it's worth noting that for inhibition purposes, the commonly employed inhibitor, GsMTx4, not only inhibits Piezo1 but also affects TRPC1 and TRPC6 (Suchyna et al 2000) , and it was not utilized in the experiments conducted in my research. As I observed some tendencies toward improvement in some series of experiments including the behavioral testing, increasing the sample size is planned to reach a defined statistical power.

Figure 5.1 shows a summary of proposed underlying mechanisms by which Piezo1 hyperactivation may affect synaptic plasticity in the aged brain, multiple aspects of which, such as the roles of IL1R receptor and modulation of CREB signaling, still need direct experimental validation.

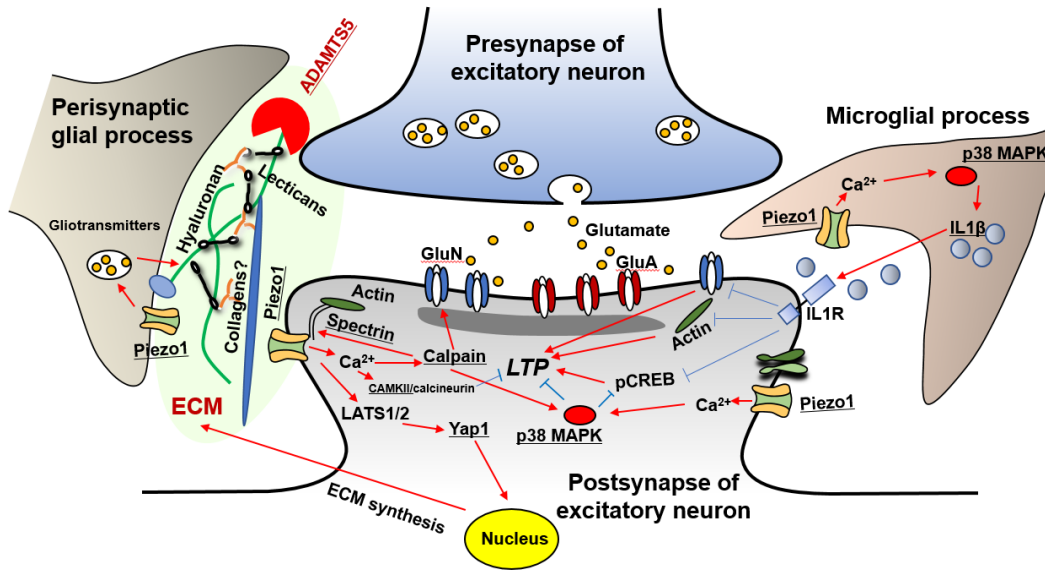


**Figure 5.1. A proposed model of how Piezo1 activation in neuronal and glial cells may lead to modulation of synaptic plasticity under aged conditions.** ECM accumulation and subsequently increased tissue stiffness can be sensed by the mechanosensitive channel Piezo1. Excessive Ca<sup>2+</sup> influx upon Piezo1 activation stimulates inflammatory pathways in glial cells and increases the release of proinflammatory cytokines such as IL-1β. IL-1β acts via IL1 receptor and inhibits NMDAR, phosphorylation of CREB and cofilin, and F-actin formation in the dendritic spines. In neurons, Piezo1 activation promotes p38 MAPK and calpain proteases, which have adverse effects on LTP. YAP nuclear translocation downstream of Piezo1 activation also contributes to transcriptional changes and remodeling of ECM in the synapse. Lectican core protein cleavage mediated by lecticanase ADAMTS5 releases the perisynaptic nano-scale tension on spines and attenuates the negative effect of Piezo1 overactivation on synaptic plasticity similar to Piezo1 knockdown. The molecules whose changes have been experimentally shown in the present work are underlined.

## 6. CONCLUSION

- Mechanosensitive ion channels in the aged hippocampus are upregulated, which coincides with increased tissue stiffness, ECM accumulation, and increased YAP dephosphorylation and nuclear translocation.
- Activation of the Piezo1 channel in the young hippocampus impairs synaptic plasticity and activation of CaMKII and increases expression of proinflammatory cytokine IL-1β, elevation in resting Ca<sup>2+</sup> concentration, phosphorylation of p38 MAPK, and calpain activation-mediated spectrin degradation.
- Impaired LTP after Piezo1 activation in young mice is rescued by p38 and calpain inhibitors.
- Aging-associated impairment in cognitive function and synaptic plasticity in aged mice are partially rescued by Piezo1 knockdown or digestion of ECM by overexpression of ADAMTS5.

## 7. REFERENCES

- Acheta J, Bhatia U, Haley J, Hong J, Rich K, et al. 2022. Piezo channels contribute to the regulation of myelination in Schwann cells. *Glia* 70: 2276-89
- Aggleton JP, Albasser MM, Aggleton DJ, Poirier GL, Pearce JM. 2010. Lesions of the rat perirhinal cortex spare the acquisition of a complex configural visual discrimination yet impair object recognition. *Behav Neurosci* 124: 55-68
- Akhmanova M, Osidak E, Domogatsky S, Rodin S, Domogatskaya A. 2015. Physical, Spatial, and Molecular Aspects of Extracellular Matrix of In Vivo Niches and Artificial Scaffolds Relevant to Stem Cells Research. *Stem Cells Int* 2015: 167025
- Alessandri-Haber N, Dina OA, Chen X, Levine JD. 2009. TRPC1 and TRPC6 channels cooperate with TRPV4 to mediate mechanical hyperalgesia and nociceptor sensitization. *J Neurosci* 29: 6217-28
- Andoh M, Koyama R. 2021. Microglia regulate synaptic development and plasticity. *Dev Neurobiol* 81: 568-90
- Andolfo I, Alper SL, De Franceschi L, Auriemma C, Russo R, et al. 2013. Multiple clinical forms of dehydrated hereditary stomatocytosis arise from mutations in PIEZO1. *Blood* 121: 3925-35, S1-12
- Arboit A, Reboreda A, Yoshida M. 2020. Involvement of TRPC4 and 5 Channels in Persistent Firing in Hippocampal CA1 Pyramidal Cells. *Cells* 9
- Arulmoli J, Pathak MM, McDonnell LP, Nourse JL, Tombola F, et al. 2015. Static stretch affects neural stem cell differentiation in an extracellular matrix-dependent manner. *Sci Rep* 5: 8499
- Asgeirsdottir HN, Cohen SJ, Stackman RW, Jr. 2020. Object and place information processing by CA1 hippocampal neurons of C57BL/6J mice. *J Neurophysiol* 123: 1247-64
- Ash JA, Lu H, Taxier LR, Long JM, Yang Y, et al. 2016. Functional connectivity with the retrosplenial cortex predicts cognitive aging in rats. *Proc Natl Acad Sci U S A* 113: 12286-91
- Asih PR, Prikas E, Stefanoska K, Tan ARP, Ahel HI, Ittner A. 2020. Functions of p38 MAP Kinases in the Central Nervous System. *Front Mol Neurosci* 13: 570586
- Assaraf E, Blecher R, Heinemann-Yerushalmi L, Krief S, Carmel Vinestock R, et al. 2020. Piezo2 expressed in proprioceptive neurons is essential for skeletal integrity. *Nat Commun* 11: 3168
- Atcha H, Jairaman A, Holt JR, Meli VS, Nagalla RR, et al. 2021. Mechanically activated ion channel Piezo1 modulates macrophage polarization and stiffness sensing. *Nat Commun* 12: 3256
- Avila J, Llorens-Martin M, Pallas-Bazarra N, Bolos M, Perea JR, et al. 2017. Cognitive Decline in Neuronal Aging and Alzheimer's Disease: Role of NMDA Receptors and Associated Proteins. *Front Neurosci* 11: 626
- Avital A, Goshen I, Kamsler A, Segal M, Iverfeldt K, et al. 2003. Impaired interleukin-1 signaling is associated with deficits in hippocampal memory processes and neural plasticity. *Hippocampus* 13: 826-34
- Bachstetter AD, Xing B, de Almeida L, Dimayuga ER, Watterson DM, Van Eldik LJ. 2011. Microglial p38alpha MAPK is a key regulator of proinflammatory cytokine up-regulation induced by toll-like receptor (TLR) ligands or beta-amyloid (Abeta). *J Neuroinflammation* 8: 79

- Bae C, Sachs F, Gottlieb PA. 2011. The mechanosensitive ion channel Piezo1 is inhibited by the peptide GsMTx4. *Biochemistry* 50: 6295-300
- Bae C, Sachs F, Gottlieb PA. 2015. Protonation of the human PIEZO1 ion channel stabilizes inactivation. *J Biol Chem* 290: 5167-73
- Baidoe-Ansah D, Sakib S, Jia S, Mirzapourdelavar H, Strackeljan L, et al. 2022. Aging-Associated Changes in Cognition, Expression and Epigenetic Regulation of Chondroitin 6-Sulfotransferase Chst3. *Cells* 11
- Basu A, Krady JK, O'Malley M, Styren SD, DeKosky ST, Levison SW. 2002. The type 1 interleukin-1 receptor is essential for the efficient activation of microglia and the induction of multiple proinflammatory mediators in response to brain injury. *J Neurosci* 22: 6071-82
- Baudry M, Bi X. 2016. Calpain-1 and Calpain-2: The Yin and Yang of Synaptic Plasticity and Neurodegeneration. *Trends Neurosci* 39: 235-45
- Baumgart E. 2000. Stiffness--an unknown world of mechanical science? *Injury* 31 Suppl 2: S-B14-23
- Benuck M, Banay-Schwartz M, DeGuzman T, Lajtha A. 1996. Changes in brain protease activity in aging. *J Neurochem* 67: 2019-29
- Bernard-Trifilo JA, Kramar EA, Torp R, Lin CY, Pineda EA, et al. 2005. Integrin signaling cascades are operational in adult hippocampal synapses and modulate NMDA receptor physiology. *J Neurochem* 93: 834-49
- Bernath E, Kupina N, Liu MC, Hayes RL, Meegan C, Wang KK. 2006. Elevation of cytoskeletal protein breakdown in aged Wistar rat brain. *Neurobiol Aging* 27: 624-32
- Berretta S. 2012. Extracellular matrix abnormalities in schizophrenia. *Neuropharmacology* 62: 1584-97
- Bikbaev A, Frischknecht R, Heine M. 2015. Brain extracellular matrix retains connectivity in neuronal networks. *Sci Rep* 5: 14527
- Binnig G, Quate CF, Gerber C. 1986. Atomic force microscope. *Phys Rev Lett* 56: 930-33
- Blanco I, Conant K. 2021. Extracellular matrix remodeling with stress and depression: Studies in human, rodent and zebrafish models. *Eur J Neurosci* 53: 3879-88
- Blaschke SJ, Demir S, Konig A, Abraham JA, Vay SU, et al. 2020. Substrate Elasticity Exerts Functional Effects on Primary Microglia. *Front Cell Neurosci* 14: 590500
- Bliss TV, Lomo T. 1973. Long-lasting potentiation of synaptic transmission in the dentate area of the anaesthetized rabbit following stimulation of the perforant path. *J Physiol* 232: 331-56
- Bloss EB, Hunter RG, Waters EM, Munoz C, Bernard K, McEwen BS. 2008. Behavioral and biological effects of chronic S18986, a positive AMPA receptor modulator, during aging. *Exp Neurol* 210: 109-17
- Blumenthal NR, Hermanson O, Heimrich B, Shastri VP. 2014. Stochastic nanoroughness modulates neuron-astrocyte interactions and function via mechanosensing cation channels. *Proc Natl Acad Sci U S A* 111: 16124-9
- Blythe NM, Muraki K, Ludlow MJ, Stylianidis V, Gilbert HTJ, et al. 2019. Mechanically activated Piezo1 channels of cardiac fibroblasts stimulate p38 mitogen-activated protein kinase activity and interleukin-6 secretion. *J Biol Chem* 294: 17395-408
- Bodhinathan K, Kumar A, Foster TC. 2010. Intracellular redox state alters NMDA receptor response during aging through Ca<sup>2+</sup>/calmodulin-dependent protein kinase II. *J Neurosci* 30: 1914-24

- Boisvert MM, Erikson GA, Shokhirev MN, Allen NJ. 2018. The Aging Astrocyte Transcriptome from Multiple Regions of the Mouse Brain. *Cell Rep* 22: 269-85
- Bolshakov VY, Carboni L, Cobb MH, Siegelbaum SA, Belardetti F. 2000. Dual MAP kinase pathways mediate opposing forms of long-term plasticity at CA3-CA1 synapses. *Nat Neurosci* 3: 1107-12
- Bonneh-Barkay D, Wiley CA. 2009. Brain extracellular matrix in neurodegeneration. *Brain Pathol* 19: 573-85
- Brakebusch C, Seidenbecher CI, Asztely F, Rauch U, Matthies H, et al. 2002. Brevican-deficient mice display impaired hippocampal CA1 long-term potentiation but show no obvious deficits in learning and memory. *Mol Cell Biol* 22: 7417-27
- Briz V, Parkash J, Sanchez-Redondo S, Prevot V, Sunol C. 2012. Allopregnanolone prevents dieldrin-induced NMDA receptor internalization and neurotoxicity by preserving GABA(A) receptor function. *Endocrinology* 153: 847-60
- Broadbent NJ, Squire LR, Clark RE. 2004. Spatial memory, recognition memory, and the hippocampus. *Proc Natl Acad Sci U S A* 101: 14515-20
- Brust TB, Cayabyab FS, Zhou N, MacVicar BA. 2006. p38 mitogen-activated protein kinase contributes to adenosine A1 receptor-mediated synaptic depression in area CA1 of the rat hippocampus. *J Neurosci* 26: 12427-38
- Burke SN, Barnes CA. 2010. Senescent synapses and hippocampal circuit dynamics. *Trends Neurosci* 33: 153-61
- Cahalan SM, Lukacs V, Ranade SS, Chien S, Bandell M, Patapoutian A. 2015. Piezo1 links mechanical forces to red blood cell volume. *Elife* 4
- Caldwell RA, Clemo HF, Baumgarten CM. 1998. Using gadolinium to identify stretch-activated channels: technical considerations. *Am J Physiol* 275: C619-21
- Calhoun ME, Fletcher BR, Yi S, Zentko DC, Gallagher M, Rapp PR. 2008. Age-related spatial learning impairment is unrelated to spinophilin immunoreactive spine number and protein levels in rat hippocampus. *Neurobiol Aging* 29: 1256-64
- Camins A, Verdaguer E, Folch J, Pallas M. 2006. Involvement of calpain activation in neurodegenerative processes. *CNS Drug Rev* 12: 135-48
- Cangalaya C, Stoyanov S, Fischer KD, Dityatev A. 2020. Light-induced engagement of microglia to focally remodel synapses in the adult brain. *Elife* 9
- Challis RC, Ravindra Kumar S, Chen X, Goertsen D, Coughlin GM, et al. 2022. Adeno-Associated Virus Toolkit to Target Diverse Brain Cells. *Annu Rev Neurosci* 45: 447-69
- Chao CC, Shen PW, Tzeng TY, Kung HJ, Tsai TF, Wong YH. 2021. Human iPSC-Derived Neurons as A Platform for Deciphering the Mechanisms behind Brain Aging. *Biomedicine* 9
- Chatelin S, Vappou J, Roth S, Raul JS, Willinger R. 2012. Towards child versus adult brain mechanical properties. *J Mech Behav Biomed Mater* 6: 166-73
- Chauhan P, Jethwa K, Rathawa A, Chauhan G, Mehra S. 2021. The Anatomy of the Hippocampus In *Cerebral Ischemia*, ed. R Pluta. Brisbane (AU)
- Chen BS, Gray JA, Sanz-Clemente A, Wei Z, Thomas EV, et al. 2012. SAP102 mediates synaptic clearance of NMDA receptors. *Cell Rep* 2: 1120-8
- Chi S, Cui Y, Wang H, Jiang J, Zhang T, et al. 2022. Astrocytic Piezo1-mediated mechanotransduction determines adult neurogenesis and cognitive functions. *Neuron* 110: 2984-99 e8

- Chighizola M, Dini T, Lenardi C, Milani P, Podesta A, Schulte C. 2019. Mechanotransduction in neuronal cell development and functioning. *Biophys Rev* 11: 701-20
- Cho H, Shin J, Shin CY, Lee SY, Oh U. 2002. Mechanosensitive ion channels in cultured sensory neurons of neonatal rats. *J Neurosci* 22: 1238-47
- Clapham DE. 2003. TRP channels as cellular sensors. *Nature* 426: 517-24
- Cohen RM, Rezai-Zadeh K, Weitz TM, Rentsendorj A, Gate D, et al. 2013. A transgenic Alzheimer rat with plaques, tau pathology, behavioral impairment, oligomeric abeta, and frank neuronal loss. *J Neurosci* 33: 6245-56
- Cornell J, Salinas S, Huang HY, Zhou M. 2022. Microglia regulation of synaptic plasticity and learning and memory. *Neural Regen Res* 17: 705-16
- Coste B, Mathur J, Schmidt M, Earley TJ, Ranade S, et al. 2010. Piezo1 and Piezo2 are essential components of distinct mechanically activated cation channels. *Science* 330: 55-60
- Cota-Coronado A, Diaz-Martinez NF, Padilla-Camberos E, Diaz-Martinez NE. 2019. Editing the Central Nervous System Through CRISPR/Cas9 Systems. *Front Mol Neurosci* 12: 110
- Cox CD, Bae C, Ziegler L, Hartley S, Nikolova-Krstevski V, et al. 2016. Removal of the mechanoprotective influence of the cytoskeleton reveals PIEZO1 is gated by bilayer tension. *Nat Commun* 7: 10366
- Crawford GE, Earnshaw JC. 1987. Viscoelastic relaxation of bilayer lipid membranes. Frequency-dependent tension and membrane viscosity. *Biophys J* 52: 87-94
- Czogalla A, Sikorski AF. 2005. Spectrin and calpain: a 'target' and a 'sniper' in the pathology of neuronal cells. *Cell Mol Life Sci* 62: 1913-24
- Dai HL, Hu WY, Jiang LH, Li L, Gaung XF, Xiao ZC. 2016. p38 MAPK Inhibition Improves Synaptic Plasticity and Memory in Angiotensin II-dependent Hypertensive Mice. *Sci Rep* 6: 27600
- Daynac M, Morizur L, Chicheportiche A, Mouthon MA, Boussin FD. 2016. Age-related neurogenesis decline in the subventricular zone is associated with specific cell cycle regulation changes in activated neural stem cells. *Sci Rep* 6: 21505
- De Felice D, Alaimo A. 2020. Mechanosensitive Piezo Channels in Cancer: Focus on altered Calcium Signaling in Cancer Cells and in Tumor Progression. *Cancers (Basel)* 12
- Delekate A, Fuchtemeier M, Schumacher T, Ulbrich C, Foddiss M, Petzold GC. 2014. Metabotropic P2Y1 receptor signalling mediates astrocytic hyperactivity in vivo in an Alzheimer's disease mouse model. *Nat Commun* 5: 5422
- Dembitskaya Y, Gavrilov N, Kraev I, Doronin M, Tang Y, et al. 2021. Attenuation of the extracellular matrix increases the number of synapses but suppresses synaptic plasticity through upregulation of SK channels. *Cell Calcium* 96: 102406
- Deng H, Yang L, Wen P, Lei H, Blount P, Pan D. 2020. Spectrin couples cell shape, cortical tension, and Hippo signaling in retinal epithelial morphogenesis. *J Cell Biol* 219
- Diaz-Alonso J, Nicoll RA. 2021. AMPA receptor trafficking and LTP: Carboxy-termini, amino-termini and TARPs. *Neuropharmacology* 197: 108710
- Diaz-Aparicio I, Paris I, Sierra-Torre V, Plaza-Zabala A, Rodriguez-Iglesias N, et al. 2020. Microglia Actively Remodel Adult Hippocampal Neurogenesis through the Phagocytosis Secretome. *J Neurosci* 40: 1453-82
- Dityatev A. 2010. Remodeling of extracellular matrix and epileptogenesis. *Epilepsia* 51 Suppl 3: 61-5
- Dityatev A, Frischknecht R, Seidenbecher CI. 2006. Extracellular matrix and synaptic functions. *Results Probl Cell Differ* 43: 69-97

- Dityatev A, Rusakov DA. 2011. Molecular signals of plasticity at the tetrapartite synapse. *Curr Opin Neurobiol* 21: 353-9
- Dityatev A, Seidenbecher C, Morawski M. 2021. Brain extracellular matrix: An upcoming target in neurological and psychiatric disorders. *Eur J Neurosci* 53: 3807-10
- Dityatev A, Wehrle-Haller B, Pitkanen A. 2014. Preface. Brain extracellular matrix in health and disease. *Prog Brain Res* 214: xiii-xvii
- Dombroski JA, Hope JM, Sarna NS, King MR. 2021. Channeling the Force: Piezo1 Mechanotransduction in Cancer Metastasis. *Cells* 10
- Doss BL, Pan M, Gupta M, Greci G, Mege RM, et al. 2020. Cell response to substrate rigidity is regulated by active and passive cytoskeletal stress. *Proc Natl Acad Sci U S A* 117: 12817-25
- Dowell-Mesfin NM, Abdul-Karim MA, Turner AM, Schanz S, Craighead HG, et al. 2004. Topographically modified surfaces affect orientation and growth of hippocampal neurons. *J Neural Eng* 1: 78-90
- Duan R, Kim JH, Shilagardi K, Schiffhauer ES, Lee DM, et al. 2018. Spectrin is a mechanoresponsive protein shaping fusogenic synapse architecture during myoblast fusion. *Nat Cell Biol* 20: 688-98
- Echeverry S, Rodriguez MJ, Torres YP. 2016. Transient Receptor Potential Channels in Microglia: Roles in Physiology and Disease. *Neurotox Res* 30: 467-78
- Eimer WA, Vassar R. 2013. Neuron loss in the 5XFAD mouse model of Alzheimer's disease correlates with intraneuronal Abeta42 accumulation and Caspase-3 activation. *Mol Neurodegener* 8: 2
- El-Tabbal M, Niekisch H, Henschke JU, Budinger E, Frischknecht R, et al. 2021. The extracellular matrix regulates cortical layer dynamics and cross-columnar frequency integration in the auditory cortex. *Commun Biol* 4: 322
- Elosegui-Artola A, Andreu I, Beedle AEM, Lezamiz A, Uroz M, et al. 2017. Force Triggers YAP Nuclear Entry by Regulating Transport across Nuclear Pores. *Cell* 171: 1397-410 e14
- Erickson KI, Prakash RS, Voss MW, Chaddock L, Heo S, et al. 2010. Brain-derived neurotrophic factor is associated with age-related decline in hippocampal volume. *J Neurosci* 30: 5368-75
- Evans EL, Cuthbertson K, Endesh N, Rode B, Blythe NM, et al. 2018. Yoda1 analogue (Dooku1) which antagonizes Yoda1-evoked activation of Piezo1 and aortic relaxation. *Br J Pharmacol* 175: 1744-59
- Faber ES, Sah P. 2007. Functions of SK channels in central neurons. *Clin Exp Pharmacol Physiol* 34: 1077-83
- Farnsworth CL, Freshney NW, Rosen LB, Ghosh A, Greenberg ME, Feig LA. 1995. Calcium activation of Ras mediated by neuronal exchange factor Ras-GRF. *Nature* 376: 524-7
- Fernandez-Sanchez ME, Brunet T, Roper JC, Farge E. 2015. Mechanotransduction's impact on animal development, evolution, and tumorigenesis. *Annu Rev Cell Dev Biol* 31: 373-97
- Ferreira SA, Romero-Ramos M. 2018. Microglia Response During Parkinson's Disease: Alpha-Synuclein Intervention. *Front Cell Neurosci* 12: 247
- Fleischmann A, Hvalby O, Jensen V, Strekalova T, Zacher C, et al. 2003. Impaired long-term memory and NR2A-type NMDA receptor-dependent synaptic plasticity in mice lacking c-Fos in the CNS. *J Neurosci* 23: 9116-22

- Foscarin S, Raha-Chowdhury R, Fawcett JW, Kwok JCF. 2017. Brain ageing changes proteoglycan sulfation, rendering perineuronal nets more inhibitory. *Aging (Albany NY)* 9: 1607-22
- Franze K, Janmey PA, Guck J. 2013. Mechanics in neuronal development and repair. *Annu Rev Biomed Eng* 15: 227-51
- Fu Y, Wan P, Zhang J, Li X, Xing J, et al. 2021. Targeting Mechanosensitive Piezo1 Alleviated Renal Fibrosis Through p38MAPK-YAP Pathway. *Front Cell Dev Biol* 9: 741060
- Fukazawa Y, Saitoh Y, Ozawa F, Ohta Y, Mizuno K, Inokuchi K. 2003. Hippocampal LTP is accompanied by enhanced F-actin content within the dendritic spine that is essential for late LTP maintenance in vivo. *Neuron* 38: 447-60
- Garg S, Timm T, Mandelkow EM, Mandelkow E, Wang Y. 2011. Cleavage of Tau by calpain in Alzheimer's disease: the quest for the toxic 17 kD fragment. *Neurobiol Aging* 32: 1-14
- Ge J, Li W, Zhao Q, Li N, Chen M, et al. 2015. Architecture of the mammalian mechanosensitive Piezo1 channel. *Nature* 527: 64-9
- Gees M, Colsoul B, Nilius B. 2010. The role of transient receptor potential cation channels in Ca<sup>2+</sup> signaling. *Cold Spring Harb Perspect Biol* 2: a003962
- Giussani M, Triulzi T, Sozzi G, Tagliabue E. 2019. Tumor Extracellular Matrix Remodeling: New Perspectives as a Circulating Tool in the Diagnosis and Prognosis of Solid Tumors. *Cells* 8
- Glisky EL. 2007. Changes in Cognitive Function in Human Aging In *Brain Aging: Models, Methods, and Mechanisms*, ed. DR Riddle. Boca Raton (FL)
- Godbout JP, Chen J, Abraham J, Richwine AF, Berg BM, et al. 2005. Exaggerated neuroinflammation and sickness behavior in aged mice following activation of the peripheral innate immune system. *FASEB J* 19: 1329-31
- Gogolla N, Caroni P, Luthi A, Herry C. 2009. Perineuronal nets protect fear memories from erasure. *Science* 325: 1258-61
- Goldsmith CS, Kim SM, Karunarathna N, Neuendorff N, Toussaint LG, et al. 2018. Inhibition of p38 MAPK activity leads to cell type-specific effects on the molecular circadian clock and time-dependent reduction of glioma cell invasiveness. *BMC Cancer* 18: 43
- Gonzalo S. 2010. Epigenetic alterations in aging. *J Appl Physiol (1985)* 109: 586-97
- Gottschling C, Wegrzyn D, Denecke B, Faissner A. 2019. Elimination of the four extracellular matrix molecules tenascin-C, tenascin-R, brevican and neurocan alters the ratio of excitatory and inhibitory synapses. *Sci Rep* 9: 13939
- Griesi-Oliveira K, Acab A, Gupta AR, Sunaga DY, Chailangkarn T, et al. 2015. Modeling non-syndromic autism and the impact of TRPC6 disruption in human neurons. *Mol Psychiatry* 20: 1350-65
- Grillo FW, Song S, Teles-Grilo Ruivo LM, Huang L, Gao G, et al. 2013. Increased axonal bouton dynamics in the aging mouse cortex. *Proc Natl Acad Sci U S A* 110: E1514-23
- Grochowska KM, Bar J, Gomes GM, Kreutz MR, Karpova A. 2021. Jacob, a Synapto-Nuclear Protein Messenger Linking N-methyl-D-aspartate Receptor Activation to Nuclear Gene Expression. *Front Synaptic Neurosci* 13: 787494
- Guerreiro R, Bras J. 2015. The age factor in Alzheimer's disease. *Genome Med* 7: 106
- Guo J, Shan C, Xu J, Li M, Zhao J, Cheng W. 2022. New Insights into TRP Ion Channels in Stem Cells. *Int J Mol Sci* 23

- Guo XW, Zhang H, Huang JQ, Wang SN, Lu Y, et al. 2021. PIEZO1 Ion Channel Mediates Ionizing Radiation-Induced Pulmonary Endothelial Cell Ferroptosis via Ca(2+)/Calpain/VE-Cadherin Signaling. *Front Mol Biosci* 8: 725274
- Guo YR, MacKinnon R. 2017. Structure-based membrane dome mechanism for Piezo mechanosensitivity. *Elife* 6
- Hall MS, Alisafaei F, Ban E, Feng X, Hui CY, et al. 2016. Fibrous nonlinear elasticity enables positive mechanical feedback between cells and ECMs. *Proc Natl Acad Sci U S A* 113: 14043-48
- Happel MF, Niekisch H, Castiblanco Rivera LL, Ohl FW, Deliano M, Frischknecht R. 2014. Enhanced cognitive flexibility in reversal learning induced by removal of the extracellular matrix in auditory cortex. *Proc Natl Acad Sci U S A* 111: 2800-5
- Harratz OF, Klug NR, Senatore AJ, Hill-Eubanks DC, Nelson MT. 2022. Piezo1 Is a Mechanosensor Channel in Central Nervous System Capillaries. *Circ Res* 130: 1531-46
- Hasegawa K, Fujii S, Matsumoto S, Tajiri Y, Kikuchi A, Kiyoshima T. 2021. YAP signaling induces PIEZO1 to promote oral squamous cell carcinoma cell proliferation. *J Pathol* 253: 80-93
- Hayashi Y. 2022. Molecular mechanism of hippocampal long-term potentiation - Towards multiscale understanding of learning and memory. *Neurosci Res* 175: 3-15
- Held K, Toth BI. 2021. TRPM3 in Brain (Patho)Physiology. *Front Cell Dev Biol* 9: 635659
- Hemonnot AL, Hua J, Ulmann L, Hirbec H. 2019. Microglia in Alzheimer Disease: Well-Known Targets and New Opportunities. *Front Aging Neurosci* 11: 233
- Heng BC, Zhang X, Aubel D, Bai Y, Li X, et al. 2021. An overview of signaling pathways regulating YAP/TAZ activity. *Cell Mol Life Sci* 78: 497-512
- Hensley K, Floyd RA, Zheng NY, Nael R, Robinson KA, et al. 1999. p38 kinase is activated in the Alzheimer's disease brain. *J Neurochem* 72: 2053-8
- Higuchi M, Iwata N, Matsuba Y, Takano J, Suemoto T, et al. 2012. Mechanistic involvement of the calpain-calpastatin system in Alzheimer neuropathology. *FASEB J* 26: 1204-17
- Hindle JV. 2010. Ageing, neurodegeneration and Parkinson's disease. *Age Ageing* 39: 156-61
- Hobohm C, Hartig W, Brauer K, Bruckner G. 1998. Low expression of extracellular matrix components in rat brain stem regions containing modulatory aminergic neurons. *J Chem Neuroanat* 15: 135-42
- Hoffmann A, Grimm C, Kraft R, Goldbaum O, Wrede A, et al. 2010. TRPM3 is expressed in sphingosine-responsive myelinating oligodendrocytes. *J Neurochem* 114: 654-65
- Hogan DB, Jette N, Fiest KM, Roberts JI, Pearson D, et al. 2016. The Prevalence and Incidence of Frontotemporal Dementia: a Systematic Review. *Can J Neurol Sci* 43 Suppl 1: S96-S109
- Hope JM, Lopez-Cavestany M, Wang W, Reinhart-King CA, King MR. 2019. Activation of Piezo1 sensitizes cells to TRAIL-mediated apoptosis through mitochondrial outer membrane permeability. *Cell Death Dis* 10: 837
- Hoshino C, Konno A, Hosoi N, Kaneko R, Mukai R, et al. 2021. GABAergic neuron-specific whole-brain transduction by AAV-PHP.B incorporated with a new GAD65 promoter. *Mol Brain* 14: 33
- Hoshino K, Hasegawa K, Kamiya H, Morimoto Y. 2017. Synapse-specific effects of IL-1beta on long-term potentiation in the mouse hippocampus. *Biomed Res* 38: 183-88
- Hosli L, Binini N, Ferrari KD, Thieren L, Looser ZJ, et al. 2022. Decoupling astrocytes in adult mice impairs synaptic plasticity and spatial learning. *Cell Rep* 38: 110484

- Hui E, Johnson CP, Yao J, Dunning FM, Chapman ER. 2009. Synaptotagmin-mediated bending of the target membrane is a critical step in Ca(2+)-regulated fusion. *Cell* 138: 709-21
- Humphrey JD, Dufresne ER, Schwartz MA. 2014. Mechanotransduction and extracellular matrix homeostasis. *Nat Rev Mol Cell Biol* 15: 802-12
- Hunter DD, Manglapus MK, Bachay G, Claudepierre T, Dolan MW, et al. 2019. CNS synapses are stabilized trans-synaptically by laminins and laminin-interacting proteins. *J Comp Neurol* 527: 67-86
- Iourov IY, Yurov YB, Vorsanova SG, Kutsev SI. 2021. Chromosome Instability, Aging and Brain Diseases. *Cells* 10
- Jantti H, Sitnikova V, Ishchenko Y, Shakirzyanova A, Giudice L, et al. 2022. Microglial amyloid beta clearance is driven by PIEZO1 channels. *J Neuroinflammation* 19: 147
- Jay DG. 2000. The clutch hypothesis revisited: ascribing the roles of actin-associated proteins in filopodial protrusion in the nerve growth cone. *J Neurobiol* 44: 114-25
- Jiang CH, Wei M, Zhang C, Shi YS. 2021a. The amino-terminal domain of GluA1 mediates LTP maintenance via interaction with neuroligin-1. *Proc Natl Acad Sci U S A* 118
- Jiang W, Del Rosario JS, Botello-Smith W, Zhao S, Lin YC, et al. 2021b. Crowding-induced opening of the mechanosensitive Piezo1 channel in silico. *Commun Biol* 4: 84
- Johnson JAG, Liu H, Hoger U, Rogers SM, Sivapalan K, et al. 2021. Mechanotransduction channel Piezo is widely expressed in the spider, *Cupiennius salei*, mechanosensory neurons and central nervous system. *Sci Rep* 11: 7994
- Johnson KM, Milner R, Crocker SJ. 2015. Extracellular matrix composition determines astrocyte responses to mechanical and inflammatory stimuli. *Neurosci Lett* 600: 104-9
- Jung H, Kim SY, Canbakis Cecen FS, Cho Y, Kwon SK. 2020. Dysfunction of Mitochondrial Ca(2+) Regulatory Machineries in Brain Aging and Neurodegenerative Diseases. *Front Cell Dev Biol* 8: 599792
- Kaech S, Banker G. 2006. Culturing hippocampal neurons. *Nat Protoc* 1: 2406-15
- Kapr J, Petersilie L, Distler T, Lauria I, Bendt F, et al. 2021. Human Induced Pluripotent Stem Cell-Derived Neural Progenitor Cells Produce Distinct Neural 3D In Vitro Models Depending on Alginate/Gellan Gum/Laminin Hydrogel Blend Properties. *Adv Healthc Mater* 10: e2100131
- Karpova A, Mikhaylova M, Bera S, Bar J, Reddy PP, et al. 2013. Encoding and transducing the synaptic or extrasynaptic origin of NMDA receptor signals to the nucleus. *Cell* 152: 1119-33
- Katanosaka K, Takatsu S, Mizumura K, Naruse K, Katanosaka Y. 2018. TRPV2 is required for mechanical nociception and the stretch-evoked response of primary sensory neurons. *Sci Rep* 8: 16782
- Kim KJ, Iddings JA, Stern JE, Blanco VM, Croom D, et al. 2015. Astrocyte contributions to flow/pressure-evoked parenchymal arteriole vasoconstriction. *J Neurosci* 35: 8245-57
- Kim Y, Meade SM, Chen K, Feng H, Rayyan J, et al. 2018. Nano-Architectural Approaches for Improved Intracortical Interface Technologies. *Front Neurosci* 12: 456
- Kimura R, Ohno M. 2009. Impairments in remote memory stabilization precede hippocampal synaptic and cognitive failures in 5XFAD Alzheimer mouse model. *Neurobiol Dis* 33: 229-35
- Kochlamazashvili G, Henneberger C, Bukalo O, Dvoretzkova E, Senkov O, et al. 2010a. The extracellular matrix molecule hyaluronic acid regulates hippocampal synaptic plasticity by modulating postsynaptic L-type Ca(2+) channels. *Neuron* 67: 116-28

- Kochlamazashvili G, Senkov O, Grebenyuk S, Robinson C, Xiao MF, et al. 2010b. Neural cell adhesion molecule-associated polysialic acid regulates synaptic plasticity and learning by restraining the signaling through GluN2B-containing NMDA receptors. *J Neurosci* 30: 4171-83
- Kopec CD, Li B, Wei W, Boehm J, Malinow R. 2006. Glutamate receptor exocytosis and spine enlargement during chemically induced long-term potentiation. *J Neurosci* 26: 2000-9
- Koskinen MK, van Mourik Y, Smit AB, Riga D, Spijker S. 2020. From stress to depression: development of extracellular matrix-dependent cognitive impairment following social stress. *Sci Rep* 10: 17308
- Kougioumoutzakis A, Pelletier JG, Laplante I, Khlaifia A, Lacaille JC. 2020. TRPC1 mediates slow excitatory synaptic transmission in hippocampal oriens/alveus interneurons. *Mol Brain* 13: 12
- Kovar H, Bierbaumer L, Radic-Sarikas B. 2020. The YAP/TAZ Pathway in Osteogenesis and Bone Sarcoma Pathogenesis. *Cells* 9
- Krapivinsky G, Medina I, Krapivinsky L, Gapon S, Clapham DE. 2004. SynGAP-MUPP1-CaMKII synaptic complexes regulate p38 MAP kinase activity and NMDA receptor-dependent synaptic AMPA receptor potentiation. *Neuron* 43: 563-74
- Krstic D, Rodriguez M, Knuesel I. 2012. Regulated proteolytic processing of Reelin through interplay of tissue plasminogen activator (tPA), ADAMTS-4, ADAMTS-5, and their modulators. *PLoS One* 7: e47793
- Kuchibhotla KV, Lattarulo CR, Hyman BT, Bacsikai BJ. 2009. Synchronous hyperactivity and intercellular calcium waves in astrocytes in Alzheimer mice. *Science* 323: 1211-5
- Kujawski S, Kujawska A, Perkowski R, Androsiuk-Perkowska J, Hajec W, et al. 2021. Cognitive Function Changes in Older People. Results of Second Wave of Cognition of Older People, Education, Recreational Activities, NutritIon, Comorbidities, fUnctional Capacity Studies (COPERNICUS). *Front Aging Neurosci* 13: 653570
- Langhans SA. 2018. Three-Dimensional in Vitro Cell Culture Models in Drug Discovery and Drug Repositioning. *Front Pharmacol* 9: 6
- Lau LW, Cua R, Keough MB, Haylock-Jacobs S, Yong VW. 2013. Pathophysiology of the brain extracellular matrix: a new target for remyelination. *Nat Rev Neurosci* 14: 722-9
- Leckband DE, de Rooij J. 2014. Cadherin adhesion and mechanotransduction. *Annu Rev Cell Dev Biol* 30: 291-315
- Lee JC, Choe SY. 2014. Age-related changes in the distribution of transient receptor potential vanilloid 4 channel (TRPV4) in the central nervous system of rats. *J Mol Histol* 45: 497-505
- Lee SLT, Lew D, Wickenheisser V, Markus EJ. 2019. Interdependence between dorsal and ventral hippocampus during spatial navigation. *Brain Behav* 9: e01410
- Lee W, Nims RJ, Savadipour A, Zhang Q, Leddy HA, et al. 2021. Inflammatory signaling sensitizes Piezo1 mechanotransduction in articular chondrocytes as a pathogenic feed-forward mechanism in osteoarthritis. *Proc Natl Acad Sci U S A* 118
- Leipzig ND, Shoichet MS. 2009. The effect of substrate stiffness on adult neural stem cell behavior. *Biomaterials* 30: 6867-78
- Lewin GR, Moshourab R. 2004. Mechanosensation and pain. *J Neurobiol* 61: 30-44
- Lewis AH, Grandl J. 2015. Mechanical sensitivity of Piezo1 ion channels can be tuned by cellular membrane tension. *Elife* 4

- Lewis AH, Grandl J. 2020. Inactivation Kinetics and Mechanical Gating of Piezo1 Ion Channels Depend on Subdomains within the Cap. *Cell Rep* 30: 870-80 e2
- Li J, Hou B, Tumova S, Muraki K, Bruns A, et al. 2014. Piezo1 integration of vascular architecture with physiological force. *Nature* 515: 279-82
- Li X, Li Q, Wang X, Li D, Li S. 2018. Differential Age-Related Changes in Structural Covariance Networks of Human Anterior and Posterior Hippocampus. *Front Physiol* 9: 518
- Liddel SA, Barres BA. 2017. Reactive Astrocytes: Production, Function, and Therapeutic Potential. *Immunity* 46: 957-67
- Lin R, Rosahl TW, Whiting PJ, Fawcett JW, Kwok JC. 2011. 6-Sulphated chondroitins have a positive influence on axonal regeneration. *PLoS One* 6: e21499
- Liu CSC, Raychaudhuri D, Paul B, Chakrabarty Y, Ghosh AR, et al. 2018a. Cutting Edge: Piezo1 Mechanosensors Optimize Human T Cell Activation. *J Immunol* 200: 1255-60
- Liu H, Bian W, Yang D, Yang M, Luo H. 2021a. Inhibiting the Piezo1 channel protects microglia from acute hyperglycaemia damage through the JNK1 and mTOR signalling pathways. *Life Sci* 264: 118667
- Liu H, Hu J, Zheng Q, Feng X, Zhan F, et al. 2022. Piezo1 Channels as Force Sensors in Mechanical Force-Related Chronic Inflammation. *Front Immunol* 13: 816149
- Liu MG, Song Q, Zhuo M. 2018b. Loss of Synaptic Tagging in the Anterior Cingulate Cortex after Tail Amputation in Adult Mice. *J Neurosci* 38: 8060-70
- Liu S, Xu X, Fang Z, Ning Y, Deng B, et al. 2021b. Piezo1 impairs hepatocellular tumor growth via deregulation of the MAPK-mediated YAP signaling pathway. *Cell Calcium* 95: 102367
- Lockhart M, Wirrig E, Phelps A, Wessels A. 2011. Extracellular matrix and heart development. *Birth Defects Res A Clin Mol Teratol* 91: 535-50
- Low SE, Amburgey K, Horstick E, Linsley J, Sprague SM, et al. 2011. TRPM7 is required within zebrafish sensory neurons for the activation of touch-evoked escape behaviors. *J Neurosci* 31: 11633-44
- Ma D, Deng B, Sun C, McComb DW, Gu C. 2022a. The Mechanical Microenvironment Regulates Axon Diameters Visualized by Cryo-Electron Tomography. *Cells* 11
- Ma T, Wang YY, Lu Y, Feng L, Yang YT, et al. 2022b. Inhibition of Piezo1/Ca(2+)/calpain signaling in the rat basal forebrain reverses sleep deprivation-induced fear memory impairments. *Behav Brain Res* 417: 113594
- Magnusson KR, Brim BL, Das SR. 2010. Selective Vulnerabilities of N-methyl-D-aspartate (NMDA) Receptors During Brain Aging. *Front Aging Neurosci* 2: 11
- Marrone MC, Morabito A, Giustizieri M, Chiurciu V, Leuti A, et al. 2017. TRPV1 channels are critical brain inflammation detectors and neuropathic pain biomarkers in mice. *Nat Commun* 8: 15292
- Martinac B, Buechner M, Delcour AH, Adler J, Kung C. 1987. Pressure-sensitive ion channel in *Escherichia coli*. *Proc Natl Acad Sci U S A* 84: 2297-301
- Martinez-Galan JR, Verdejo A, Caminos E. 2018. TRPC1 Channels Are Expressed in Pyramidal Neurons and in a Subset of Somatostatin Interneurons in the Rat Neocortex. *Front Neuroanat* 12: 15
- Martino F, Perestrelo AR, Vinarsky V, Pagliari S, Forte G. 2018. Cellular Mechanotransduction: From Tension to Function. *Front Physiol* 9: 824

- Matuszko G, Curreli S, Kaushik R, Becker A, Dityatev A. 2017. Extracellular matrix alterations in the ketamine model of schizophrenia. *Neuroscience* 350: 13-22
- McGregor G, Clements L, Farah A, Irving AJ, Harvey J. 2018. Age-dependent regulation of excitatory synaptic transmission at hippocampal temporoammonic-CA1 synapses by leptin. *Neurobiol Aging* 69: 76-93
- McMillen P, Holley SA. 2015. Integration of cell-cell and cell-ECM adhesion in vertebrate morphogenesis. *Curr Opin Cell Biol* 36: 48-53
- Meng Y, Zhang Y, Jia Z. 2003. Synaptic transmission and plasticity in the absence of AMPA glutamate receptor GluR2 and GluR3. *Neuron* 39: 163-76
- Menigoz A, Boudes M. 2011. The expression pattern of TRPV1 in brain. *J Neurosci* 31: 13025-7
- Metwally E, Zhao G, Zhang YQ. 2021. The calcium-dependent protease calpain in neuronal remodeling and neurodegeneration. *Trends Neurosci* 44: 741-52
- Minegishi T, Kastian RF, Inagaki N. 2022. Mechanical regulation of synapse formation and plasticity. *Semin Cell Dev Biol*
- Mitchison T, Kirschner M. 1988. Cytoskeletal dynamics and nerve growth. *Neuron* 1: 761-72
- Miyata S, Komatsu Y, Yoshimura Y, Taya C, Kitagawa H. 2012. Persistent cortical plasticity by upregulation of chondroitin 6-sulfation. *Nat Neurosci* 15: 414-22, S1-2
- Mohri Z, Del Rio Hernandez A, Krams R. 2017. The emerging role of YAP/TAZ in mechanotransduction. *J Thorac Dis* 9: E507-E09
- Morawski M, Filippov M, Tzinia A, Tsilibary E, Vargova L. 2014. ECM in brain aging and dementia. *Prog Brain Res* 214: 207-27
- Moreno-Cugnon L, Revuelta M, Arrizabalaga O, Colie S, Moreno-Valladares M, et al. 2019. Neuronal p38alpha mediates age-associated neural stem cell exhaustion and cognitive decline. *Aging Cell* 18: e13044
- Morrison DK. 2012. MAP kinase pathways. *Cold Spring Harb Perspect Biol* 4
- Mortera P, Herculano-Houzel S. 2012. Age-related neuronal loss in the rat brain starts at the end of adolescence. *Front Neuroanat* 6: 45
- Mulholland PJ, Luong NT, Woodward JJ, Chandler LJ. 2008. Brain-derived neurotrophic factor activation of extracellular signal-regulated kinase is autonomous from the dominant extrasynaptic NMDA receptor extracellular signal-regulated kinase shutoff pathway. *Neuroscience* 151: 419-27
- Murphy MC, Jones DT, Jack CR, Jr., Glaser KJ, Senjem ML, et al. 2016. Regional brain stiffness changes across the Alzheimer's disease spectrum. *Neuroimage Clin* 10: 283-90
- Nakamichi R, Ma S, Nonoyama T, Chiba T, Kurimoto R, et al. 2022. The mechanosensitive ion channel PIEZO1 is expressed in tendons and regulates physical performance. *Sci Transl Med* 14: eabj5557
- Nestor MW, Cai X, Stone MR, Bloch RJ, Thompson SM. 2011. The actin binding domain of betaI-spectrin regulates the morphological and functional dynamics of dendritic spines. *PLoS One* 6: e16197
- Nichol RHt, Catlett TS, Onesto MM, Hollender D, Gomez TM. 2019. Environmental Elasticity Regulates Cell-type Specific RHOA Signaling and Neuritogenesis of Human Neurons. *Stem Cell Reports* 13: 1006-21
- Nicholson DA, Yoshida R, Berry RW, Gallagher M, Geinisman Y. 2004. Reduction in size of perforated postsynaptic densities in hippocampal axospinous synapses and age-related spatial learning impairments. *J Neurosci* 24: 7648-53

- Niekisch H, Steinhardt J, Berghauer J, Bertazzoni S, Kaschinski E, et al. 2019. Learning Induces Transient Upregulation of Brevican in the Auditory Cortex during Consolidation of Long-Term Memories. *J Neurosci* 39: 7049-60
- O'Leary LA, Davoli MA, Belliveau C, Tanti A, Ma JC, et al. 2020. Characterization of Vimentin-Immunoreactive Astrocytes in the Human Brain. *Front Neuroanat* 14: 31
- Oh MM, Oliveira FA, Disterhoft JF. 2010. Learning and aging related changes in intrinsic neuronal excitability. *Front Aging Neurosci* 2: 2
- Ojo JO, Rezaie P, Gabbott PL, Stewart MG. 2015. Impact of age-related neuroglial cell responses on hippocampal deterioration. *Front Aging Neurosci* 7: 57
- Origlia N, Righi M, Capsoni S, Cattaneo A, Fang F, et al. 2008. Receptor for advanced glycation end product-dependent activation of p38 mitogen-activated protein kinase contributes to amyloid-beta-mediated cortical synaptic dysfunction. *J Neurosci* 28: 3521-30
- Palmer AL, Ousman SS. 2018. Astrocytes and Aging. *Front Aging Neurosci* 10: 337
- Pandya JD, Grondin R, Yonutas HM, Haghazadeh H, Gash DM, et al. 2015. Decreased mitochondrial bioenergetics and calcium buffering capacity in the basal ganglia correlates with motor deficits in a nonhuman primate model of aging. *Neurobiol Aging* 36: 1903-13
- Paoletti P, Bellone C, Zhou Q. 2013. NMDA receptor subunit diversity: impact on receptor properties, synaptic plasticity and disease. *Nat Rev Neurosci* 14: 383-400
- Parpaite T, Coste B. 2017. Piezo channels. *Curr Biol* 27: R250-R52
- Passini FS, Jaeger PK, Saab AS, Hanlon S, Chittim NA, et al. 2021. Shear-stress sensing by PIEZO1 regulates tendon stiffness in rodents and influences jumping performance in humans. *Nat Biomed Eng* 5: 1457-71
- Pathak MM, Nourse JL, Tran T, Hwe J, Arulmoli J, et al. 2014. Stretch-activated ion channel Piezo1 directs lineage choice in human neural stem cells. *Proc Natl Acad Sci U S A* 111: 16148-53
- Payan-Gomez C, Rodriguez D, Amador-Munoz D, Ramirez-Clavijo S. 2018. Integrative Analysis of Global Gene Expression Identifies Opposite Patterns of Reactive Astroglia in Aged Human Prefrontal Cortex. *Brain Sci* 8
- Peebles CL, Yoo J, Thwin MT, Palop JJ, Noebels JL, Finkbeiner S. 2010. Arc regulates spine morphology and maintains network stability in vivo. *Proc Natl Acad Sci U S A* 107: 18173-8
- Perea JR, Garcia E, Valles-Saiz L, Cuadros R, Hernandez F, et al. 2022. p38 activation occurs mainly in microglia in the P301S Tauopathy mouse model. *Sci Rep* 12: 2130
- Pielage J, Fetter RD, Davis GW. 2005. Presynaptic spectrin is essential for synapse stabilization. *Curr Biol* 15: 918-28
- Pizzorusso T, Medini P, Berardi N, Chierzi S, Fawcett JW, Maffei L. 2002. Reactivation of ocular dominance plasticity in the adult visual cortex. *Science* 298: 1248-51
- Popov A, Brazhe A, Denisov P, Sutyagina O, Li L, et al. 2021. Astrocyte dystrophy in ageing brain parallels impaired synaptic plasticity. *Aging Cell* 20: e13334
- Prieto GA, Smith ED, Tong L, Nguyen M, Cotman CW. 2019. Inhibition of LTP-Induced Translation by IL-1 $\beta$  Reduces the Level of Newly Synthesized Proteins in Hippocampal Dendrites. *ACS Chem Neurosci* 10: 1197-203
- Pruitt BL, Dunn AR, Weis WI, Nelson WJ. 2014. Mechano-transduction: from molecules to tissues. *PLoS Biol* 12: e1001996
- Qiu Z, Guo J, Kala S, Zhu J, Xian Q, et al. 2019. The Mechanosensitive Ion Channel Piezo1 Significantly Mediates In Vitro Ultrasonic Stimulation of Neurons. *iScience* 21: 448-57

- Quick K, Zhao J, Eijkelkamp N, Linley JE, Rugiero F, et al. 2012. TRPC3 and TRPC6 are essential for normal mechanotransduction in subsets of sensory neurons and cochlear hair cells. *Open Biol* 2: 120068
- Redmon SN, Yarishkin O, Lakk M, Jo A, Mustafic E, et al. 2021. TRPV4 channels mediate the mechanoreponse in retinal microglia. *Glia* 69: 1563-82
- Richard AD, Tian XL, El-Saadi MW, Lu XH. 2018. Erasure of striatal chondroitin sulfate proteoglycan-associated extracellular matrix rescues aging-dependent decline of motor learning. *Neurobiol Aging* 71: 61-71
- Rizvi S, Raza ST, Mahdi F. 2014. Telomere length variations in aging and age-related diseases. *Curr Aging Sci* 7: 161-7
- Ryu Y, Iwashita M, Lee W, Uchimura K, Kosodo Y. 2021. A Shift in Tissue Stiffness During Hippocampal Maturation Correlates to the Pattern of Neurogenesis and Composition of the Extracellular Matrix. *Front Aging Neurosci* 13: 709620
- Saito K, Elce JS, Hamos JE, Nixon RA. 1993. Widespread activation of calcium-activated neutral proteinase (calpain) in the brain in Alzheimer disease: a potential molecular basis for neuronal degeneration. *Proc Natl Acad Sci U S A* 90: 2628-32
- Sappington RM, Sidorova T, Ward NJ, Chakravarthy R, Ho KW, Calkins DJ. 2015. Activation of transient receptor potential vanilloid-1 (TRPV1) influences how retinal ganglion cell neurons respond to pressure-related stress. *Channels (Austin)* 9: 102-13
- Satoh K, Hata M, Takahara S, Tsuzaki H, Yokota H, et al. 2006. A novel membrane protein, encoded by the gene covering KIAA0233, is transcriptionally induced in senile plaque-associated astrocytes. *Brain Res* 1108: 19-27
- Schneider H, Pitossi F, Balschun D, Wagner A, del Rey A, Besedovsky HO. 1998. A neuromodulatory role of interleukin-1beta in the hippocampus. *Proc Natl Acad Sci U S A* 95: 7778-83
- Segel M, Neumann B, Hill MFE, Weber IP, Viscomi C, et al. 2019. Niche stiffness underlies the ageing of central nervous system progenitor cells. *Nature* 573: 130-34
- Senkov O, Andjus P, Radenovic L, Soriano E, Dityatev A. 2014. Neural ECM molecules in synaptic plasticity, learning, and memory. *Prog Brain Res* 214: 53-80
- Shi Y, Ethell IM. 2006. Integrins control dendritic spine plasticity in hippocampal neurons through NMDA receptor and Ca<sup>2+</sup>/calmodulin-dependent protein kinase II-mediated actin reorganization. *J Neurosci* 26: 1813-22
- Shibasaki K, Ishizaki Y, Mandadi S. 2013. Astrocytes express functional TRPV2 ion channels. *Biochem Biophys Res Commun* 441: 327-32
- Shigetomi E, Tong X, Kwan KY, Corey DP, Khakh BS. 2011. TRPA1 channels regulate astrocyte resting calcium and inhibitory synapse efficacy through GAT-3. *Nat Neurosci* 15: 70-80
- Shimada A, Keino H, Satoh M, Kishikawa M, Hosokawa M. 2003. Age-related loss of synapses in the frontal cortex of SAMP10 mouse: a model of cerebral degeneration. *Synapse* 48: 198-204
- Sierra A, Encinas JM, Deudero JJ, Chancey JH, Enikolopov G, et al. 2010. Microglia shape adult hippocampal neurogenesis through apoptosis-coupled phagocytosis. *Cell Stem Cell* 7: 483-95
- Siiskonen H, Oikari S, Pasonen-Seppanen S, Rilla K. 2015. Hyaluronan synthase 1: a mysterious enzyme with unexpected functions. *Front Immunol* 6: 43

- Song Y, Li D, Farrelly O, Miles L, Li F, et al. 2019. The Mechanosensitive Ion Channel Piezo Inhibits Axon Regeneration. *Neuron* 102: 373-89 e6
- Sorra KE, Harris KM. 2000. Overview on the structure, composition, function, development, and plasticity of hippocampal dendritic spines. *Hippocampus* 10: 501-11
- Squire LR. 2009. The legacy of patient H.M. for neuroscience. *Neuron* 61: 6-9
- Startek JB, Boonen B, Talavera K, Meseguer V. 2019. TRP Channels as Sensors of Chemically-Induced Changes in Cell Membrane Mechanical Properties. *Int J Mol Sci* 20
- Stearns-Reider KM, D'Amore A, Beezhold K, Rothrauff B, Cavalli L, et al. 2017. Aging of the skeletal muscle extracellular matrix drives a stem cell fibrogenic conversion. *Aging Cell* 16: 518-28
- Steinkuhler J, Sezgin E, Urbancic I, Eggeling C, Dimova R. 2019. Mechanical properties of plasma membrane vesicles correlate with lipid order, viscosity and cell density. *Commun Biol* 2: 337
- Stevens B, Allen NJ, Vazquez LE, Howell GR, Christopherson KS, et al. 2007. The classical complement cascade mediates CNS synapse elimination. *Cell* 131: 1164-78
- Storm C, Pastore JJ, MacKintosh FC, Lubensky TC, Janmey PA. 2005. Nonlinear elasticity in biological gels. *Nature* 435: 191-4
- Suchyna TM, Johnson JH, Hamer K, Leykam JF, Gage DA, et al. 2000. Identification of a peptide toxin from *Grammostola spatulata* spider venom that blocks cation-selective stretch-activated channels. *J Gen Physiol* 115: 583-98
- Sun Y, Li M, Liu G, Zhang X, Zhi L, et al. 2020. The function of Piezo1 in colon cancer metastasis and its potential regulatory mechanism. *J Cancer Res Clin Oncol* 146: 1139-52
- Syeda R. 2021. Physiology and Pathophysiology of Mechanically Activated PIEZO Channels. *Annu Rev Neurosci* 44: 383-402
- Syeda R, Xu J, Dubin AE, Coste B, Mathur J, et al. 2015. Chemical activation of the mechanotransduction channel Piezo1. *Elife* 4
- Takada Y, Numata T, Mori Y. 2013. Targeting TRPs in neurodegenerative disorders. *Curr Top Med Chem* 13: 322-34
- Takei Y. 2019. Age-dependent decline in neurogenesis of the hippocampus and extracellular nucleotides. *Hum Cell* 32: 88-94
- Tanaka H, Homma H, Fujita K, Kondo K, Yamada S, et al. 2020. YAP-dependent necrosis occurs in early stages of Alzheimer's disease and regulates mouse model pathology. *Nat Commun* 11: 507
- Tao W, Lee J, Chen X, Diaz-Alonso J, Zhou J, et al. 2021. Synaptic memory requires CaMKII. *Elife* 10
- Tojkander S, Gateva G, Lappalainen P. 2012. Actin stress fibers--assembly, dynamics and biological roles. *J Cell Sci* 125: 1855-64
- Tong L, Prieto GA, Kramar EA, Smith ED, Cribbs DH, et al. 2012. Brain-derived neurotrophic factor-dependent synaptic plasticity is suppressed by interleukin-1beta via p38 mitogen-activated protein kinase. *J Neurosci* 32: 17714-24
- Tyler WJ. 2012. The mechanobiology of brain function. *Nat Rev Neurosci* 13: 867-78
- Tyrrell DJ, Blin MG, Song J, Wood SC, Zhang M, et al. 2020. Age-Associated Mitochondrial Dysfunction Accelerates Atherogenesis. *Circ Res* 126: 298-314

- van Helvert S, Friedl P. 2016. Strain Stiffening of Fibrillar Collagen during Individual and Collective Cell Migration Identified by AFM Nanoindentation. *ACS Appl Mater Interfaces* 8: 21946-55
- VanGuilder HD, Farley JA, Yan H, Van Kirk CA, Mitschelen M, et al. 2011. Hippocampal dysregulation of synaptic plasticity-associated proteins with age-related cognitive decline. *Neurobiol Dis* 43: 201-12
- Vegh MJ, Heldring CM, Kamphuis W, Hijazi S, Timmerman AJ, et al. 2014a. Reducing hippocampal extracellular matrix reverses early memory deficits in a mouse model of Alzheimer's disease. *Acta Neuropathol Commun* 2: 76
- Vegh MJ, Rausell A, Loos M, Heldring CM, Jurkowski W, et al. 2014b. Hippocampal extracellular matrix levels and stochasticity in synaptic protein expression increase with age and are associated with age-dependent cognitive decline. *Mol Cell Proteomics* 13: 2975-85
- Velasco-Estevez M, Gadalla KKE, Linan-Barba N, Cobb S, Dev KK, Sheridan GK. 2020. Inhibition of Piezo1 attenuates demyelination in the central nervous system. *Glia* 68: 356-75
- Velasco-Estevez M, Mampay M, Boutin H, Chaney A, Warn P, et al. 2018. Infection Augments Expression of Mechanosensing Piezo1 Channels in Amyloid Plaque-Reactive Astrocytes. *Front Aging Neurosci* 10: 332
- Verkhatsky A. 2019. Astroglial Calcium Signaling in Aging and Alzheimer's Disease. *Cold Spring Harb Perspect Biol* 11
- Verkhatsky A, Reyes RC, Parpura V. 2014. TRP channels coordinate ion signalling in astroglia. *Rev Physiol Biochem Pharmacol* 166: 1-22
- Vining KH, Mooney DJ. 2017. Mechanical forces direct stem cell behaviour in development and regeneration. *Nat Rev Mol Cell Biol* 18: 728-42
- Viviani B, Bartesaghi S, Gardoni F, Vezzani A, Behrens MM, et al. 2003. Interleukin-1beta enhances NMDA receptor-mediated intracellular calcium increase through activation of the Src family of kinases. *J Neurosci* 23: 8692-700
- von Strauss E, Viitanen M, De Ronchi D, Winblad B, Fratiglioni L. 1999. Aging and the occurrence of dementia: findings from a population-based cohort with a large sample of nonagenarians. *Arch Neurol* 56: 587-92
- Wang H, Katagiri Y, McCann TE, Unsworth E, Goldsmith P, et al. 2008. Chondroitin-4-sulfation negatively regulates axonal guidance and growth. *J Cell Sci* 121: 3083-91
- Wang J, La JH, Hamill OP. 2019. PIEZO1 Is Selectively Expressed in Small Diameter Mouse DRG Neurons Distinct From Neurons Strongly Expressing TRPV1. *Front Mol Neurosci* 12: 178
- Wang L, Xia J, Li J, Hagemann TL, Jones JR, et al. 2018a. Tissue and cellular rigidity and mechanosensitive signaling activation in Alexander disease. *Nat Commun* 9: 1899
- Wang L, You X, Lotinun S, Zhang L, Wu N, Zou W. 2020. Mechanical sensing protein PIEZO1 regulates bone homeostasis via osteoblast-osteoclast crosstalk. *Nat Commun* 11: 282
- Wang Y, Chi S, Guo H, Li G, Wang L, et al. 2018b. A lever-like transduction pathway for long-distance chemical- and mechano-gating of the mechanosensitive Piezo1 channel. *Nat Commun* 9: 1300
- Wang Y, Xiao B. 2018. The mechanosensitive Piezo1 channel: structural features and molecular bases underlying its ion permeation and mechanotransduction. *J Physiol* 596: 969-78

- Watson PA, Hannan R, Carl LL, Giger KE. 1996. Contractile activity and passive stretch regulate tubulin mRNA and protein content in cardiac myocytes. *Am J Physiol* 271: C684-9
- Wen Q, Janmey PA. 2013. Effects of non-linearity on cell-ECM interactions. *Exp Cell Res* 319: 2481-9
- White JP, Cibelli M, Urban L, Nilius B, McGeown JG, Nagy I. 2016. TRPV4: Molecular Conductor of a Diverse Orchestra. *Physiol Rev* 96: 911-73
- Winkler J, Abisoye-Ogunniyan A, Metcalf KJ, Werb Z. 2020. Concepts of extracellular matrix remodelling in tumour progression and metastasis. *Nat Commun* 11: 5120
- Wong LW, Chong YS, Lin W, Kisiswa L, Sim E, et al. 2021. Age-related changes in hippocampal-dependent synaptic plasticity and memory mediated by p75 neurotrophin receptor. *Aging Cell* 20: e13305
- Wong PC, Marszalek J, Crawford TO, Xu Z, Hsieh ST, et al. 1995. Increasing neurofilament subunit NF-M expression reduces axonal NF-H, inhibits radial growth, and results in neurofilamentous accumulation in motor neurons. *J Cell Biol* 130: 1413-22
- Wu D, Huang W, Richardson PM, Priestley JV, Liu M. 2008. TRPC4 in rat dorsal root ganglion neurons is increased after nerve injury and is necessary for neurite outgrowth. *J Biol Chem* 283: 416-26
- Wu J, Lewis AH, Grandl J. 2017a. Touch, Tension, and Transduction - The Function and Regulation of Piezo Ion Channels. *Trends Biochem Sci* 42: 57-71
- Wu J, Young M, Lewis AH, Martfeld AN, Kalmeta B, Grandl J. 2017b. Inactivation of Mechanically Activated Piezo1 Ion Channels Is Determined by the C-Terminal Extracellular Domain and the Inner Pore Helix. *Cell Rep* 21: 2357-66
- Wu LJ, Sweet TB, Clapham DE. 2010. International Union of Basic and Clinical Pharmacology. LXXVI. Current progress in the mammalian TRP ion channel family. *Pharmacol Rev* 62: 381-404
- Xiong Y, Dong L, Bai Y, Tang H, Li S, et al. 2022. Piezo1 activation facilitates ovarian cancer metastasis via Hippo/YAP signaling axis. *Channels (Austin)* 16: 159-66
- Xu J, Kurup P, Zhang Y, Goebel-Goody SM, Wu PH, et al. 2009. Extrasynaptic NMDA receptors couple preferentially to excitotoxicity via calpain-mediated cleavage of STEP. *J Neurosci* 29: 9330-43
- Xu K, Zhong G, Zhuang X. 2013. Actin, spectrin, and associated proteins form a periodic cytoskeletal structure in axons. *Science* 339: 452-6
- Xue YX, Xue LF, Liu JF, He J, Deng JH, et al. 2014. Depletion of perineuronal nets in the amygdala to enhance the erasure of drug memories. *J Neurosci* 34: 6647-58
- Yan C, Wang F, Peng Y, Williams CR, Jenkins B, et al. 2018. Microtubule Acetylation Is Required for Mechanosensation in *Drosophila*. *Cell Rep* 25: 1051-65 e6
- Yang S, Gigout S, Molinaro A, Naito-Matsui Y, Hilton S, et al. 2021. Chondroitin 6-sulphate is required for neuroplasticity and memory in ageing. *Mol Psychiatry* 26: 5658-68
- Yang XL, Wang X, Shao L, Jiang GT, Min JW, et al. 2019. TRPV1 mediates astrocyte activation and interleukin-1beta release induced by hypoxic ischemia (HI). *J Neuroinflammation* 16: 114
- Young JL, Holle AW, Spatz JP. 2016. Nanoscale and mechanical properties of the physiological cell-ECM microenvironment. *Exp Cell Res* 343: 3-6
- Yu JY, Fang P, Wang C, Wang XX, Li K, et al. 2018. Dorsal CA1 interneurons contribute to acute stress-induced spatial memory deficits. *Neuropharmacology* 135: 474-86

- Yuan A, Rao MV, Veeranna, Nixon RA. 2017. Neurofilaments and Neurofilament Proteins in Health and Disease. *Cold Spring Harb Perspect Biol* 9
- Zappia KJ, O'Hara CL, Moehring F, Kwan KY, Stucky CL. 2017. Sensory Neuron-Specific Deletion of TRPA1 Results in Mechanical Cutaneous Sensory Deficits. *eNeuro* 4
- Zeng Y, Zhang J, Zhu Y, Zhang J, Shen H, et al. 2015. Tripchlorolide improves cognitive deficits by reducing amyloid beta and upregulating synapse-related proteins in a transgenic model of Alzheimer's Disease. *J Neurochem* 133: 38-52
- Zhang J, Mao X, Zhou T, Cheng X, Lin Y. 2014. IL-17A contributes to brain ischemia reperfusion injury through calpain-TRPC6 pathway in mice. *Neuroscience* 274: 419-28
- Zhang X, Hu M, Yang Y, Xu H. 2018. Organellar TRP channels. *Nat Struct Mol Biol* 25: 1009-18
- Zhang Y, Su SA, Li W, Ma Y, Shen J, et al. 2021. Piezo1-Mediated Mechanotransduction Promotes Cardiac Hypertrophy by Impairing Calcium Homeostasis to Activate Calpain/Calcineurin Signaling. *Hypertension* 78: 647-60
- Zhao Q, Zhou H, Chi S, Wang Y, Wang J, et al. 2018. Structure and mechanogating mechanism of the Piezo1 channel. *Nature* 554: 487-92
- Zheng J. 2013. Molecular mechanism of TRP channels. *Compr Physiol* 3: 221-42
- Zhou FW, Roper SN. 2014. TRPC3 mediates hyperexcitability and epileptiform activity in immature cortex and experimental cortical dysplasia. *J Neurophysiol* 111: 1227-37
- Zhou X, Zhu D, Katsuki F, Qi XL, Lees CJ, et al. 2014. Age-dependent changes in prefrontal intrinsic connectivity. *Proc Natl Acad Sci U S A* 111: 3853-8
- Zhu B, Qian W, Han C, Bai T, Hou X. 2021. Piezo 1 activation facilitates cholangiocarcinoma metastasis via Hippo/YAP signaling axis. *Mol Ther Nucleic Acids* 24: 241-52